Release of a Natural mRNA During Recycling of the Prokaryotic Ribosome

Dissertation

for the award of the degree

“Doctor rerum naturalium“ (Dr. rer. nat.)

of the Georg-August University of Göttingen

within the doctoral program:

GGNB Biomolecules: Structure – Function – Dynamics

of the Georg-August University School of Science (GAUSS)

submitted by

Moritz Willy Rudolf Willmer

from Kronach, Germany

Göttingen, 2022

Members of the Thesis Committee

Prof. Dr. Marina V. Rodnina
Department of Physical Biochemistry
Max Planck Institute for Multidisciplinary Sciences, Göttingen, Germany

Prof. Dr. Kai Tittmann
Department of Molecular Enzymology
Georg-August-Universität Göttingen, Göttingen, Germany

Prof. Dr. Holger Stark
Department of Structural Dynamics
Max Planck Institute for Multidisciplinary Sciences, Göttingen, Germany

Members of the Examination Board

Reviewer: Prof. Dr. Marina Rodnina
Department of Physical Biochemistry
Max Planck Institute for Multidisciplinary Sciences, Göttingen, Germany

Second Reviewer: Prof. Dr. Kai Tittmann
Department of Molecular Enzymology
Georg-August-Universität Göttingen, Göttingen, Germany

Further members of the Examination Board

Dr. Alexis C. Faesen
Research Group Biochemistry of Signal Dynamics
Max Planck Institute for Multidisciplinary Sciences, Göttingen, Germany

Dr. Sonja Lorenz
Research Group Ubiquitin Signaling Specificity
Max Planck Institute for Multidisciplinary Sciences, Göttingen, Germany

Prof. Dr. Hauke Hillen
Department of Cellular Biochemistry
University Medical Center Göttingen, Göttingen, Germany

Date of oral examination: 2nd of February 2023

Affidavit

I hereby declare that the presented dissertation entitled "Release of a Natural mRNA During Recycling of the Prokaryotic Ribosome" has been written independently and with no other sources and aids than quoted.

Göttingen, December 19th, 2022

Moritz Willy Rudolf Willmer

Table of Contents

Abstract

Ribosome recycling is the last step of the bacterial translation cycle. The release of the peptide leaves a 70S ribosome with a deacylated tRNA in the P site and the stop codon of the mRNA in the A site. The combined action of the ribosome recycling factor (RRF) and elongation factor G (EF-G) cause the splitting of the ribosomal subunits. The mechanism of tRNA and mRNA release and the order of events are less well understood and are controversially discussed in the literature. Based on studies using various non-native model mRNAs different orders of events were proposed. In this thesis the release of a natural mRNA and subunit splitting in a native termination context are investigated. A system had to me established to measure the recycling reaction at the stop codon of a previously fully translated ORF of an mRNA featuring a natural 3'-UTR. Using a bioinformatic transcriptome analysis, the lpp mRNA (coding for the major outer membrane prolipoprotein Lpp) was chosen as a representative natural mRNA. The lpp mRNA features a structured 3'-UTR with a transcription terminator hairpin, which is a predominant feature of terminal OFRs. To observe mRNA release from the 30S subunit, a FRET-assay was developed. For that purpose, a bioconjugation method utilizing the lipoic acid ligase $LplA^{W37V}$ was utilized and adapted for site-specific introduction of a fluorophore to the 30S subunit. Subunit splitting and mRNA release were measured in bulk kinetic experiments using the stopped-flow technique. The results show that mRNA release of the natural lpp mRNA happens almost simultaneously to subunit splitting, with subunit splitting being necessary for the fast release of the structured natural mRNA. mRNAs with truncated or no 3'-UTR, i.e. without the native mRNA hairpin, can dissociate from the ribosome without requiring subunit splitting. Single molecule TIRF microscopy was used as an additional technique and supported the results obtained with the bulk kinetic experiments. In conclusion, the results demonstrate the context dependence of ribosome function, the importance of choosing a physiological relevant model system and explain the partially contradicting models of previous studies. This study contributes towards integrating mRNA release into a comprehensive model of prokaryotic ribosome recycling and adds to understanding this vital step in bacterial translation.

1 Introduction

The ribosome comes from a vanished world that existed on the early earth long before the first biological life as we know it emerged. The discussions about the origins of life on earth are centered about the questions if RNA or proteins preceded the other. The ribosome, as a remainder of this time, in its core consists of RNA, but synthesizes all the proteins that are the vital building blocks of life. So far, we can only speculate whether the ribosome is one of the last artifacts from a world where RNA molecules both stored genetic information and served as the major catalysts, finally paving the way for proteins to take over their today's role from metabolism through gene regulation onto being structural components, or if in a co-existing RNA-and-protein world the separately evolved major components of the ribosome found together and henceforth fulfilled their todays function. As far as we can imagine, the ribosome, connecting RNA/DNA stored information and protein driven execution of this information, sparked the biogenesis of all life (Bowman et al., 2015).

In all life forms on earth, genetic information is stored as DNA, with only few exceptions being viruses that use RNA instead. Transcription of DNA into RNA makes this information accessible. RNAs can interact with DNA (regulatory RNAs) or small molecules (aptamers), or even catalyze chemical reactions (ribozymes). But the majority of RNAs function together at the ribosome, they deliver the building plan for proteins (messenger RNAs, mRNAs), build the structural basis for the core parts of the ribosome (ribosomal RNAs, rRNAs), or deliver the amino acids to the ribosome (transfer RNAs, tRNAs). The ribosome carries out the synthesis of proteins in a process called translation. Protein-encoding open reading frames (ORFs) on mRNAs store the information as base triplets (codons) that can be identified by the different tRNAs in the decoding center of the ribosome. The tRNAs ensure that the codon-corresponding amino acids are brought to the peptidyl transferase center (PTC) where peptide bond formation is catalyzed and the protein is synthesized. Translation is a cyclic and highly dynamic process. Various translation factors are involved in the different phases: ribosome assembly on an mRNA, decoding, translocation of the mRNA, release of the finished protein and disassembly of ribosome complexes (Rodnina, 2018).

Aside from being a fascinating molecular machine that utilizes chemical energy to synthesize the most abundant yet diverse building blocks of all life, researching the ribosome can also have immediate benefits. For example, most antibiotic compounds target the subtle differences between the ribosomes of bacteria and mammals (Wilson, 2014). Also, viruses are completely dependent on hijacking their host cell's ribosomes for replication. Gaining more insights into these

processes could help to give humanity effective tools to fight against many diseases like the recent SARS-CoV-2 pandemic and whatever comes next.

1.1 Bacterial Ribosome

Bacterial ribosomes consist of two subunits, the small 30S subunit and the large 50S subunit. Both subunits consist of both rRNA and proteins. The core of the ribosome consists almost exclusively of rRNA while the proteins are located on the solvent exposed surface. In *E. coli*, the 30S subunit consists of the 16S rRNA and 21 ribosomal proteins. The 50S subunit consists of the 5S rRNA, the 23S rRNA and 33 proteins (Fig. 1). The rRNA core of the ribosome features the catalytic active sites. The 30S subunit consists of two major domains, the “head” and the “body”. Rotation or “swiveling” of the head relative to the body is a requirement for many reactions of the translation cycle (Bock et al., 2013). Characteristic extensions of the head and the body are the “beak” and the “shoulder”, respectively. The mRNA enters the 30S subunit between the beak and helix 16 of the shoulder, the ribosomal proteins S3, S4 and S5 are located around this site forming a tunnel. The positively charged residues of these proteins also significantly contribute to the ribosome’s helicase activity (Takyar et al., 2005). The mRNA path continues towards the decoding center on the subunit interface side where the base pairing of mRNA and tRNAs happens. The subunit interface side features the three tRNA binding sites, the aminoacyl (A site), peptidyl (P site) and exit (E site) site. The mRNA path ends near the E site where the proteins S1, S6, S18, S21 are located as well as the anti-Shine-Dalgarno (aSD) sequence, an rRNA motif that can base-pair with the Shine Dalgarno (SD) sequence of mRNAs. The 50S subunit harbors three pockets for the A-, P-, and E-site tRNAs with the peptidyl transferase center (PTC) between the A and P site. The polypeptide exit tunnel emerges from the PTC through the 50S subunit towards the solvent side where the tunnel is extended through the proteins L23, L24 and L29. Other characteristic features or the 50S subunit are the L1 stalk at the E site and and the L7/L12 stalk at the A site (Ban et al., 2000; Melnikov et al., 2012; Nissen et al., 2000; Ramakrishnan, 2014; Weisser and Ban, 2019; Yusupov et al., 2001).

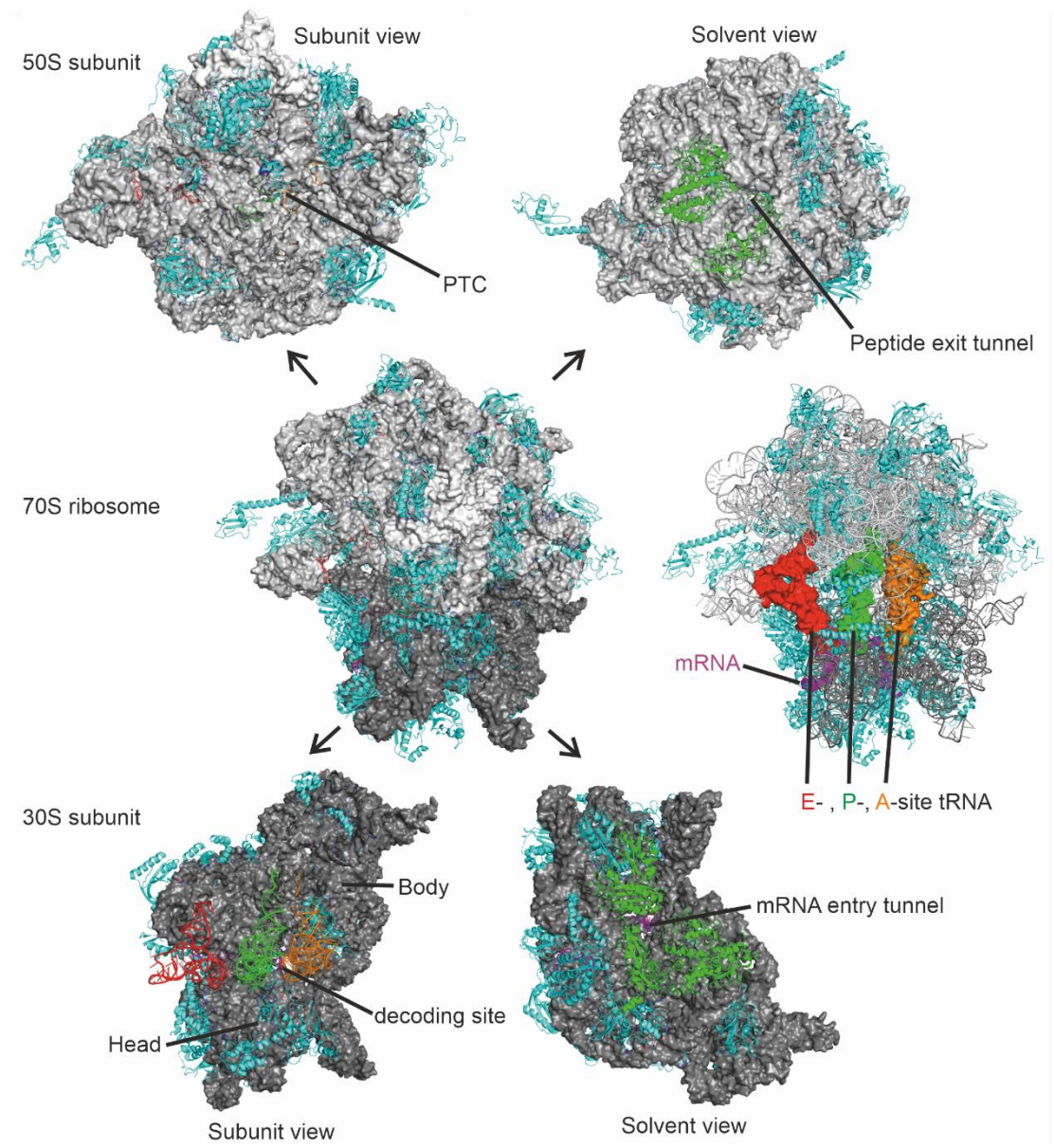

Figure 1. Bacterial ribosome. The 70S ribosome, here shown is an X-ray structure from *T. thermophilus and E. coli*, consisting of the large 50S and the small 30S subunit. The 50S subunit comprises the 23S and the 5S rRNA light grey) and 33 ribosomal proteins (top row) with the PTC in the center and the peptide exit tunnel that extends into the solvent by the proteins L23, L24 and L29 (green). The small 30S subunit (bottom row) with its head and body domains consists of the 16S rRNA (dark grey) and 21 ribosomal proteins. The mRNA (purple) enters through the mRNA entry tunnel surrounded by the ribosomal proteins S3, S4 and S5 (green) and binds between the head and the body of the 30S subunit. E, P and A site are occupied by tRNAs (red, green, orange). Structure from PDB: 6QNR (Rozov et al., 2019).

1.2 Bacterial Translation

Translation in its main steps is highly conserved through all life forms. Generally, translation cycles through four phases (Fig. 2). In the initiation phase, the ribosome complex is assembled on the mRNA at the start codon of the open reading frame (ORF). During multiple cycles of the elongation phase, amino acids are added to the growing polypeptide chain. The finished protein is released from the ribosome in the termination phase. To complete the cycle, the ribosome is then primed for the next round of translation in the recycling phase (Rodnina, 2018).

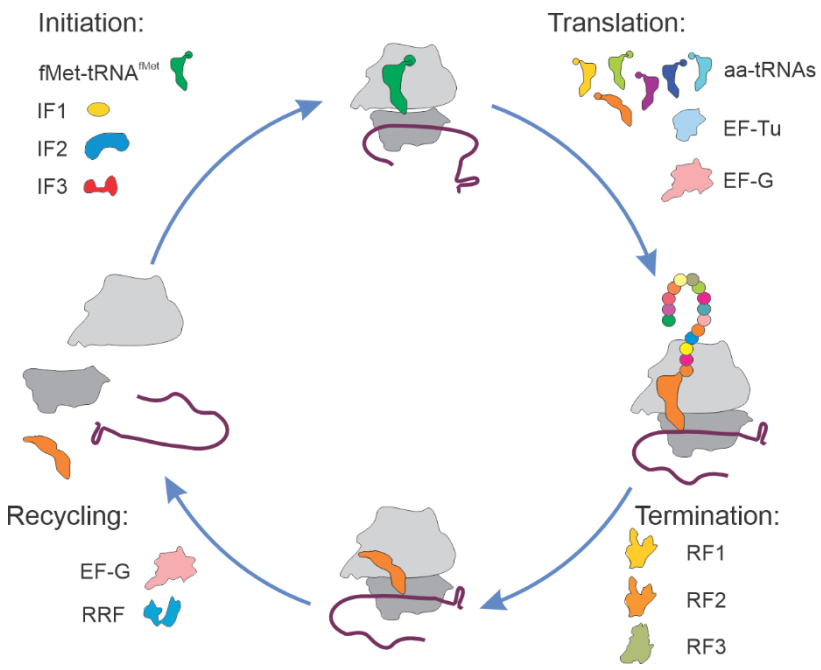

Figure 2. Translation cycle. In bacteria, translation of an mRNA (purple) by the ribosome (grey) requires four distinct steps: initiation, elongation, termination and recycling.

Through evolution, prokaryotes have conserved the ribosome and the translation cycle in its very basic form. This adds further relevance to studying the prokaryotic translation cycle as the findings often help to understand also other organisms. To start the prokaryotic translation cycle, the ribosome must bind to an mRNA, select the correct reading frame and acquire the initiator tRNA. The most common initiation pathway requires initiation factors IF1, IF2 and IF3 alongside the initiator tRNA and the mRNA to bind to the 30S subunit prior 50S subunit joining (Fig. 3). The events do not follow a strict order and may vary depending on abundance of the factors (Milon and Rodnina, 2012; Rodnina, 2018). IF3 binding near the platform is also considered the final step of

ribosome recycling and blocks subunit association during the early stages of initiation (Goyal et al., 2017; Hussain et al., 2016; Karimi et al., 1999; Peske et al., 2005). IF1 binds to the A-site and the translational GTPase IF2 binds near the P-site (Carter et al., 2001; Goyal et al., 2015; Milon et al., 2010; Milon et al., 2012; Milon and Rodnina, 2012; Sette et al., 1997). Initiator tRNA forms an Initiator-tRNA-IF2-GTP complex that is then recruited to the 30S subunit, to form the 30S pre-initiation complex (PIC) (Milon *et al.*, 2010; Milon *et al.*, 2012; Milon and Rodnina, 2012). In prokaryotes, mRNA binding to the 30S subunit is independent of initiation factors and 30S subunit conformation and instead is influenced by individual properties of the mRNA. Secondary structure elements in the so-called translation initiation region (TIR), describing the nucleotide positions of -20 to +15 around the start codon (Dreyfus, 1988; Milon and Rodnina, 2012), and the presence of a SD sequence can have a major influence on the binding kinetics of mRNAs. Ribosomal proteins S1, S2, S7, S11, S18 and S21 seem to have varying affinities to structured, unstructured or truncated mRNAs, with S1 playing the major role of recruiting the mRNA into the right position on the 30S subunit (Milon and Rodnina, 2012). mRNAs that contain a SD sequence are then stabilized through binding to the aSD motif. This stabilization alongside the general properties of the TIR help placing the start codon in the P site ready to interact with the initiator tRNA (Milon and Rodnina, 2012). Correct start codon recognition is mediated by the initiation factors (Milon and Rodnina, 2012). Once the initiator tRNA has been base paired with the start codon, the 30 PIC undergoes conformational rearrangements to become the 30S initiation complex (IC), characterized by a rotated conformation of the 30S subunits head relative to the body that leads to stabilization of IF1, IF2, mRNA and tRNA but destabilization of IF3 (Hussain *et al.*, 2016; Julian et al., 2011; Milon *et al.*, 2010; Milon et al., 2008). The 50S subunit can then join to the 30S IC, mediated by interactions between IF2 and L12 (Huang et al., 2010; Milon and Rodnina, 2012). GTP hydrolysis by IF2 leads to stabilization of the initiator tRNA in the P site (Goyal *et al.*, 2015; Rodnina, 2018). IF3 dissociates or is displaced to a non-canonical binding site on the 50S subunit (Goyal *et al.*, 2017). Conformational changes and release of the inorganic phosphate (Pi) loosen the interactions of IF2 and the initiator tRNA (Rodnina, 2018). Dissociation of IF1 and IF2 lead to conformational changes that allow formation of intersubunit bridges between the 30S and the 50S subunit to form the mature 70S IC (Milon and Rodnina, 2012; Rodnina, 2018).

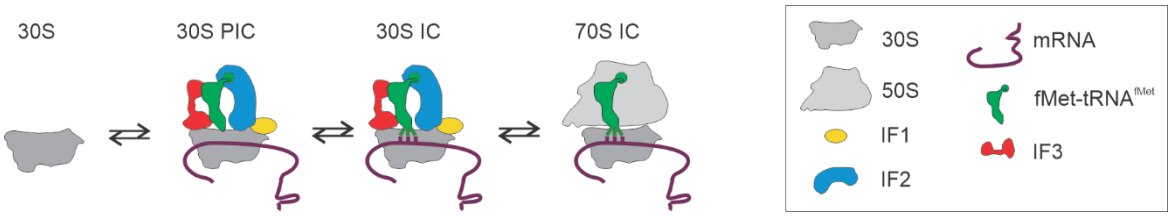

Figure 3. Initiation. Initiation: IF1 (yellow), IF2 (blue), IF3 (red), fMet-tRNA^{fMet} (green) bind to the 30S subunit (grey) with mRNA (purple). fMet-tRNA^{fMet} recognizes the start codon. The 50S subunit (light grey) binds and IF1, IF2 and IF3 are released. Modified from (Milon and Rodnina, 2012).

Elongation is a cyclic process that features the two most fundamental ribosome functions: decoding and peptide bond formation. The decoding step ensues the correct interpretation of the mRNA's information. The ribosome selects an aa-tRNA matching the codon on the mRNA in the decoding center, followed by peptide bond formation in the PTC (Fig. 4). Translocation, the movement of the mRNA and tRNAs, completes a round of elongation. Various factors and mechanistic checkpoints ensure directionality of this process (Rodnina, 2018).

The central elongation factor for the decoding step is the translational GTPase elongation factor Tu (EF-Tu). EF-Tu forms a ternary complex (TC) with an aa-tRNA and GTP. The TC delivery to the ribosome is mediated by the L12/L7 stalk (Diaconu et al., 2005; Kothe et al., 2004). For the decoding step, the 70S ribosome complex with mRNA and P-site-bound peptidyl- or initiator-tRNA (70S IC) requires an empty A site and resides in an open conformation. The anticodon of the aa-tRNA is stepwise brought into proximity with the corresponding mRNA codon residing in the A site. Establishment of cognate codon-anticodon base pairing leads to activation of EF-Tu's GTPase activity. This acts as a fist checkpoint where near-cognate base pairing might be accepted under circumstances, but incorrect base pairing usually leads to ejection of the TC. GTP hydrolysis and subsequent Pi release, lead to a conformation change of EF-Tu to the GDP-bound form. EF-Tu-GDP loses its tRNA affinity and can dissociate from the ribosome. Accommodation of the aa-tRNA in the A site serves as a second checkpoint. Cognate aa-tRNAs undergo structural rearrangements and accommodate with its 3'-end into the PTC. Closing of the ribosome leads to stabilization of correct aa-tRNAs whereas incorrect ones are released (Rodnina, 2018; Rodnina et al., 2017).

Close proximity of the P-site-bound peptidyl-tRNA and the A-site-bound aa-tRNA leads to peptide bond formation in the PTC. The nascent peptide chain from the P-site tRNA is transferred to the

A-site tRNA. Unlike classic enzymes, the reaction is not directly carried out but accelerated by the ribosome. The PTC, consisting of rRNA, provides a shielded reaction environment (Rodnina, 2013; 2018; Rodnina et al., 2007).

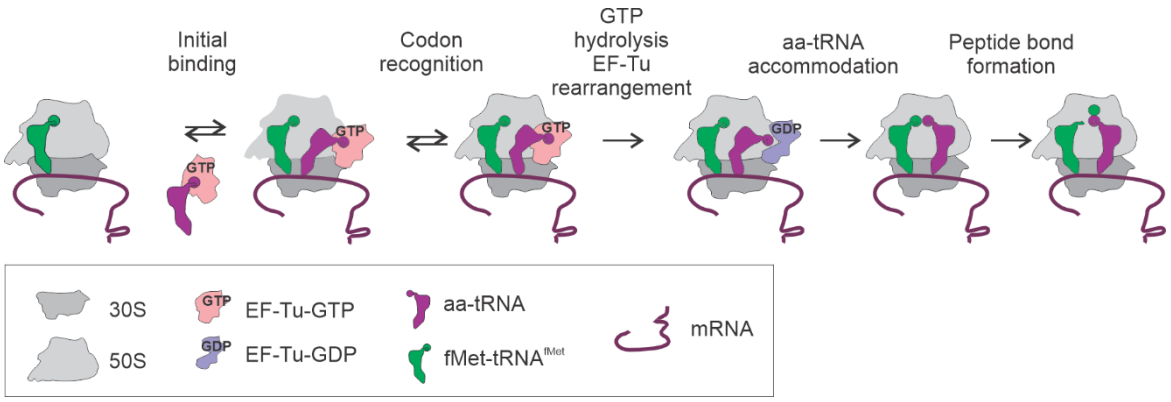

Figure 4. Elongation. aa-tRNA in complex with EF-Tu-GTP complex (purple and pink, respectively) binds to the ribosome and recognizes the codon through the tRNA's anticodon. Correct pairing results in GTP hydrolysis and EF-Tu rearrangement. EF-Tu-GDP (purple) is released, and the peptide bond forms inside the PTC. Modified from (Maracci and Rodnina, 2016).

To enable the next round of elongation, the ribosome needs to free the A site by moving the A-site-bound peptidyl-tRNA to the P site and thus the P-site bound deacylated tRNA to the E site, and correspondingly translocate the mRNA to present the next codon in the A site (Fig. 5). This movement is mediated by the translational GTPase elongation factor G (EF-G) (Maracci and Rodnina, 2016; Rodnina et al., 2019). EF-G-GTP binds to the pre-translocation complex mediated by the L12/L7 stalk (Diaconu *et al.*, 2005). Rotation of the 30S subunit head and body to the rotated state enables the tRNAs to adopt hybrid P/E and A/P states. After GTP hydrolysis, the body rotates backward, but the head stays in a forward swiveled conformation, enabling the tRNAs to adopt chimeric states where they retain their 50S and mRNA binding sites but the 30S subunit repositions (Adio et al., 2015; Belardinelli et al., 2016a; Belardinelli et al., 2016b). Alongside the following backwards rotation of the head, the tRNAs adopt their new positions in the classic P and E sites. The E-site-bound deacylated tRNA loses codon-anticodon interaction, ultimately leading to its release from the ribosome mediated by the L1 stalk (Belardinelli *et al.*, 2016a; Rodnina, 2018). Pi release leads to conformational change of EF-G promoting directionality to the entire translocation

process (Rodnina *et al.*, 2019). EF-G dissociation finally empties the A site for the next decoding step (Belardinelli *et al.*, 2016a; Rodnina, 2018).

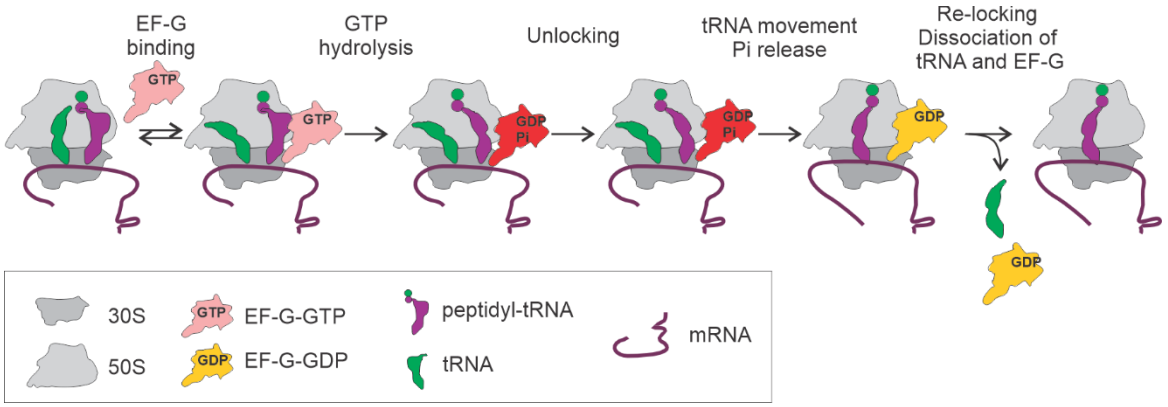

Figure 5. Translocation. EF-G-GTP (pink) binds to the ribosome complex. GTP hydrolysis and 30S subunit unlocking (light green) results in translocation of the A-site peptidyl-tRNA (purple) to the P site. Deacylated P-site tRNA (green) is translocated to the E site and released as well as EF-G-GDP (yellow). Modified from (Rodnina and Wintermeyer, 2011).

Elongation usually ends when a stop codon is presented in the A site. The release factors RF1 and RF2 recognize the stop codon and facilitate peptide release from the ribosome (Fig. 6). The translational GTPase RF3 mediates the following release of RF1 or RF2 from the ribosome (Rodnina, 2018).

The stop codon UAG is recognized by RF1, UGA by RF2 and UAA by both. RF1 or RF2 bind to the A site of the ribosome and read the A-site codon. Binding promotes the ribosome to adopt the nonrotated state. Recognition of the correct codon enables positioning of the factors GGQ motif in the PTC. The GGQ motif catalyzes hydrolysis of the nascent peptide chain from the P-site tRNA. While RF3 is optional for the release of RF2 from the ribosome following peptide release, it is required for RF1. Binding of RF3-GTP to the ribosome induces fluctuations between the rotated and nonrotated state that destabilize RF1 leading to its dissociation. The ribosome then adopts the rotated state. Conformational changes upon GTP hydrolysis then allow the dissociation of RF3 (Adio et al., 2018; Rodnina, 2018).

Ribosome recycling is the final step of the translation cycle. After synthesis and release of the synthesized protein, the ribosome needs to be prepared for the next round of translation (Rodnina, 2018).

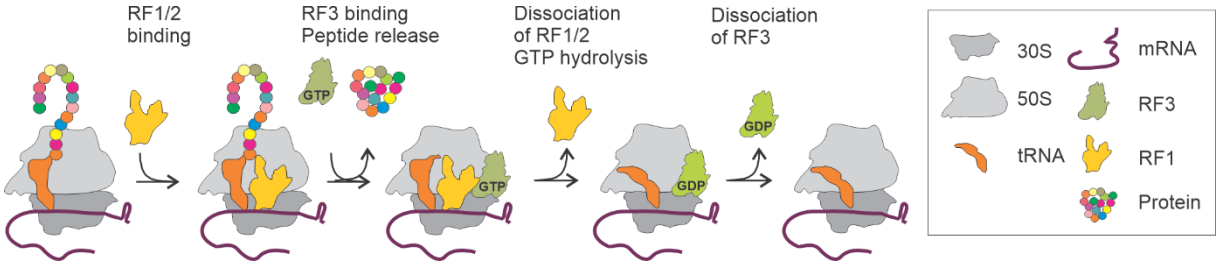

Figure 6. Termination. RF1 (yellow) binds to the ribosome containing the peptidyl-tRNA (orange with polypeptide) in the P site. RF3-GTP (green) binds to the complex and the protein is released. RF1 dissociates and RF3 dissociates after GTP hydrolysis. The PoTC remains to be recycled. Modified from (Adio *et al.*, 2018).

1.3 Ribosome Recycling

Termination of translation results in a ribosome complex that still contains the mRNA and a deacylated tRNA. In this post-termination complex (PoTC), the deacylated tRNA sits in the P site attached to the last codon on the ORF on the ribosome bound mRNA (Fig. 7). During recycling, the large and the small subunit dissociate and the mRNA and the deacylated tRNA are released. Recycling is carried out by the ribosome recycling factor (RRF), EF-G and IF3 (Rodnina, 2018).

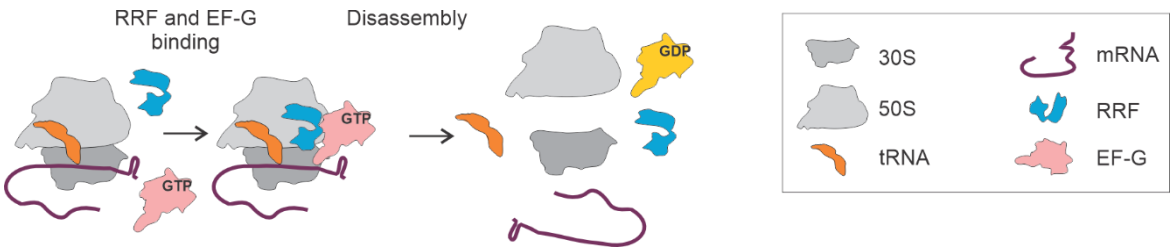

Figure 7. Recycling. RRF (blue) and EF-G-GTP (pink) bind to the PoTC harboring the mRNA and deacylated tRNA in the P site. This leads to GTP hydrolysis and complex disassembly. Modified from (Peske *et al.*, 2005).

1.3.1 Ribosome Recycling Factor (RRF)

RRF is a L-shaped protein with two domains. Domain I consists of three α-helices, the N-terminal helix H1 and the two C-terminal helices H5 and H6, in a bundle. Domain II consists of a β/α/β sandwich with helix H4 in addition to the two very small helices H2 and H3. Domain II has an overall rather globular shape and is located at the base of Domain I in a perpendicular orientation (Fig. 8A). The overall size and shape of RRF is very similar to that of a tRNA (Fig. 8B) (Selmer et al., 1999). Initially it was assumed that RRF binds to the ribosomal A site and is translocated like a tRNA (Selmer *et al.*, 1999) but later it was shown that RRF binds very differently compared to tRNAs (discussed below). The structural similarities of RRF and tRNA are best explained by their parallel evolution together with the ribosome. The shape likely is a necessity to fit into the ribosome where RRF can then fulfill its function. The combined action of RRF and EF-G cause the subunit splitting (Janosi et al., 1996).

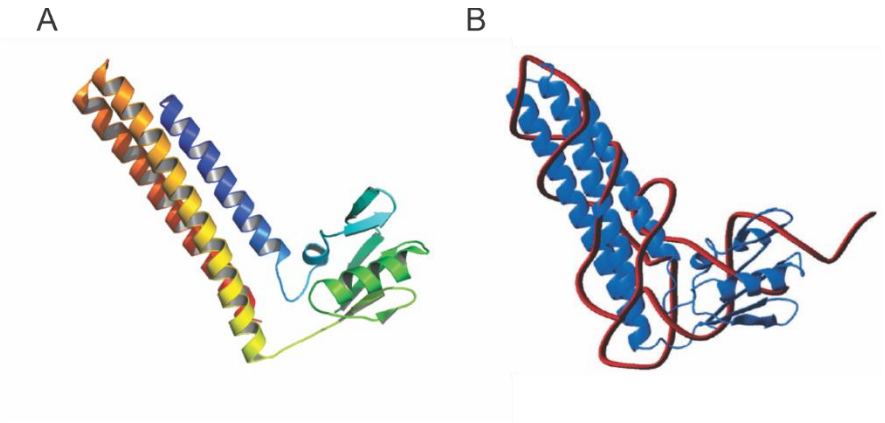

Figure 8. RRF. (A) Crystal structure of RRF from *Thermotoga maritima* at 2.55 Å resolution. Domain I consists of three α-helices (red to yellow and blue), domain II contains two small α-helices and a β-sheet (green and teal). Structure from PDB: 1DD5 (Selmer *et al.*, 1999) (B) Similar shape of RRF (blue) and a tRNA (red) (Selmer *et al.*, 1999).

1.3.2 Elongation Factor G (EF-G)

Besides its various roles during translocation, EF-G also enables the subunit splitting of the recycling step. EF-G has five domains (Fig. 9) (AEvarsson et al., 1994). Domain I is the G domain that binds GTP or GDP and is therefore the key domain of EF-Gs GTPase function (Cunha et al., 2013) that promotes translocation through GTP hydrolysis (Rodnina et al., 1997). Domain I and II can also be found in other translational GTPases such as EF-Tu or RF3. Through domain IV, EF-G carries out its various roles in the translation cycle, such as accelerating translocation (Savelsbergh et al., 2000) or reading frame maintenance (Peng et al., 2019). Inside the ribosome, domain IV points towards the A site to speed up translocation and help the ribosome to maintain the reading frame (Katunin et al., 2002; Peng *et al.*, 2019; Petrychenko et al., 2021). Conformational changes induced by GTP hydrolysis on EF-G leads to conformational changes in the ribosome enabling translocation (Adio *et al.*, 2015; Belardinelli *et al.*, 2016a). For recycling, EF-G binds to the PoTC subsequently to RRF (Dunkle et al., 2011). While GTP hydrolysis during translocation only accelerates the reaction (Katunin *et al.*, 2002; Peng *et al.*, 2019), during recycling it is a requirement to induce conformational changes that lead to subunit splitting (Fu et al., 2016; Karimi *et al.*, 1999; Savelsbergh et al., 2009).

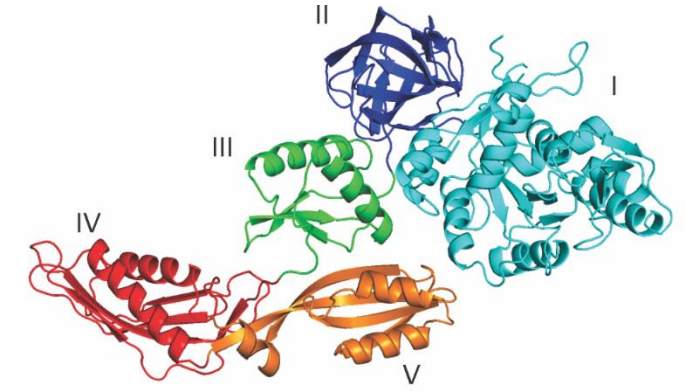

Figure 9. EF-G. EF-G with its five domains from PDB: 4V7D (Brilot et al., 2013).

1.3.3 Initiation Factor 3 (IF3)

IF3 connects recycling with the initiation on a new mRNA and closes the translation cycle. IF3 has two globular domains connected by a flexible linker region (Fig. 10) (Kycia et al., 1995; Moreau et al., 1997). During various stages of initiation, IF3 changes position and conformation on the 30S subunit (Hussain *et al.*, 2016). On an empty 30S subunit, the N-terminal domain binds near the platform of the 30S subunit while the C-terminal domain would position itself near the P site, interacting with the mRNA to scan for the correct start codon (Hussain *et al.*, 2016). The presence of an initiator tRNA on the correct start codon displaces the C-terminal domain and the N-terminal domain interacts with the tRNAs elbow (Hussain *et al.*, 2016). During both initiation and recycling, IF3 blocks subunit association (Dallas and Noller, 2001; Julian *et al.*, 2011). While during initiation this blocking function is dispersed upon start codon recognition with the help of the other initiation factors (Hussain *et al.*, 2016; MacDougall and Gonzalez, 2015), it promotes irreversibility to the recycling reaction (Hirokawa et al., 2005; Peske *et al.*, 2005).

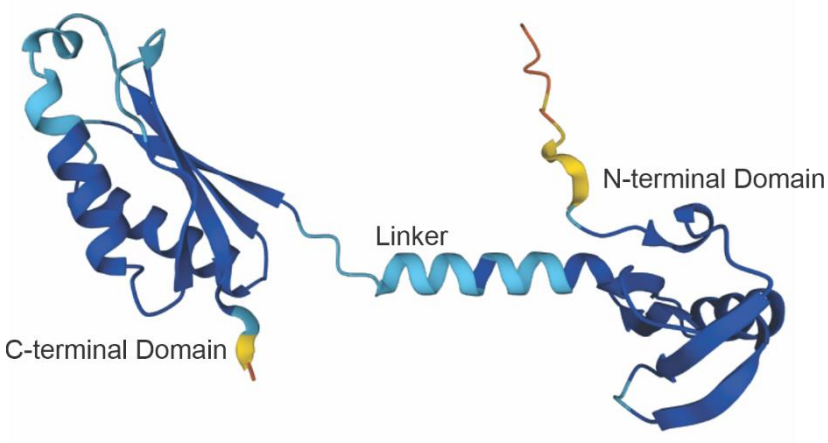

Figure 10. IF3. IF3 with its two domains and flexible linker. Structure prediction from Alphafold on UniProt entry: A0A5B9AIA3 (Jumper et al., 2021; Varadi et al., 2022).

1.3.4 Mechanism of Ribosome Recycling

After termination, the post-termination complex (PoTC) must be disassembled to free the ribosome for a new round of translation. This requires the release of mRNA and tRNA from the ribosome, as well as splitting of the subunits. The combined actions of RRF and EF-G cause subunit splitting (Karimi *et al.*, 1999). After subunit splitting IF3 promotes directionality through prevention of subunit reassociation, priming the ribosome for the next round of translation (Hirokawa *et al.*, 2005). Requirements and mechanism of tRNA and mRNA release are controversially discussed (Rodnina, 2018).

To separate the ribosomal subunits, RRF enters the PoTC through the A site (Fujiwara et al., 2001; Gao et al., 2005). Binding of RRF to the ribosome stabilizes the 30S subunit in a fully rotated state with the P-site tRNA adopting to the hybrid P/E binding state (Fig. 11A) (Dunkle *et al.*, 2011). Ribosome bound RRF occupies an area entirely inside the 50S subunit but unlike tRNAs not on the 30s subunit. Its domain I spans from the P site through the A site overlapping with the binding sites of the CCA-ends of A- and P-site tRNAs while a significant part of RRFs domain II is located outside of the A site (Fig. 11B) (Agrawal et al., 2004). There, domain II and parts of domain I overlap with the canonical binding site of EF-G (Agrawal *et al.*, 2004). Binding of EF-G to the PoTC-RRF-complex leads to GTP hydrolysis and subsequent splitting of the ribosomal subunits (Borg et al., 2016; Fu *et al.*, 2016; Hirokawa et al., 2008; Hirokawa *et al.*, 2005; Karimi *et al.*, 1999; Pavlov et al., 2008; Peske *et al.*, 2005; Prabhakar et al., 2017; Savelsbergh *et al.*, 2009; Zavialov et al., 2005). While earlier studies suggested a tRNA-like translocation movement of RRF through the ribosome (Hirokawa et al., 2002b), it was shown that the conformational changes of EF-G induced by GTP hydrolysis push RRF against ribosomal inter-subunit bridges (Fig. 11C) leading to their disruption and thereby causing the dissociation of the 30S and the 50S subunit (Agrawal *et al.*, 2004; Barat et al., 2007; Gao et al., 2007; Gao *et al.*, 2005; Pai et al., 2008; Yokoyama et al., 2012). While GTP hydrolysis only accelerates translocation, it is crucial for the action of EF-G in recycling (Fujiwara et al., 2004; Savelsbergh *et al.*, 2009). After splitting of the subunits, IF3 can bind to the 30S subunit and prevent subunit re-association (Hirokawa *et al.*, 2005) and RRF and EF-G dissociate from the 50S subunit (Barat *et al.*, 2007; Fu *et al.*, 2016; Peske *et al.*, 2005).

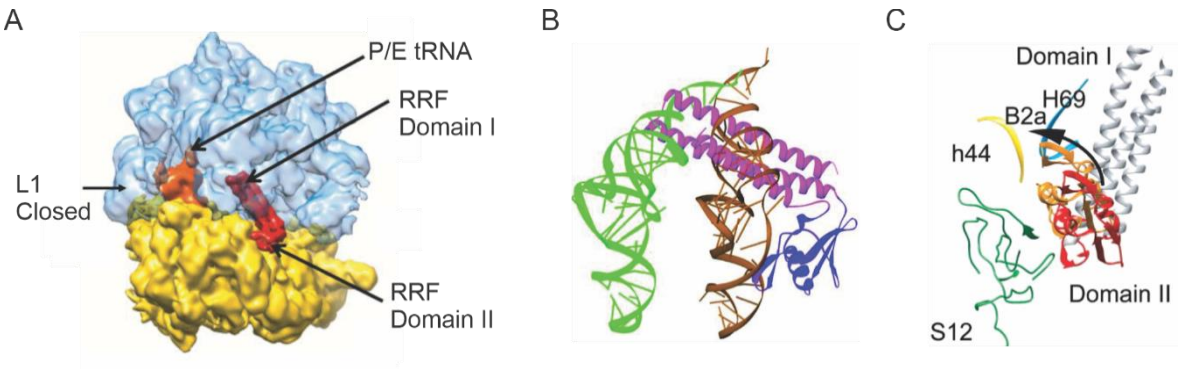

Figure 11. Key structure intermediates during recycling. (A) Cryo-EM structure of the bacterial post-termination complex (PoTC) in closed conformation with the deacylated tRNA (orange) in the P/E conformation and bound RRF (red) (Fu *et al.*, 2016). (B) On the ribosome (not shown) the binding site of RRF (purple and pink) overlaps with the binding sites of the A-site tRNA (orange) and the P-site tRNA (green) (Agrawal *et al.*, 2004). (C) Visualization of the movement of RRFs domain II (red and orange) against the ribosomal intersubunit bridge B2a between helix H69 and helix H44(Fu *et al.*, 2016).

The dissociation of mRNA and tRNA is still controversially discussed and different orders of events have been proposed. The differences between the proposed models may reflect variations in the experimental setups and model systems, such as the use of unnatural translation termination contexts and low temporal resolution of experiments. Polysome breakdown assays, where ribosomes bound to small fragments of RNase digested mRNAs were used, as well as structural studies, suggested that the tRNA might be pushed out of the ribosome by the action of EF-G and RRF before subunit splitting happens (Fig. 11A) (Agrawal *et al.*, 2004; Barat *et al.*, 2007; Hirokawa et al., 2006; Hirokawa *et al.*, 2008; Hirokawa et al., 2002a; Hirokawa *et al.*, 2002b; Hirokawa *et al.*, 2005; Iwakura et al., 2017; Janosi *et al.*, 1996; Kaji et al., 2001; Kiel et al., 2007; Selmer *et al.*, 1999). tRNA release might be followed by rapid release of mRNAs (or mRNA fragments) (Hirokawa *et al.*, 2002b; Iwakura *et al.*, 2017). Contrary to those findings, other structural studies and kinetic experiments with PoTCs containing short synthetic mRNAs that commonly feature a 5'-UTR with an SD sequence, suggest that the tRNA and mRNA remain bound to the 30S subunit after subunit splitting and their release might be facilitated by IF3 (Fig. 11B) (Borg *et al.*, 2016; Chen et al., 2017; Fu *et al.*, 2016; Fujiwara *et al.*, 2001; Fujiwara *et al.*, 2004; Karimi *et al.*, 1999; Pavlov *et al.*, 2008; Peske *et al.*, 2005; Prabhakar *et al.*, 2017; Savelsbergh *et al.*, 2009; Zavialov *et al.*, 2005). Kinetic experiments with short synthetic mRNAs that do not have a SD Sequence hint to rapid mRNA release followed by tRNA release and significantly slower subunit splitting (Fig. 11C) (Chen *et al.*, 2017).

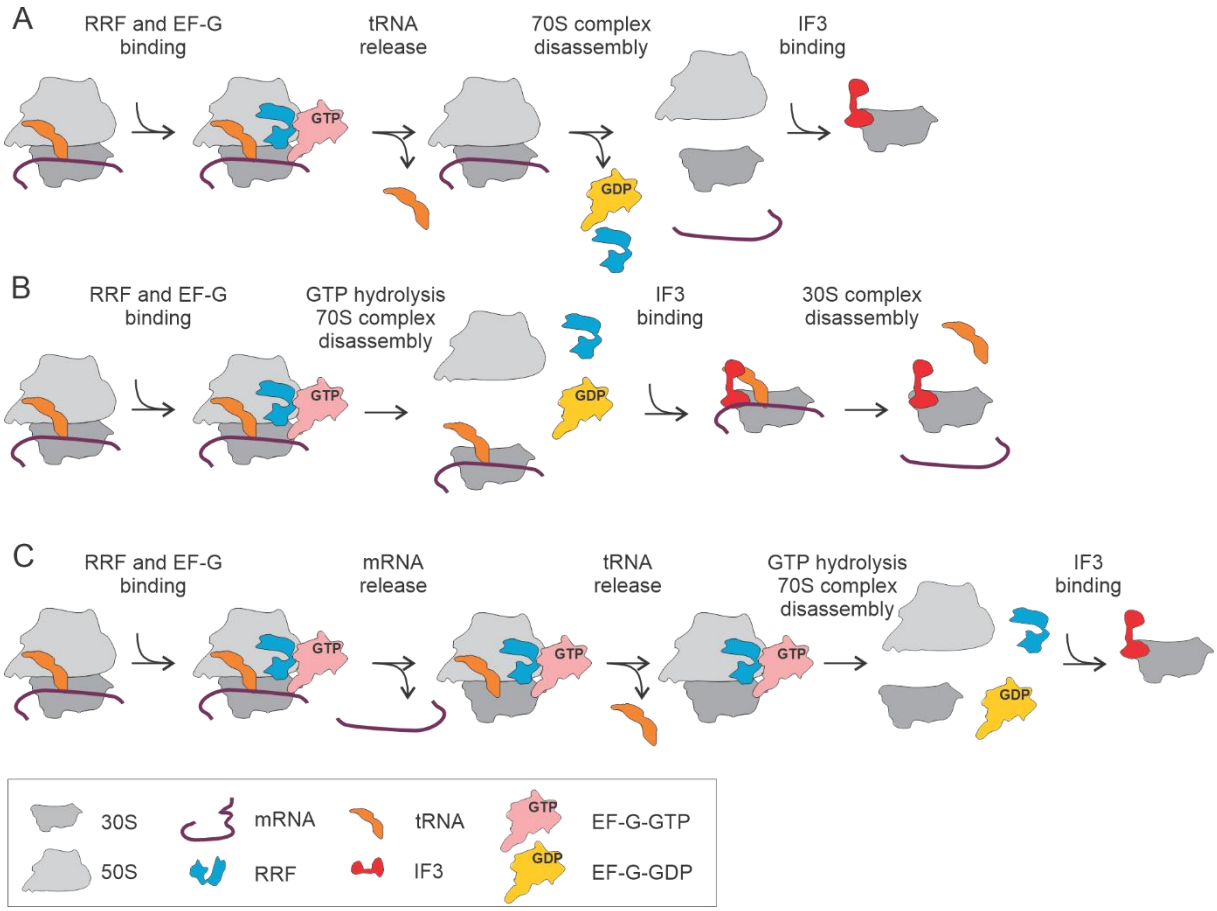

Figure 12. Different models of recycling. Different and in parts conflicting models of recycling based on studies with different model mRNAs and experimental approaches have been suggested. (A) Model based on low time resolution experiments with small mRNA fragments from polysome breakdown assays. RRF and EF-G binding to the PoTC results in fast tRNA release. Subunit splitting and mRNA release happen after RRF and EF-G-GDP are released. In the end IF3 binds to the empty 30S subunit (Iwakura *et al.*, 2017). (B) Model based on rapid kinetic experiments with small mRNAs containing a SD sequence. GTP hydrolysis induced structural rearrangements result in subunit splitting. RRF and EF-G-GDP dissociate from the 50S subunit. tRNA and mRNA stay attached to the 30S subunit. IF3 binds, promoting tRNA and mRNA dissociate from the 30S subunit (Chen *et al.*, 2017; Peske *et al.*, 2005) (C) Model based on fast kinetic experiments with small mRNAs that do not contain a SD sequence. RRF and EF-G-GTP binding to the PoTC results in fast release of the mRNA. Then the tRNA is released. GTP hydrolysis and subunit splitting happen afterwards. In the end IF3 binds to the 30S subunit (Chen *et al.*, 2017).

1.4 Prokaryotic mRNAs

The controversy regarding the order of events in recycling likely results from the use of various non-native mRNAs with unnatural translation termination contexts. The rate of mRNA release may be highly context dependent. Structure and sequence of mRNA play a major role in many ribosome-related processes. Structure elements, such as hairpins, are together with an UGA stop codon necessary for incorporation of selenocysteine (Rodnina *et al.*, 2017), or modulate frameshifting in viruses (Korniy et al., 2019). So far, the influence of structures in proximity to the ribosome during recycling have never been investigated. Bacterial mRNAs are produced by the transcription machinery transcribing a designated genome sequence. Prokaryotic mRNAs can consist of one or more open reading frames (ORFs). An ORF contains the genetic information for the ribosome to synthesize a protein. mRNAs also feature untranslated but functionally important regions flanking the ORF (Kushner, 2018). Appearance of prokaryotic mRNAs is reliant on the specific genome organization. The bacterial genome is organized in operons. Those are single genes or clusters of multiple genes, often related in function, that feature a transcription start site (TSS) often accompanied by sequences for transcription regulation upstream of the gene/genes and end with a downstream transcription termination site (TTS). In general, transcription of single gene operons leads to single-gene mRNAs (monocistronic) and multi gene operons lead to multi-gene mRNAs (polycistronic). Operons can feature multiple TSS and TTS that allow the creation of multiple different mRNAs (Conway et al., 2014; Yan et al., 2018). Internal TSS and TTS of multigene operons are enabling the production of mRNAs containing varying sets of ORFs (Yan *et al.*, 2018). Up and down regulation of TSS and TTS to shape the transcriptome is one of the major ways of prokaryotic gene regulation (Conway *et al.*, 2014).

TSS are accompanied by promoter sequences that recruit the RNA polymerase. Once the RNA polymerase is recruited to the promotor DNA, typically with the help of transcription factors, it creates a transcription bubble by separating the DNA double strands. The RNA polymerase then proceeds on the antisense strand using the DNA to copy it to synthesize an mRNA from 5’ to 3’ direction. mRNA transcription usually halts when a TTS is encountered. Transcription termination is achieved either by the action of the transcription termination factor Rho, or by the RNA polymerase encountering an intrinsic Rho-independent termination signal (Kushner, 2018).

Rho-dependent transcription termination happens when Rho binds to a pyrimidine-rich rho utilization (*rut*) site on the newly synthesized mRNA (Mitra et al., 2017). Rho then travels on the mRNA towards the RNA polymerase (Mitra *et al.*, 2017). Meeting of the two complexes will then induce transcription to stop, leading to release of mRNA, Rho and RNA polymerase from the DNA

(Mitra *et al.*, 2017; Peters et al., 2011). However, Rho-dependent termination is very situational. In prokaryotes, transcription and translation can happen simultaneous. As soon as the start of an mRNA is synthesized, ribosomes can initiate on the 5'-end and start translation. This leads to occupation by ribosomes on mRNAs while those are still being synthesized. Under optimal growth conditions, ribosomal occupation will block Rho binding and processing of the nascent mRNA (Mitra *et al.*, 2017). It is assumed, that Rho plays a more significant role under stress conditions by blocking dispensable downstream translation via early translation termination of lengthy operons. Further functions of Rho are the rescue of RNA polymerases from dysfunctional mRNAs, regulation of sRNA functions (small RNAs that bind to proteins or mRNAs often with regulatory function), controlling of riboswitch actions and more (Mitra *et al.*, 2017; Peters *et al.*, 2011).

Rho-independent transcription termination through intrinsic terminators is the default mechanism of termination under optimal conditions. Intrinsic terminator sequence consists of a GC rich dyad repeat followed by a stretch of T nucleotides (nts) in the coding DNA strand (Peters *et al.*, 2011; Platt, 1981; Wu and Platt, 1978). During transcription of this region, the RNA will fold into a GC-rich hairpin followed by several U nucleotides (Kushner, 2018; Peters *et al.*, 2011; Platt, 1981; Wu and Platt, 1978). Formation of this hairpin weakens the cohesion of the RNA:DNA hybrid as well as it inflicts conformational changes within the RNA polymerase, ultimately leading to the dissociation of mRNA and RNA polymerase from the DNA (Kushner, 2018; Peters *et al.*, 2011).

Bacterial mRNAs feature not only the ORFs for peptide synthesis, but also a 5' untranslated region (UTR) and a 3'-UTR (Fig. 12) (Kushner, 2018). The 5'-UTR is defined by the transcription start at the TSS and reaches from there towards the start codon of the ORF (Kushner, 2018). The 5'-UTR features sequences for the recruitment of ribosomes onto the mRNA (ribosome binding site, RBS) and sequences that guide the ribosome onto the start codon, such as the Shine-Dalgarno (SD) sequence (Kushner, 2018). The 3'-UTR starts after the stop codon of the ORF. In case of an intrinsic termination of the mRNA at the TTS, the 3'-UTR ends with the transcription terminator hairpin structure (Kushner, 2018; Peters *et al.*, 2011). Like all RNA molecules, mRNAs can form various secondary and tertiary structures. Accumulation of hairpins in the 5'-UTR or 3'-UTR can have regulatory reasons (Kushner, 2018). For example, riboswitches are aptameric 5'-UTR regions that switch conformation upon binding of a certain small molecule and thus masking the RBS to inhibit translation (Kushner, 2018). Most structures such as extensively structured 5'-UTRs or REP-elements (large hairpin structures from repetitive extragenic palindromes) however, are believed to simply improve mRNA stability by granting protection from endonucleases (Emory et al., 1992; Kushner, 2018; Newbury et al., 1987).

Prokaryotic mRNAs are often polycistronic (Kushner, 2018). The multiple ORFs of a polycistronic mRNA can overlap, but are usually separated by an intercistronic spacer region (Huvet and Stumpf, 2014; Kushner, 2018; Salgado et al., 2000). RBS and SD sequences can be found in the intercistronic regions. When the space is limited and the ORFs are very close to each other or even overlap, SD sequences can also be found inside a previous ORF (Kushner, 2018). In general, bacterial genomes are very compressed (Conway *et al.*, 2014; Salgado *et al.*, 2000; Yan *et al.*, 2018). Operons on one DNA strand often overlap with operons on the other DNA strand (Conway *et al.*, 2014; Yan *et al.*, 2018). Transcription terminators work bidirectionally in some cases while they have to be attenuated in other cases to prevent preliminary termination (Kushner, 2018). The overall complexity makes computational prediction of operons very challenging. While promotor regions can be reliably identified, the effectiveness in transcription termination of an individual hairpin structure found in the 3'-region cannot be evaluated easily (Yan *et al.*, 2018). RNA sequencing achieves better mapping of the bacterial transcriptome in usable detail and even allow a quantitative analysis (Conway *et al.*, 2014; Creecy and Conway, 2015; Yan *et al.*, 2018). 5'-Ends of mRNAs can be enriched allowing precise localization of TSS (Creecy and Conway, 2015). 3'-Ends of mRNAs cannot be studied in such detail and thus have been widely ignored in bioinformatic publications (Creecy and Conway, 2015; Peters *et al.*, 2011). Intrinsic transcription termination is typically not fully efficient (Creecy and Conway, 2015; Peters *et al.*, 2011; Yan *et al.*, 2018). Transcription read-through can happen and is often functional (Yan *et al.*, 2018). Even with successful transcription termination, the exact position at which the mRNA ends varies (Creecy and Conway, 2015). On top of that, the 3'-end of an mRNA is the primary site of exonuclease-dependent degradation (Creecy and Conway, 2015; Kushner, 2018). Still, RNA sequencing can give very valuable insights into the bacterial transcriptome (Conway *et al.*, 2014; Creecy and Conway, 2015; Yan *et al.*, 2018).

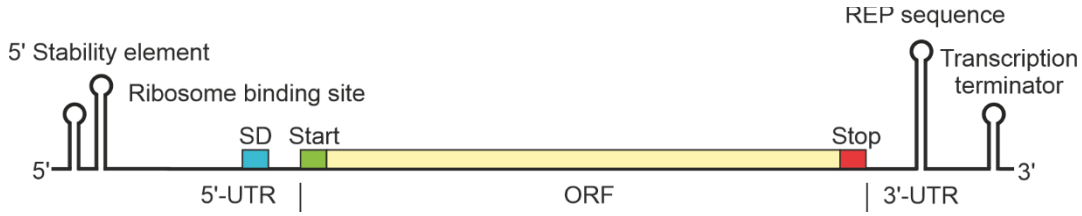

Figure 13. mRNA. The 5'-UTR of bacterial mRNAs often features several stem-loop structures that serve as a stability element. Before the translation start featuring the start codon AUG, a ribosomal binding site (RBS) which entails a Shine-Dalgarno (SD) sequence can be found in many mRNAs in *E. coli*. The translation stop codon acts as a termination signal and is followed by the 3'-UTR. The 3'-UTR often contains stem-loop structures derived from transcription termination and sometimes additional repetitive extragenic palindromic (REP) sequences (Kushner, 2018).

1.5 Differences Throughout the Domains of Life

The rRNA core of the ribosome featuring the decoding center, peptidyl transferase center, tRNA binding sites and the peptide exit tunnel is universally conserved throughout all domains of life (Ben-Shem et al., 2011; Klinge et al., 2011; Rabl et al., 2011; Spahn et al., 2001). The solvent-exposed face of ribosomes from the three domains of life, however, feature differences that have been added throughout evolution (Bowman et al., 2020).

The outer rRNA of the archaeal ribosome resembles the prokaryotic one, but in the eukaryotic ribosome so called expansion segments are inserted into the eukaryotic rRNA that have many variations throughout different eukaryotic species (Bowman *et al.*, 2020; Melnikov *et al.*, 2012). This contributes to the eukaryotic 80S ribosome with a mass of ca. 4.3 MDa being considerable larger than the 2.3 MDa bacterial 70S ribosome (Melnikov *et al.*, 2012). The eukaryotic ribosome consists of the large 60S and the small 40S subunit (Klinge *et al.*, 2011; Rabl *et al.*, 2011) while the archaeal ribosome also has a 50S and 30S subunit (Bowman *et al.*, 2020). The most fundamental ribosomal proteins, like L23, L29 and L24 on the peptide exit tunnel, L3, L4 and L5 around the mRNA entry site or the L1 stalk (Ben-Shem *et al.*, 2011; Klinge *et al.*, 2011) are highly conserved throughout all domains of life. Eukaryotic and archaeal ribosomes contain a larger and very different set of common ribosomal proteins (Bowman *et al.*, 2020; Melnikov *et al.*, 2012). In eukaryotes, additional ribosomes exist in the mitochondria and chloroplasts. Chloroplast ribosomes do not diverge much from other bacterial ribosomes found in cyanobacteria (Bieri et al., 2017). The mitochondrial ribosome (mitoribosome) also stems from a bacterial ancestor but has evolved to be optimized for the synthesis of the few mitochondrial proteins, among them many membrane proteins (Greber and Ban, 2016). The mammalian 55S mitoribosome consists of a small 28S and a large 39S subunit. The mitoribosome is has an unusual ratio of lower rRNA and higher protein content. Throughout evolution, the rRNA core has been reduced and numerous ribosomal proteins have been added, especially in the fungal and metazoan lines (Greber and Ban, 2016).

The ribosomes core function, protein translation, however, remains unsurprisingly conserved (Weisser and Ban, 2019). Most steps in eukaryotic translation are very similar to their prokaryotic counterparts and are carried out by homologous translation factors, but there are also fundamental differences. In general, eukaryotes have a larger number of translation factors of which many consist of different subunits. While elongation is relatively similar, especially the initiation is designed to fit to the needs of eukaryotic mRNAs. Eukaryotic mRNAs are usually monocistronic and only in rare cases contain a small uORF upstream of the main gene for regulatory purposes. In Eukaryotes, the mRNA is transcribed in the nucleus while translation is carried out in the cytosol.

The eukaryotic gene transcript undergoes significantly posttranscriptional modifications before the matured mRNA will be translated. Splicing removes untranslated introns. Polyadenylation adds a tail of adenines to the 3'-UTR. The often structured 5'-UTR is modified with a 7-methylguanosin cap (Leppek et al., 2018). The mRNAs are then transported into the cytosol, simultaneous transcription and translation as in prokaryotes is therefore not possible. Eukaryotic mRNAs appear circularized through the connection of the 5' cap binding initiation factor eIF4F with the poly-A-binding protein PABP on the 3' end (Wells et al., 1998). Eukaryotic initiation factors then mediate the interaction of the 40S subunit with the mRNA leading to the joining of the 60S subunit upon start codon recognition.

Archaeal translation initiation appears to be a mixture of both pro- and eukaryotes (Schmitt et al., 2020). Archaeal mRNAs closely resemble the prokaryotic ones albeit appear to have slightly shorter 5'-UTRs (Schmitt *et al.*, 2020). Like in prokaryotes, interaction with the ribosome relies on the recognition of a SD sequence while the aSD sequence is missing from the eukaryotic ribosome. The involved proteins however are near identical to the eukaryotic set of translation factors. Some factors like eIF3 or eIF5 are not necessary due to the simpler and non-processed mRNA (Schmitt *et al.*, 2020).

There are also significant differences regarding release and recycling. Unlike in bacteria, eukaryotes have only one class I release factor, eRF1, that recognizes all three stop codons (Brown et al., 2015). eRF1 forms a ternary complex with the GTPase eRF3 and GTP that can bind to the ribosome (Alkalaeva et al., 2006). When a stop codon is recognized by eRF1, it changes its conformation to induce GTPase activity of eRF3 (Brown *et al.*, 2015; Preis et al., 2014). GTP hydrolysis leads to the release of eRF3-GDP from the ribosome while eRF1 remains bound (Jackson et al., 2012). Termination and recycling are coupled in eukaryotes as the ATPase ABCE1 contributes to both, peptide release and subunit splitting (Pisarev et al., 2010). ABCE1 binds to the ribosome once eRF3 has dissociated and it stimulates peptide release activity of eRF1 (Pisarev *et al.*, 2010; Weisser and Ban, 2019). ATP hydrolysis of ABCE1 causes conformational changes in its RNA-binding iron sulfur cluster domain that lead to subunit splitting and subsequent dissociation of ABCE1 and eRF1 (Heuer et al., 2017; Pisarev *et al.*, 2010; Weisser and Ban, 2019). After subunit splitting the 40S subunit stays on the mRNA with a deacylated tRNA bound to the P site. The initiation factors eIF1, eIF1A and eIF3 then bind to the 40S subunit to prevent subunit reassociation (Jackson *et al.*, 2012; Rabl *et al.*, 2011; Weisser and Ban, 2019). eIF1 promotes tRNA release and eIF3, especially subunit eIF3j, mediates mRNA release by binding to the 40S subunit with negative cooperativity to mRNA (Fraser et al., 2007). The 40S subunit can then start a new round of translation. This mechanism of coupled

peptide release and recycling dependent on ABCE1 is shared among eukaryotes and archaea (Nurenberg and Tampe, 2013).

1.6 Scope of Thesis

Aim of this thesis is to study the mechanism and the order of the release of a native mRNA from the ribosome and the splitting of the ribosome subunits during prokaryotic ribosome recycling in a physiological termination and recycling situation. To achieve this goal, it was necessary to identify a natural mRNA as a model mRNA and to develop new fluorescence assays and labeling strategies for fast kinetic and single molecule studies.

A detailed analysis of the *E. coli* transcriptome was performed to characterize the native termination context in *E. coli* mRNA. As a representative model mRNA the natural mRNA of the major outer membrane prolipoprotein Lpp was chosen (Nakamura and Inouye, 1979). To study the mRNA release, the mRNA was labeled at the 3'-end and a FRET partner position was introduced at the 30S subunit. For this purpose, a recently published bioconjugation method utilizing the lipoic acid ligase $LplA^{W37V}$ was used to site-specifically introduce a fluorophore to the 30S subunit. Significant adaptions had to be made to the original protocol (Baalmann et al., 2018) to enable its use for ribosome labeling. After step assignment of the acceptor fluorescence signal from the mRNA-S3-FRET pair measured in the stopped-flow apparatus during elongation, release and recycling, the mRNA release phase was compared to the subunit splitting measured via light scattering. Mechanistic insights were also gained by comparison to lpp variants with truncated 3'-UTR. While experiments using the stopped-flow technique show the combined signal from the bulk of the sample, single molecule TIRF microscopy allows to observe mRNA release from the ribosome and subunit splitting on single ribosomes. In conclusion, the results explain the partially contradicting models of previous studies. Further, this study contributes towards integrating mRNA release into a summarizing model of prokaryotic ribosome recycling.

2 Materials and Methods

2.1 Chemicals

Chemicals were purchased from Sigma-Aldrich (Steinheim, Germany), Roche Diagnostics (Mannheim, Germany), Merck (Darmstadt, Germany), Carl Roth (Karlsruhe, Germany) and Serva (Heidelberg, Germany), unless stated otherwise. GTP and DNase I was from Jena Bioscience (Jena, Germany), dNTP and Color Prestained Protein Standard was from NEB (Frankfurt, Germany), DNA SmartLadder was from Eurogentec (Seraing, Belgium).

Kits for plasmid DNA purification, NucleoSpin® Gel and PCR Clean-up kits were from Macherey-Nagel (Düren, Germany). Nitrocellulose and cellulose acetate filters and syringe filters were from Sartorius Biolab (Göttingen, Germany). DNA oligonucleotides were from IDT (Leuven, Belgium) and from Eurofins Genomics (Ebersberg, Germany). Cloning Enzymes were from New England Biolabs (Massachusetts, USA). Radioactive amino acids were from Hartmann Analytic (Braunschweig, Germany) and PerkinElmar (Massachusetts, USA). Scintillation fluids Ultima Gold™ XR and Quickzint 361 were purchased from PerkinElmar (Massachusetts, USA) and Zinsser analytic (Frankfurt, Germany), respectively. Glass coverslips and objective slides were from Menzel-Gläser (Braunschweig, Germany). Preparative columns were from GE Healthcare (Chicago, USA).

2.2 Fluorophores

Name	**max. Excitation, nm**	**max. Emission, nm**	**Extinction coefficient, ε / L · mol^{-1} · cm^{-1}**	**Supplier**
ATTO488-Me-Tetrazine	500	520	90 000	ATTO-TEC
ATTO647N-hydrazide	646	664	150 000	ATTO-TEC
Cy3-hydrazide	555	570	150 000	Lumiprobe
Sulfo-Cy3-Me-Tetrazine	548	563	162 000	Lumiprobe
Sulfo-Cy5-Me-Tetrazine	646	662	271 000	Lumiprobe
BODIPY-FL-NHS-Ester	503	509	92 000	Thermo Fischer Scientific
Cy3-maleimide	555	570	150 000	Cytiva
Cy5-maleimide	646	662	271 000	Cytiva

2.3 Buffer

Buffer	Content
2x Translation gel sample buffer	100 mM Tris/HCl, pH 6.8 280 mM 2-mercaptoethanol 24% (w/v) glycerol 10% SDS (w/v)
4x Protein sample buffer	200 mM Tris/HCl, pH 6.8 8% SDS (w/v) 40% glycerol (v/v) 0.4% bromophenol (w/v) 400 mM 2-mercaptoethanol
DNA extraction buffer	10 mM Tris/HCl 1 mM EDTA 0.1% Triton x 100
$HAKM_X$	50 mM HEPES/KOH, pH 7.5 70 mM NH_4Cl 30 mM KCl X mM $MgCl_2$
HKM HiFi	50 mM HEPES/KOH, pH 7.5 100 mM KCl 3.5 mM $MgCl_2$ 8 mM putrescine 0.5 mM spermidine
HKM_X	50 mM HEPES/KOH, pH 7.5 100 mM KCl X mM $MgCl_2$
Isotherm buffer	100 mM Tris/HCl, pH 7.5 10 mM $MgCl_2$ 10 mM DTT 25% (w/v) PEG-8000 1 mM NAD
LB	1% NaCl (w/v) 1% tryptone (w/v) 0.5% yeast extract pH 7.0 (HCl/NaOH)
LplA purification buffer	20 mM Tris/HCl, pH 8.0 300 mM NaCl 5 mM 2-mercaptoethanol 15% glycerol (v/v)
mRNA purification buffer A	30 mM BisTris, pH 6.0 300 mM NaCl 1 mM EDTA
mRNA purification buffer B	30 mM BisTris, pH 6.0 1.5 M NaCl 1 mM EDTA

RNA sample buffer	80% formamide 89 mM Tris/HCl 89 mM H_3BO_3 2 mM EDTA 0.25% bromophenol (w/v) 0.25% xylencyanol (w/v)
SDS-PAGE running buffer	25 mM Tris/HCl 200 mM glycine 0.1% SDS (w/v)
TAE	40 mM Tris/HCl 20 mM acetic acid 1 mM EDTA
TAKM HiFi	50 mM Tris/HCl, pH 7.5 70 mM NH_4Cl 30 mM KCl 3.5 mM $MgCl_2$ 8 mM putrescine 0.5 mM spermidine
$TAKM_X$	50 mM Tris/HCl, pH 7.5 70 mM NH_4Cl 30 mM KCl X mM $MgCl_2$
TBE	89 mM Tris/HCl 89 mM H_3BO_3 2 mM EDTA
Transcription buffer	40 mM Tris/HCl, pH 7.5 15 mM MgCl2 2 mM spermidine 10 mM NaCl
tRNA purification buffer A	50 mM NaOAc, pH 4.5 10 mM $MgCl_2$
tRNA purification buffer B	50 mM NaOAc, pH 4.5 10 mM $MgCl_2$ 1.1 M KCl
Von Jagow anode buffer	200 mM Tris/HCl, pH 8.9
Von Jagow cathode buffer	100 mM Tris/HCl, pH 8.25 100 mM Tricine 0.1% SDS (w/v) final pH 8.25

2.4 *E. coli* Strains

Strain	Genotype	Supplier
MRE 600		UAB Fermentation Facility
NovaBlue Singles™ Competent Cells	endA1 hsdR17 (rK12– mK12+) supE44 thi-1 recA1 gyrA96 relA1 lac F'[proA+B+ lacIqZΔM15::Tn10] (TetR)	Novagen, Merck
BL21 (DE3)	F– ompT gal dcm lon hsdSB(rB- mB-) λ(DE3 [lacI lacUV5-T7 gene 1 ind1 sam7 nin5])	Novagen, Merck
BW25113	F- DE(araD-araB)567 lacZ4787(del)::rrnB-3 LAM- rph-1 DE(rhaD-rhaB)568 hsdR514	DMSZ – German Collection of Microorganisms and Cell Cultures GmbH

2.5 Plasmids

Plasmid	Insert	Resistance	Supplier
pUC19		Carbenicillin	Novagen, Merck
pET24a		Kanamycin	Novagen, Merck
pYFJ16-LplA(W37V)	LplA(W37V)	Carbenicillin, Chloramphenicol	Addgene, plasmid #34838 from Alice Ting
pMW2-S3C	S3-LAP (C term.)	Carbenicillin	
pMW2d-S2C	S2-LAP (C term.)	Carbenicillin	
pMW2d-S5C	S5-LAP (C term.)	Carbenicillin	
pMW2d-S5N	S5-LAP (N term.)	Carbenicillin	
pMW2d-S9N	S9-LAP (N term.)	Carbenicillin	
pMW2c-S10C	S10-LAP (C term.)	Carbenicillin	
pMW2c-S16C	S16-LAP (C term.)	Carbenicillin	
pMW5-lpp	lpp mRNA	Carbenicillin	
pMW5-lpp58	lpp58 mRNA	Carbenicillin	
pMW5-lpp38	lpp38 mRNA	Carbenicillin	
pMW5-lpp18	lpp18 mRNA	Carbenicillin	

2.6 Primers

2.6.1 Primers for the Generation of Transcription Templates

Primer	Sequence (5‘ to 3‘)	Function
oliMW003	AGGTACTATTACTTGCGGTATTTAGTAGCCATGT	rev primer lpp-no-Pin
oliMW325	GAATTCGAGCTCGGTACCC	fwd primer
oliMW326	TTACTTGCGGTATTTAGTAGCCATGTTG	rev primer lpp-stop

2.6.2 Primers for Site-specific Mutagenesis

Primer	Sequence (5’ to 3’)
oliMW007	TAATAGTACCTGTGAAGTGAAAAATGGCG
oliMW100	TGAATTCGAGCTCGGTACCCCTGTACACAGCGCCAACAAT
oliMW101	GTCGACTCTAGAGGATCCCCGCGACATTGTACGTCGCTTT
oliMW102	TGAATTCGAGCTCGGTACCCAAATCCCCATATCGAGGGCG
oliMW103	GTCGACTCTAGAGGATCCCCGTTGTGTCCGATCGCTGAGA
oliMW104	TGAATTCGAGCTCGGTACCCAGCCAGCTCAACCCAACTTT
oliMW105	GTCGACTCTAGAGGATCCCCGGCGCTGATAAGCAGGTGAT
oliMW106	TGAATTCGAGCTCGGTACCCGAGATTCCCACAGGGTCAGC
oliMW107	GTCGACTCTAGAGGATCCCCCGGACTTTGTCGTGTGAACC
oliMW108	TGAATTCGAGCTCGGTACCCTGGCCAGCCCTTCTTAACAG
oliMW109	GTCGACTCTAGAGGATCCCCGGTGACGGCTTCGATCTCAA
oliMW120	GATAAAGTTTGGTATGACCTGGACGCGTAATAAGGCTTGATAACTCCCCC
oliMW121	AATTTCGAAACCGCTACCGCCACCACCCTCAGCTTCTACGAAGCTTTCTT
oliMW124	GATAAAGTTTGGTATGACCTGGACGCGTAAGGAGCGTCGCTGATGTTACAACC
oliMW125	AATTTCGAAACCGCTACCGCCACCACCTTTACGGCCTTTACGCTGCTG
oliMW126	GATAAAGTTTGGTATGACCTGGACGCGTAAACCATGGCAAAGACTATTAAAATTACTCA AACCC
oliMW127	AATTTCGAAACCGCTACCGCCACCACCTTTCCCCAGAATTTCTTCAACGGA
oliMW128	GACCTGGACGCGGGTGGTGGCGGTAGCGCTCACATCGAAAAACAAGCTGG
oliMW129	ATACCAAACTTTATCAATTTCGAAACCCATCTTACACCTCTACCTTAGAACTG
oliMW130	GACCTGGACGCGGGTGGTGGCGGTAGCGCTGAAAATCAATACTACGGCACTG
oliMW131	ATACCAAACTTTATCAATTTCGAAACCCATTGCCTATAATCCCGATTAGATG
oliMW136	GATAAAGTTTGGTATGACCTGGACGCGTAATCTGTCACGGTGGTCATGATG
oliMW137	AATTTCGAAACCGCTACCGCCACCACCAGCTGCTTTGTTTACTTCTTTGATCAGC
oliMW143	TAGTACGAGACACAGGAAACAGCTATGACCATGA
oliMW145	GGGGATCCTCTAGAGTCGACC
oliMW146	GGGTACCGAGCTCGAATTC
oliMW237	CACTGATTAAGCATTGGTAAAACACCCCTTGTATTACTGTTTATGTAAGC
oliMW239	TTACCAATGCTTAATCAGTGAGGCACC
oliMW245	GATTCATTAATGCAGCTGGCACG
oliMW246	GCCAGCTGCATTAATGAATCAAACGTTTCGGCGAGAAGC
oliMW247	CATAGCTGTTTCCTGTGTGAAATTGTTATC
oliMW248	GAATTCGAGCTCGGTACCCTTAACCCAGGCTGATCTGCACG

oliMW249	TCACACAGGAAACAGCTATGCAGAACCAAAGAATCCGTATCC
oliMW250	GATAAAGTTTGGTATGACCTGGACGCGTAAGGGTACCGAGCTCGAATTC
oliMW251	AATTTCGAAACCGCTACCGCCACCACCACCCAGGCTGATCTGCAC
oliMW276	GAATTCGAGCTCGGTACCCTTACGCGTCCAGGTCATACCAAAC
oliMW277	GAATTCGAGCTCGGTACCCTTATTTCCCCAGAATTTCTTCAACGGATTTACC
oliMW278	GAATTCGAGCTCGGTACCCTTAACGTTTGGAGAACTGCGGAC
oliMW280	TCACACAGGAAACAGCTATGGCAACTGTTTCCATGCG
oliMW281	TCACACAGGAAACAGCTATGGGTCAGAAAGTACATCCTAATGGT
oliMW282	TCACACAGGAAACAGCTATGGCTCACATCGAAAAACAAGC
oliMW283	TCACACAGGAAACAGCTATGGGTTTCGAAATTGATAAAGTTTGGTATGAC
oliMW284	TCACACAGGAAACAGCTATGACACCGGACTCCGTTCC
oliMW295	TTCCACACATTATACGAGCCGGAAGCA
oliMW296	TTGTGAGCGGATAACAATTTCACACAG
oliMW297	ATAACAATTTCACACAGGAAACAGCTATG
oliMW306	CGTGCCAGCTGCATTAATGAATC
oliMW310	GTCGACTCTAGAGGATCCCCGGTCTCTAAAAAAATGGCGCACAATGTGC
oliMW311	TGAATTCGAGCTCGGTACCCGCTACATGGAGATTAACTCAATCTAGAGGG
oliMW312	TAATACGACTCACTATAGGGCTACATGGAGATTAACTCAATCTAGAGGG
oliMW332	AGCAGCCTGAACGTCGG
oliMW333	GTTCAGAGTCTGAACGTCAGAAGACAG
oliMW334	CAGCAGAGTAGAACCCAGGATTACC

2.6.3 Primers for Sequencing

Primer	**Sequence (5’ to 3’)**
oliMW160	GGGCAAATTGAGAATCATTCTGAATTTCG
oliMW161	GTTTATAGACGGGTTTTGCATTGGT
oliMW162	GACGTTCAGCATAGTCTGTTCTTGG
oliMW163	CGGATCCAGATCTTACCTTGACG
oliMW164	GCGCATTATGCCGCGTG
oliMW165	CATGCTGAAAAGCCCGTTTTCAG
oliMW166	AGACACGACGACCTTGCTG
oliMW167	ACCGCCAGCAGCTTCG
oliMW168	ATCCTGTTGACCATCAGCTGC
oliMW169	GCGAGCTACCGGGTAAACAG
oliMW170	ATCCTGCGACCCCACG
oliMW171	CGCGTCGCAGTGGTGATTACTA
oliMW172	CATTGCTGGTAACTCACCACCAC
oliMW173	GAGTTAGCAACTGTTGATTGCAATTCC
oliMW174	GTCGCTGATCGAAGATATCGAAAGC
oliMW185	CGCGTCCAGGTCATACCAAAC

2.7 List of mRNAs

mRNA	Sequence (5' to 3')
mUUC	GGCAAGGAGGUAAAUA**AUGUUCGUUAUU**
mlpp-test	GGGAGUUCAAAAAUUUAAAAGUUAACAGGUAUACAUACU**AUGGACAACAUGGCUA CUAAAUACCGCAAGUAA**UAGUACCU
lpp	GGGCUACAUGGAGAUUAACUCAAUCUAGAGGGUAUUAAUA**AUGAAAGCUACUAA ACUGGUACUGGGCGCGGUAAUCCUGGGUUCUACUCUGCUGGCAGGUUGCUCCAG CAACGCUAAAAUCGAUCAGCUGUCUUCUGACGUUCAGACUCUGAACGCUAAAGU UGACCAGCUGAGCAACGACGUGAACGCAAUGCGUUCCGACGUUCAGGCUGCUAAA GAUGACGCAGCUCGUGCUAACCAGCGUCUGGACAACAUGGCUACUAAAUACCGCA AGUAA**UAGUACCUGUGAAGUGAAAAAUGGCGCACAUUGUGCGCCAUUUUUU
lpp58	GGGCUACAUGGAGAUUAACUCAAUCUAGAGGGUAUUAAUA**AUGAAAGCUACUAA ACUGGUACUGGGCGCGGUAAUCCUGGGUUCUACUCUGCUGGCAGGUUGCUCCAG CAACGCUAAAAUCGAUCAGCUGUCUUCUGACGUUCAGACUCUGAACGCUAAAGU UGACCAGCUGAGCAACGACGUGAACGCAAUGCGUUCCGACGUUCAGGCUGCU UAA**UAGUACCUGUGAAGUGAAAAAUGGCGCACAUUGUGCGCCAUUUUUUU
lpp38	GGGCUACAUGGAGAUUAACUCAAUCUAGAGGGUAUUAAUA**AUGAAAGCUACUAA ACUGGUACUGGGCGCGGUAAUCCUGGGUUCUACUCUGCUGGCAGGUUGCUCCAG CAACGCUAAAAUCGAUCAGCUGUCUUCUGACGUUCAGACUCUGAAC UAA**UAGUAC CUGUGAAGUGAAAAAUGGCGCACAUUGUGCGCCAUUUUUUU
lpp18	GGGCUACAUGGAGAUUAACUCAAUCUAGAGGGUAUUAAUA**AUGAAAGCUACUAA ACUGGUACUGGGCGCGGUAAUCCUGGGUUCUACUCUGCUG UAA**UAGUACCUGUG AAGUGAAAAAUGGCGCACAUUGUGCGCCAUUUUUUU
lpp-no-Pin	GGGCUACAUGGAGAUUAACUCAAUCUAGAGGGUAUUAAUA**AUGAAAGCUACUAA ACUGGUACUGGGCGCGGUAAUCCUGGGUUCUACUCUGCUGGCAGGUUGCUCCAG CAACGCUAAAAUCGAUCAGCUGUCUUCUGACGUUCAGACUCUGAACGCUAAAGU UGACCAGCUGAGCAACGACGUGAACGCAAUGCGUUCCGACGUUCAGGCUGCUAAA GAUGACGCAGCUCGUGCUAACCAGCGUCUGGACAACAUGGCUACUAAAUACCGCA AGUAA**UAGUACCU
lpp-stop	GGGCUACAUGGAGAUUAACUCAAUCUAGAGGGUAUUAAUA**AUGAAAGCUACUAA ACUGGUACUGGGCGCGGUAAUCCUGGGUUCUACUCUGCUGGCAGGUUGCUCCAG CAACGCUAAAAUCGAUCAGCUGUCUUCUGACGUUCAGACUCUGAACGCUAAAGU UGACCAGCUGAGCAACGACGUGAACGCAAUGCGUUCCGACGUUCAGGCUGCUAAA GAUGACGCAGCUCGUGCUAACCAGCGUCUGGACAACAUGGCUACUAAAUACCGCA AGUAA**

AUG start codon is highlighted in green, UAA stop codon in red, GG T7-transcription start site in grey, **ORF** in bold, hairpin structure is underlined

2.8 Software

Software	Manufacturer and References
Anaconda Distribution Spyder IDE 5.1.5 Python version 3.9.7 Matplotlib 3.5.0 Numpy 1.20.3 Pandas 1.3.5	Anaconda, Inc. Python Software Foundation (Van Rossum and Drake, 2009) (Hunter, 2007) (Harris et al., 2020) (McKinney, 2010)
KNIME Analytics Software 4.2.1	KNIME AG (Berthold et al., 2008)
GraphPad Prism 9	GraphPad Software
TableCurve 2D v5.01	Systat Software Inc.
ImageJ 1.53k	(Schneider et al., 2012)
Snapgene 4.3.8.1	Dotmatics
ViennaRNA Package 2.0	(Lorenz et al., 2011)
Powershell 1.0	Microsoft Corporation
Microsoft Office	Microsoft Corporation
pymol 1.5	Schrödinger
AlphaFold	DeepMind (Jumper *et al.*, 2021; Varadi *et al.*, 2022)

2.9 Preparation of Ribosomes, Proteins and tRNAs

Wild type ribosomes (70S), initiation factors (IF1, IF2 and IF3), elongation factors (EF-Tu and EF-G), release factors (RF1 and RF3), recycling factor RRF, and tRNAs were from *E. coli* and were prepared as described (Holtkamp et al., 2014; Milon et al., 2007; Peske *et al.*, 2005; Rodnina et al., 1999; Rodnina and Wintermeyer, 1995; Savelsbergh et al., 2003).

2.10 Vector Construction and Mutation

Primer and plasmid design were done in Snapgene (Dotmatics).

PCR was used to introduce site-specific mutations into plasmids or to generate fragments for vector assembly. PCR was carried out using Q5® High-Fidelity DNA Polymerase (New England Biolabs) according to the manufacturer's protocol. Typically, 100-200 pg plasmid DNA was used. Alternatively, 1 µL of genomic DNA was used as template. Genomic DNA was harnessed by lysing

one colony of BW25113 cells in 50 µL DNA extraction buffer (10 mM Tris/HCl, 1 mM EDTA, 0.1% TritonX100).

PCR products were analyzed on an agarose gel (0.5 to 2% of agarose in TAE buffer supplemented with DNA Stain G, Serva, 1:20 000) and Gel Loading Dye Purple (New England Biolabs) was added to the samples prior to loading. The electrophoresis was performed with a gel electrophoresis system (Peqlab) at 120 V for 40 to 60 min. The DNA was visualized with a UV gel documentation system (Peqlab).

PCR products were purified using the Nucleospin® Gel and PCR Clean-up Kit (Macherey-Nagel). Blunt end ligation was performed using the Quick Ligation™ Kit (New England Biolabs) combined with T4 Polynucleotide Kinase (New England Biolabs) for 5'-phosphorylation of PCR products. Alternatively, plasmids were created via Gibson assembly from multiple fragments. For Gibson assembly, 0.05 pmol of every fragment was incubated for 1 h at 50°C in 20 µL isotherm buffer supplemented with 0.15 mM dNTPs (New England Biolabs), 0.025 U/µL Phusion Polymerase (New England Biolabs), 4 U/µL Taq DNA Ligase (New England Biolabs), 0.0075 U/µL T5 Exonuclease (New England Biolabs), 0.003 µg/µL Extreme Thermostable Single-Stranded DNA Binding Protein (ET SSB, New England Biolabs).

Assembled plasmids were transformed via heat shock at 42°C for 45 s into NovaBlue Singles™ Competent Cells (Novagen). For transformation, 10 ng plasmid DNA, 10 µL ligation mix or Gibson mix were used for 50 µL of competent cells. Cells were cultivated on LB-agar plates (LB with 1.5% (w/v) agar) supplemented with the required antibiotic (100 µg/mL carbenicillin, 50 µg/mL kanamycin, 25 µg/mL chloramphenicol) for selection and incubated at 37°C overnight. Single colonies were transferred to LB supplemented with the selection antibiotic and incubated overnight with shaking at 200 rpm. Cells were harvested via centrifugation (small tabletop centrifuge, Eppendorf, 5 min, 11000 rpm). Plasmid concentrations were determined by measuring the absorption at 260 nm via Nanodrop 2000c (Peqlab).

Plasmids were purified using the NucleoBond® Plasmid Purification Kit (Macherey-Nagel). Sequencing was commissioned to Seqlab (Microsynth). Standard primers (M13, M13r or pUCM13-rev-157) or premixed primers were used.

2.11 Preparation of mRNAs

For mRNA preparation, vector pMW5-lpp was created. The pMW5 vector is based on the pUC19 vector but features a T7-polymerase promoter sequence (5'-TAATACGACTCACTATAGGGAG-3') for *in vitro* transcription prior to the full native lpp-mRNA sequence including the 5' and 3' UTRs. For convenient sequencing, the promoter and mRNA region of pMW5 is 5' and 3' flanked by an M13 and an M13r binding site, respectively. A BsaI cleavage site was introduced to cut the plasmid DNA right after the mRNA-coding sequence to perform run-off transcription.

A promoterless variant of pUC19 was created using the primers oliMW143 and oliMW306 (primer list) on pUC19 (Novagen). The vector backbone fragment was obtained from this vector by PCR with the primers oliMW145 and oliMW146. This fragment and the lpp mRNA coding DNA fragment, created by PCR with primers oliMW310 and oliMW311 and using BW25113 genomic DNA as a template, were assembled using the Gibson cloning method. oliMW310 also introduces the BsaI site right after the lpp mRNAs 3'-UTR. The T7 promoter sequence was introduced by PCR with the primers oliMW312 and oliMW146 to create the pMW5-lpp vector. Vectors pMW5-lpp58, pMW5-lpp38 and pMW5-lpp18, whose lpp mRNAs contain only the first 58, 38, 18 amino acids of the ORF prior to the native 3'-UTR, respectively, were created by PCR with the reverse primer oliMW007 and the forward primers oliMW332, oliMW333 and oliMW334, respectively.

The templates for the *in vitro* transcription of mRNAs were obtained either by PCR with the corresponding primers or by linearization of plasmid DNA using restriction endonuclease BsaI-HF®v2 (New England Biolabs).

In vitro transcription of mRNAs was performed in transcription buffer (40 mM Tris-HCl pH 7.5, 15 mM MgCl2, 2 mM spermidine, 10 mM NaCl) supplemented with 10 mM DTT, 3 mM NTPs (each), 5 mM GMP, 5 u/mL pyrophosphatase (from yeast, Sigma) and 0.2 u/µL RNase inhibitor (Molox) with 1.6 u/µL T7 RNA-polymerase per 100 µL/mL PCR mix or 100 ng/mL linearized plasmid for 4 h at 37°C. The mRNAs were purified on an ÄKTA system (GE Amersham ÄKTA FPLC UPC-960, P-920, Frac-920) via a HiTrap Q HP column (GE Healthcare) with a linear gradient (0 – 100%, 40 min, 3 mL/min, mRNA purification buffer A30 mM Bis-Tris, pH 6.0, 300 mM NaCl, 1 mM EDTA, mRNA purification buffer B: 30 mM Bis-Tris, pH 6.0, 1.5 M NaCl, 1 mM EDTA). The mRNA containing fractions were pooled and precipitated with ethanol (2.5 volumes) and KOAc (1/10 volume of 3 M solution) at -20°C. mRNA concentrations were determined by their extinction at 260 nm spectrophotometrically using a Nanodrop 2000c (Thermo Fischer Scientific). The extinction coefficient of mRNAs was calculated using the RNA Molecular Weight Calculator (AAT Bioquest). The size and homogeneity

of the mRNAs was checked via UREA-PAGE (RNA loading buffer, 8 – 15% acrylamide/Bis solution (19:1), 7 M urea, 0.1% APS and 0.1% TEMED in TBE buffer, gel electrophoresis kit (BioRad) at 250 V for 50 min) and methylene blue staining.

2.12 Labeling of mRNAs

In vitro transcribed mRNAs were labeled with hydrazide conjugated dyesat the 3'-end. Firstly, the mRNA (10-15 nmol in 150 µL) was oxidized with 1 mM KIO_4 in 100 mM NaOAc (pH 5.3) on ice for 45 min. The reaction was quenched by adding ethylene glycol (40 mM final concentration). The mRNA was precipitated twice with ethanol (2.5 volumes) or 2-propanol (0.9 volumes) and NaOAc (1/10 volume of 3 M solution) at -20°C. The pellet was resolved in as little 100 mM NaOAc (pH 5.3) as possible (2 µL per nmol mRNA). For the labeling reaction, 0.1 µL of 20 mM hydrazide dye in DMSO was added per 1 µL of reaction volume. Labeling reactions were performed at 37°C for 1 h. To remove excess dye, mRNAs were repeatedly precipitated with ethanol (2.5 volumes) and NaOAc (1/10 volume of 3 M solution) at -20°C. Pellets were resolved in water. mRNA concentrations were determined spectrophotometrically at 260 nm using a Nanodrop 2000c (Thermo Fischer Scientific). The extinction coefficients of mRNAs were calculated using the RNA Molecular Weight Calculator (AAT Bioquest). Absorption of the dye (A_{dye}) was determined by its extinction at the dye specific extinction maximum. The degree of labeling (DOL) was calculated according to following equation (Eq. 1):

$$\mathrm{DOL} = \frac{A_{dye}/\varepsilon_{dye}}{A_{RNA}/\varepsilon_{RNA}} \quad (1)$$

where A_{dye} is the absorbance of the dye at the absorbance maximum and ε_{dye} denotes the extinction coefficient at the absorbance maximum of the dye. The extinction coefficient ε_{RNA} describes the calculated extinction at 260 nm for the mRNA. The absorbance of the mRNA A_{RNA} was measured at 260 nm. The absorption of the dye at 260 nm was insignificant for the large mRNAs used, hence a correction was not required. The quality of the labeled mRNAs was checked via UREA-PAGE (RNA loading buffer, 8 – 15% acrylamide/Bis solution (19:1), 7 M urea, 0.1% APS and 0.1% TEMED in TBE buffer, gel electrophoresis kit (BioRad) at 250 V for 50 min, Amersham Typhoon, GE Healthcare).

2.13 Preparation of Total aa-tRNAs

The aminoacylation of total tRNA from *E. coli* (Roche, 80 units A_{260}/mL) was performed in $HAKM_{20}$ buffer supplemented with 3 mM ATP, 2 mM DTT, L-amino acids (Sigma, 300 µM each) and 3% (v/v) S100 extract for 30 min at 37°C (Cunha *et al.*, 2013; Milon *et al.*, 2007; Wieden et al., 2002). The reaction was quenched by adding 1/10 volume 3 M KOAc. The reaction mixture was phenol-extracted and precipitated with ethanol (2.5 volumes) and KOAc (1/10 volume of 3 M solution) at -20°C. The pellet was briefly dried, dissolved in water and purified by FPLC (GE Amersham ÄKTA Primewith a HiTrap) on a Q HP column (GE Healthcare) using a linear gradient (0 – 100%, 40 min, 2 mL/min, tRNA purification buffer A: 50 mM NaOAc, pH 4.5, 10 mM $MgCl_2$, tRNA purification buffer B: 50 mM NaOAc, pH 4.5, 10 mM $MgCl_2$, 1.1 M KCl). The tRNA containing fractions were pooled and precipitated with ethanol (2.5 volumes) and KOAc (1/10 volume of 3 M solution) at -20°C. The pellet was briefly dried and dissolved in water. The tRNA concentration was determined spectrophotometrically at 260 nm (extinction coefficient 575 000 M^{-1} cm^{-1}, Lambda Bio+ spectrophotometer, PerkinElmer).

2.14 Preparation of S3-labeled Ribosomes

The protein S3 of the 30S subunit was labeled at the C-terminal position utilizing the lipoic acid ligase $LplA^{W37V}$ and biorthogonal inverse electron demand Diels-Alder reaction. This method has been previously described (Baalmann *et al.*, 2018), but adaptations had to be made to the original protocol. Ribosomes were purified from BW25113 cells overexpressing S3 with C-terminal LAP-tag. The LAP tag was site specifically modified with a norbornene moiety utilizing $LplA^{W37V}$. In a second step, Me-tetrazine conjugated dyes (dye chapter) could react with the norbornene handle.

For overexpression of ribosomal proteins in BW25113, the pMW2 vector was created. The pMW2 vector is based on the pUC19 vector (Novagen) but features the low copy origin of replication (ORI) of pET24a (Novagen). To boost expression in BW25113, the variants pMW2c and pMW2d have the supposedly stronger lacUV5 promotor instead of the lac promotor from pUC19. Additionally, in the variant pMW2d, the lac operator was mutated dysfunctional to prevent repression by the lac repressor. The vector pMW2d should not need IPTG induction. pMW2 was created via Gibson assembly of the pUC19 vector backbone amplified with the primers oliMW239 and oliMW245 and the pET24a ORI fragment amplified with the primers oliMW237 and oliMW246. For improved

primer binding, the S3 ORF was amplified with its flanking regions with the primers oliMW102 and oliMW103. For cloning, this fragment was inserted into the pUC19 vector amplified with the primers oliMW145 and oliMW146 via Gibson assembly. A C-terminal LAP-tag (GFEIDKVWYDLDA) with a GGGGS-linker was added to S3 via the primers oliMW124 and oliMW125. The LAP-tagged S3 ORF was amplified with the primers oliMW281 and oliMW276 and inserted into the pMW2 vector amplified using primers oliMW247 and oliMW146 via Gibson assembly to create the expression vector pMW2-S3C.

Like for plasmid pMW2-S3C, the ORFs of S2, S5, S9 and S16 were amplified from the genome (primer oliMW100, oliMW101, oliMW104, oliMW105, oliMW106, oliMW107, oliMW108, oliMW109). A C-terminal LAP-tag was added to S2, S5, S16 (primer oliMW120, oliMW121, oliMW126, oliMW127, oliMW136, oliMW137). Inserts were amplified and inserted into pMW2 to create pMW2-S2C (oliMW280, oliMW276), pMW2-S5C (oliMW282, oliMW276) and pMW2-S16C (oliMW284, oliMW276). An N-terminal LAP-tag was added to S5 and S9 (primer oliMW128, oliMW129, oliMW130, oliMW131). Inserts were amplified and inserted into pMW2 to create pMW2-S5N (oliMW283, oliMW277) and pMW2-S9N (oliMW283, oliMW278). S10 was directly inserted into the pMW2 vector (oliMW248, oliMW249) and a C-terminal LAP tag was added (oliMW250, oliMW251). To improve expression, the promotor of pMW2 was changed to the lacUV5 promotor using the primers oliMW296 and oliMW295 for the inserts S10C and S16C to create the vectors pMW2c-S10C and pMW2c-S16C. To further improve expression, the lac-operator was made unfunctional for the inserts S2C, S5C, S5N and S9N using the primers oliMW296 and oliMW297 to create the vectors pMW2d-S2C, pMW2d-S5C, pMW2d-S5N, pMW2d-S9N.

To grow cells for the purification of ribosomes, electrocompetent BW25113 cells were transformed with pMW2-S3C by electroporation (3 ms, 1250 V, Electroporator, Eppendorf). Electrocompetent BW25113 cells were created by growing BW25113 to an OD_{600} of 0.6 (mid-exponential phase) in LB, repeatedly washing of cells in LB with 10% glycerol and finally, creating a 100x concentrated stock (OD_{600} of 60) in LB with 10% glycerol. Cells from a single colony of BW25113 with pMW2-S3C were grown overnight in LB supplemented with 100 µg/mL carbenicillin at 37°C. 2x 25 mL of this pre-culture were used to inoculate fresh 2x 200 mL LB and the cultures were grown to an OD_{600} of 1.25 (135 min). 30 mL of this second pre-culture were used to inoculate 500 mL of LB supplemented with carbenicillin. After 50 min of growth to an OD_{600} of 0.25, IPTG was added to a final concentration of 1 mM. Cells were grown to an OD_{600} of 2.0 (total 190 min at 37°C) and subsequently harvested (10 min, 7 k rpm, 4 °C, Avanti J-26 XP centrifuge with JLA-8.1000, Beckmann Coulter). A total of 36 flasks with 500 mL culture each was used, yielding 75 g of cells for preparation of tagged ribosomes.

Ribosomes were purified as described (Rodnina and Wintermeyer, 1995).

The lipoic acid ligase LplA^{W37V} was purified as described (Baalmann *et al.*, 2018). pYFJ16-LplA(W37V) was expressed in BL21 (DE3). Cells were grown in LB supplemented with 25 µg/mL chloramphenicol at 37°C. Expression was induced with 1 mM IPTG at an OD_{600} of 0.45. Cells were harvested after 4 h by centrifugation (10 min, 7 k rpm, 4 °C, Avanti J-26 XP centrifuge with JLA-8.1000, Beckmann Coulter). The cell pellet was resuspended in LplA purification buffer (20 mM Tris-HCl pH 8.0, 300 mM NaCl, 5 mM 2-mercaptoethanol, 15% glycerol) supplemented with cOmplete protease inhibitors (1 tablet per 100 mL) and DNase I (2 u/mL). Cells were opened by pressure using an Emulsiflex C-3 homogenizer (Avestin). The cell lysate was centrifuged (30 min, 30 k rpm, 4°C, Avanti J-30 I centrifuge with JA30.50, Beckmann Coulter) and the protein was subsequently purified via Protino Ni-IDA Resin (Macherey-Nagel) in a gravity flow column as suggested by the manufacturer. The LplA^{W37V} containing eluted fractions were concentrated via a Vivaspin 20 filtration unit (Sartorius) with a 10 kDa MWCO cut-off. The buffer was changed to $TAKM_7$ with 50% glycerol for storage. Protein size and purity were analyzed via SDS-PAGE (4x protein sample buffer, 12% acrylamide/Bis solution (19:1), 1% SDS, 0.1% APS and 0.1% TEMED in SDS-PAGE running buffer, gel electrophoresis kit (BioRad) at 200 V for 1 h, Coomassie Brilliant Blue staining).

The norbornene handle (7-(exo-norborn-5-ene-carboxamido)heptanoic acid) was synthesized in the Facility for Synthetic Chemistry (Max Planck Institute for Multidisciplinary Sciences, Göttingen) according to a published protocol (Baalmann *et al.*, 2018) from *N*-hydroxysuccinimidyl exo-norborn-5-ene-carboxylate and 7-aminoheptanoic acid. Quality of the substance was confirmed via HPLC and ^{1}H-NMR. A purity of 99.4% was achieved.

Labeling of LAP-tagged ribosomes was carried out according to the published protocol (Baalmann *et al.*, 2018) which has been developed further and optimized for the present purpose as follows. In a first step, the LAP tag on the C-terminal end of S3 on the 30S subunit was modified utilizing the lipoic acid ligase LplA^{W37V}. This modified ligase binds to the LAP tag and catalyzes the reaction of the lysine residue in the tag with the carboxylic acid group of the norbornene substrate. This reaction consumes ATP. Modification of tagged ribosomes (2.5 µM) was performed with 1 µM LplA^{W37V}, 5 mM ATP and 1 mM norbornene substrate (from 200 mM stock solution in DMSO) in $TAKM_7$ for 30 min at 37°C. At 30 min incubation, a labeling efficiency of 55 – 60% (determined spectrophotometrically) can be achieved with 95% of dye molecules at the specific labeling position (determined via gel quantification). Longer incubation periods lead to higher labeling efficiencies, but this also caused unspecific modification of ribosomal protein residues by LplA^{W37V}. After the modification reaction, the Mg^{2+} concentration was increased to 21 mM. Ribosomes were purified

from the reaction mixture by ultracentrifugation (3 h, 55 k rpm, 4°C, Optima MAX-XP ultracentrifuge with TLS55, Beckmann Coulter) through a 40% sucrose cushion in $TAKM_{21}$. Pelleted ribosomes were resuspended in $TAKM_7$ to a concentration of 15 µM.

In a second step, Me-tetrazine conjugated dyes react with the norbornene moiety on the ribosome via biorthogonal inverse electron demand Diels-Alder cycloaddition (Baalmann *et al.*, 2018). For the labeling reaction, 0.2 mg/mL (0.2 to 0.5 mM) of Me-tetrazine conjugated dyes (from 20 mg/mL stock solution in DMSO) was added to 15 µM modified ribosomes in $TAKM_7$. Reaction was performed at 37°C for 1 h. After the labeling reaction, Mg^{2+} concentration was increased to 21 mM. Ribosomes were purified from excess dye by ultracentrifugation (3 h, 55 k rpm, 4°C, Optima MAX-XP ultracentrifuge with TLS55, Beckmann Coulter) through a 40% sucrose cushion in $TAKM_{21}$. Pelleted ribosomes were resuspended and stored in $TAKM_7$. Ribosome concentration was determined by its extinction at 260 nm assuming 23 pmol of 70S ribosomes per absorption unit (Lambda Bio+ spectrophotometer, PerkinElmer). Dye concentration was determined by its extinction at the dye specific manufacturer provided wavelength and extinction coefficient via a Nanodrop 2000c (Peqlab) and labeling efficiency was calculated using Eq. 1 (chapter 2.12). Specificity of labeling was checked via SDS-PAGE (4x protein sample buffer, 15% acrylamide/Bis solution (19:1), 1% SDS, 0.1% APS and 0.1% TEMED in SDS-PAGE running buffer, gel electrophoresis kit (BioRad) at 200 V for 1 h, Amersham Typhoon, GE Healthcare). Gel quantification was done with the imageJ software (Schneider *et al.*, 2012).

2.15 Preparation of L9- and S6-labeled Ribosomal Subunits

50S subunits with Cy5-labeled L9 and 30S subunits with Cy3-labeled S6 were prepared as described (Sharma et al., 2016). L9(N11C) and S6(D41C) were from *E. coli* BW25113 and prepared as described (Ermolenko et al., 2007; Hickerson et al., 2005; Lieberman et al., 2000; Sharma *et al.*, 2016). Proteins were labeled with Cy5-maleimide or Cy3-maleimide as described (Sharma *et al.*, 2016). Ribosomal subunits were prepared from ΔL9 or ΔS6 deletion strains as described (Rodnina and Wintermeyer, 1995). Reconstitution of ΔL9 50S subunits with Cy5-labeled L9(N11C-Cy5) and ΔS6 30S subunits with Cy3-labeled S6(D41C-Cy3) was performed as described (Sharma *et al.*, 2016).

2.16 Formation of Initiation Complexes

Initiation complexes (ICs) were formed in $TAKM_7$ buffer or in HKM_7 to minimize spontaneous peptide drop off possibly caused by ammonium. HKM_7 buffer was preferred when ICs were subsequent used for translation or rapid kinetic experiments. If not stated otherwise, initiation complexes (ICs) were formed by incubating 1 µM 70S ribosomes with 2 µM IF1, IF2, IF3, 3 µM mRNA and 3 µM f[^{3}H]Met-tRNA^{fMet} and 1 mM GTP at 37°C for 20 min. The efficiency of initiation complexes formation was determined by measuring the ^{3}H-radioactivity after filtration through cellulose nitrate filters (0.45 µm pore size, Sartorius), to which ribosomes and with them bound f[^{3}H]Met-tRNA^{fMet} but not free tRNA bind. Filters were dissolved in 10 mL Quickscint 361 scintillation cocktail (Zinsser Analytic) and counted in a Tri-Carb® 3110 TR Liquid Scintillation Analyzer (PerkinElmer).

2.17 *In vitro* Translation

Translation was carried out *in vitro* by mixing ICs with ternary complex (TC) containing aa-tRNAs and EF-Tu in HKM HiFi buffer supplemented with 3 mM phosphoenolpyruvic acid (PEP), 1 mM GTP, 1 mM dithiothreitol DTT and 0.5% (v/v) pyruvate kinase (PK). Translation was performed with 0.1 µM ICs, 1 µM EF-G, 50 µM aa-tRNA, 50 µM EF-Tu and 1 µM RF1 to prevent stop codon read through. EF-Tu, EF-G, RF1, GTP, DTT, PEP and PK were incubated at 37°C for 15 min to convert GDP to GTP. Subsequently, aa-tRNAs were added and incubated for 1 min at 37 °C before adding IC to start the reaction. To create pre-recycling complexes (PRCs) for smFRET experiments, translation was carried out for 20 s before the reaction was stopped by rapid cooling on ice.

2.18 Separation of Translation Products on von Jagow Gels

To monitor the translational progress, the peptide products were separated on high resolution von Jagow gels, which resolve not only large full-length products but also small peptide intermediates. ICs were formed as described using BODIPY-FL-labeled f[^{3}H]Met-tRNA^{fMet}. *In vitro* translation was carried out as described. Samples (25 µL) were taken and the reaction was stopped by addition to 5 µL 2 M NaOH (final concentration of 0.4 M) at 37°C for 30 min. HEPES pH 5 (5.5 µL of 2 M, final

concentration of 0.2 M) was added for neutralization. Samples were mixed with equal volumes of 2x translation gel sample buffer (35.5 µL) and separated by Tris-Tricine gel electrophoresis (Schagger, 2006; Schagger and von Jagow, 1987). Peptides were separated on a 16.5% acrylamide gel (6% w/w bis-acrylamide in total acrylamide, 1 M Tris/HCl pH 8.45, 0.1% SDS, 0.1% APS, 0.1% TEMED). The gel featured also a 4% acrylamide stacking gel and a 10% acrylamide spacer gel between the layers (3% w/w bis-acrylamide in total acrylamide, 1 M Tris/HCl pH 8.45, 0.1% SDS, 0.1% APS, 0.1% TEMED). Electrophoresis was carried out at 40°C with von Jagow cathode buffer and von Jagow anode buffer for 1 h at 30 V followed by 30 min at 80 V, 30 min at 100 V and finally 1 h at 140 V (large gel electrophoresis kit, Peqlab). Bodipy-FL-labeled translation products were visualized by fluorescence scanning of the gels on an Amersham Typhoon Scanner (GE Healthcare). Gel quantification was carried out using the imageJ software (Schneider *et al.*, 2012) and the resulting data was fitted with a delay phase followed by a single exponential equation (association) in GraphPad Prism (Eq. 2):

$$Y = IF\ (X < X_0, Y_0\ , Y_0 + (Amp - Y_0) * (1\ -\ exp(-k * (X - X_0)))) \qquad (2)$$

Here, X_0 describes the delay time of the exponential phase and the relative amount of translation products Y equals Y_0 for the duration of the delay. The amplitude is denoted by Amp. The delay phase is followed by a one phase exponential association where k is the rate constant.

2.19 Rapid Kinetics

Rapid kinetic experiments were performed with a SX-20 stopped-flow apparatus (Applied Photophysics) by rapidly mixing equal volumes (55 µL) of the reactants. mRNA release was measured with ICs featuring the S3-ATTO488 and mRNA-ATTO647N FRET-pair. Acceptor fluorescence was observed by exciting with a 470 nm LED light source (10 mA) and measuring with a red sensitive photomultiplier (680 V) after passing a RG665 filter. Subunit splitting was observed using the same ICs featuring the S3-ATTO488 and mRNA-ATTO647N FRET-pair, but as light source either a xenon lamp with a monochromator set to 350 nm or a 435 nm LED light source (16 mA) was used. Measurements were performed with a standard photomultiplier (350V for Xenon lamp, 180 V for LED) without a filter.

ICs featuring the S3-ATTO488-labeled 70S ribosomes and 3'-labeled mRNA-ATTO647N were formed as described and subsequently purified via ultracentrifugation through a sucrose cushion

(40% sucrose cushion in $TAKM_{21}$). The Mg^{2+} concentration of the sample solution was increased to 21 mM. Ultracentrifugation was performed at 55 k rpm and 4°C for 2 h in an Optima MAX-XP ultracentrifuge and a TLS55 rotor (Beckmann Coulter). Pelleted ribosomes were resuspended and stored in $TAKM_7$. Ribosome concentration was determined by its extinction at 260 nm assuming 23 pmol of 70S ribosomes per absorption unit (Lambda Bio+ spectrophotometer, PerkinElmer). The concentration of formed initiation complexes was determined via ^{3}H-radioactivity by adding 2 mL Ultima Gold™ XR scintillation cocktail (Perkin Elmer) to the sample followed by counting with a Tri-Carb® 3110 TR Liquid Scintillation Analyzer (PerkinElmer).

Translation was monitored after rapid mixing of 50 nm ICs with 1 µM EF-G, 50 µM aa-tRNA, 50 µM EF-Tu, 1 µM RF1 in HKM HiFi buffer supplemented with 3 mM PEP, 1 mM GTP, 1 mM DTT and 0.5% (v/v) PK the stopped flow apparatus. To observe the recycling reaction after translation in the stopped-flow apparatus, 50 nm ICs were mixed with 2.5 µM EF-G, 50 µM aa-tRNA, 50 µM EF-Tu, 1 µM RF1, 1 µM RF3, 5 µM RRF 1 µM IF3. 0.25 µM non-labeled mUUC mRNA was also added to prevent reassociation of recycled labeled mRNAs. In each measurement, 4 – 8 data traces were averaged. The averaged traces were fitted with TableCurve 2D software (SYSTAT) or GraphPad Prism (GraphPad software) to determine kinetic properties of the observed reactions. Recycling phases were fitted with a delay followed by two exponential phases (decay) equation in GraphPad Prism (Eq. 3):

$$Y = IF(X < X_0, Y_0, Y_0 + Amp_1 * (1 - exp(-k_1 * (X - X_0))) + Amp_2 * (1 - exp(-k_2 * (X - X_0)))) \quad (3)$$

As for equation (2), X_0 describes the delay time of the exponential phase and Y equals Y_0 for the duration of the delay. The amplitudes Amp_1 and Amp_2 are corresponding to the two rate constants k_1 and k_2.

2.20 Single-molecule Experiments using TIRF Microscopy

TIRF imaging was performed using an IX 81 inverted objective-based microscope with a PLAPON 100 x 1.45 numerical aperture objective (Olympus), a 561 nm solid-state laser at 30 mW, a CCD-C9100-13 camera (Hamamatsu), a dual view micro imager DV2 splitter (Photometrics) and HQ 605/40 and HQ 680/30 filters (Chroma Technology) as described (Adio *et al.*, 2015).

Experiments were carried out at 22°C in TAKM HiFi buffer supplemented with an oxygen-scavenging system (2.5 mM protocatechuic acid (PCA), 50 nM protocatechuate 3,4-dioxygenase (PCD)) and a triplet-state quencher mixture (1 mM Trolox and 1 mM methylviologen (MV)) (imaging buffer).

Flow chambers containing biotin-polyethylene glycol quartz slides were prepared as described (Adio *et al.*, 2015) and subsequently washed with TAKM HiFi buffer supplemented with 10 mg/mL BSA and 1 µM neutravidin. After additional washing step with TAKM HiFi buffer supplemented with 1 mg/mL BSA, 0.5 - 1 nM ribosome complexes diluted in TAKM HiFi buffer were immobilized on quartz slides using the mRNA annealed to a biotinylated primer.

To monitor the release of mRNA from 30S subunits, ICs with the S3-Cy5 and mRNA-Cy3 FRET pair were formed by incubating 2 µM 70S ribosomes with Cy3-label on the C-terminal LAP-tag of S3 with 3 µM IF1, IF2, IF3, 1 µM mRNA with Cy5-label on the 3'-end and 3 µM f[^{3}H]Met-tRNA^{fMet} at 37°C for 30 min. The mRNA was incubated with equimolar amounts of 5'-Biotin-TEG labeled DNA oligo (3'-GAGTTAATCTCCATGTAGCC-5') at 37°C for 30 min prior to IC formation.

To monitor subunit splitting, ICs with the S6-Cy3 and L9-Cy5 FRET pair were formed from separated subunits by incubating 1 µM S6-Cy3 labeled 30S subunits with 2 µM L9-Cy5 labeled 50S subunits with 1.5 µM IF1, IF2, IF3, 3 µM mRNA and 2 µM f[^{3}H]Met-tRNA^{fMet} at 37°C for 30 min. S6-Cy3 labeled 30S subunits were activated in TAKM$_{20}$ prior to IC formation. The mRNA was incubated with equimolar amounts of 5'-Biotin-TEG labeled DNA oligo (3'-GAGTTAATCTCCATGTAGCC-5') at 37°C for 30 min prior to IC formation.

To create pre-recycling complexes (PRCs), in vitro translation of these ICs was performed as described by incubating ICs with elongation factors (1 µM EF-G, 50 µM aa-tRNA, 50 µM EF-Tu) and 1 µM RF1 for 20 s.

PRCs were diluted in TAKM HiFi buffer to a concentration of 1 nM and applied to the flow chamber. To observe the recycling reaction, RF3, RRF, EF-G and GTP were added to the imaging buffer. If not stated otherwise, the following concentrations were used: 1 µM EF-G, 1 µM RF3, 1 µM RRF, 1 mM GTP.

Movies were recorded at 100 ms per frame. A semi-automated algorithm was used to select anti-correlated fluorescence traces exhibiting characteristic single fluorophore intensities (Adio *et al.*, 2015). Bleed-through of Cy3 signal into the Cy5 channel was corrected using an experimentally determined coefficient of 0.13. FRET efficiency was calculated as the ratio of measured emission fluorescence intensities (I), $I_{Cy5}/(I_{Cy3} + I_{Cy5})$. Fluorescence time courses were extracted and analyzed using Matlab (Mathworks) with custom scripts as described (Adio *et al.*, 2015; Fei et al., 2008; Roy

et al., 2008). The distributions of FRET states were fitted to a sum of Gaussian functions using a nonlinear minimization procedure (fminsearch, Matlab, R2011b). The lengths of FRET trajectories were used to obtain the rate constants corresponding to the release of mRNA from 30S subunit and subunits splitting. The normalized dependence of non-recycled complexes on time was fitted to an exponential function (Eq. 4):

$$y = A\, exp(-k_{obs}) \tag{4}$$

where k_{obs} is the observed decay rate. The observed rates k_{obs} were corrected (k_{cor}) according to the equation (Eq. 5):

$$\mathrm{k}_{cor} = \frac{1}{t_d + \frac{1}{k_{obs} - k_{ph}}} \tag{5}$$

where t_d is the delay time between the factors adding and start of the measurement. The photobleaching correction rate k_{ph} was derived from independent experiments performed without any factors in the imaging buffer to correct for photobleaching and intrinsic complex instability.

2.21 Transcriptome Analysis

A bioinformatics analysis of the *E. coli* transcriptome was performed to assess occurrence of hairpin structures in 3'-UTRs of mRNAs. A data-pipeline was created in the KNIME Analytics Software (KNIME AG) (Berthold *et al.*, 2008) to merge *E. coli* K-12 MG1655 genome and gene annotations from GenBank (U00096.3) with RNASeq confirmed operon annotations (Conway *et al.*, 2014) (GEO database accession number GSE52059). Forward and complement genes were extracted separately from GenBank U00096.3 with their attributed genome positions. Sequence and 3' regions of all genes were extracted from GenBank U00096.3 and merged to create a dataset containing all *E. coli* genes with their start and end position, calculated gene length, gene sequence and 3' region sequence. In addition, a dictionary for alternative gene names was created as well as lists of all GenBank U00096.3 entries attributed as coding sequence (CDS) or RNA. Forward and complement RNASeq confirmed operons were extracted separately from confirmed operon annotations (GSE52059) (Conway *et al.*, 2014) with their attributed genome positions and merged to create a dataset containing all RNASeq confirmed *E. coli* operons with their start and end position and calculated operon length. Since dataset GSE52059 refers to *E. coli* K-12 strain BW38028, which is

the slightly different from *E. coli* K-12 MG1655, an algorithm had to be created to merge the datasets. For named operons, operon start and end was compared to first gene start positions and last gene end positions from GenBank U00096.3. Genes deposited with alternative or outdated names were corrected with help of the previously created dictionary for alternative gene names. Operon start and end positions were corrected to match GenBank U00096.3 annotations of the corresponding genes. Unnamed operons were treated in the same way as the previous named operon. Additionally, the preceding and the following 50 nucleotides (nts) of the genome sequence were added to the corrected operon start and end annotations, respectively. Finally, the algorithm checked which genes from GenBank U00096.3 fit inside the corrected operon annotations of dataset GSE52059. Out of 750 RNASeq confirmed operons on the forward strand (760 on the complementary strand) 599 (609) were correctly named, 62 (67) had alternative names that needed the alternative gene name dictionary correction and 89 (74) were unnamed. 1414 (1587) genes were fitted in 666 (695) of these RNASeq found operons. The separately treated forward and complement datasets were merged and duplicates, as well as faulty entries were removed. With help of the previously created lists of CDS and RNA genes, operons that contain non-coding or RNA genes at the last position were removed. Finally, a set of 1249 RNASeq confirmed operons containing 2826 genes was created. For analysis, the 1249 terminal genes of these RNASeq confirmed operons were selected and the terminal 200 nts from the gene sequence including the stop codon and the first 200 nts of the 3' region (after the stop codon) were used. For comparison, a more inclusive dataset containing all 4153 protein coding genes was created from GenBank U00096.3 by removal of non-coding genes and RNAs. Additionally, a dataset representing the intergenic regions of polycistronic operons was created by collecting the 3' regions of 1450 non-terminal genes from polycistronic operons. For comparison, the data pipeline was also tested on a set of 1000 random DNA regions. Due to exceptionally short ORFs, some genes had to be excluded from analysis. Datasets for analysis were exported in fasta format from the KNIME pipeline and passed on to the RNALfold algorithm (ViennaRNA Package 2.0) (Lorenz *et al.*, 2011) to analyze the folding properties of the operons 3' regions. The RNALfold algorithm was operated within Powershell (Microsoft) and used to screen the 3' environments for hairpin structures in 50 nt windows (RNALfold arguments: -L 50 -o –i). The RNALfold output was reimported into the data-pipeline for sorting and statistical analysis. Histograms depicting fold distribution and corresponding folding energy were created in Python (version 3.9.7, Python Software Foundation) (Van Rossum and Drake, 2009) using Matplotlib (Hunter, 2007), Numpy (Harris *et al.*, 2020) and Pandas (McKinney, 2010).

3 Results

3.1 Transcriptome Analysis

Previous studies on recycling relied on small model mRNAs or mRNA fragments. The results were likely influenced by the unnatural context used. The proximity of the ribosome to the model mRNA's start codon and the 5'-UTR, if containing a SD sequence for efficient initiation, could potentially favor re-initiation and thus prevent timely mRNA release (Chen *et al.*, 2017; Peske *et al.*, 2005). Random mRNA fragments resulting from RNase degraded polysomes lack stop codons and 3'-UTRs (Iwakura *et al.*, 2017). So far recycling has never been studied at the translation end of a long natural mRNA. While it is generally known that mRNAs have 3'-UTRs and often end with a transcription terminator hairpin, the prevalence of these and similar structures within the 3'-regions of genes was not well explored. For this reason, a detailed analysis of the *E. coli* transcriptome was performed to characterize the native termination context in *E. coli* mRNA. The aim was to identify a natural mRNA as a model mRNA for ribosome recycling studies in a physiological termination and recycling situation.

A data pipeline was created in the KNIME Analytics Software (Berthold *et al.*, 2008) to merge the *E. coli* genome and gene annotations from GenBank entry U00096.3 with the GSE52059 dataset containing RNASeq confirmed operon annotations (Conway *et al.*, 2014).The data pipeline allows to create subsets of specific gene regions for subsequent analysis (Fig. 14). A rather inclusive dataset containing the 3'-regions of 4153 protein coding genes was created. While non-protein coding genes like tRNAs have been eliminated from this list, it still contains pseudo genes, predicted genes and evolutionary artifacts. For a significant number of these genes, it is unclear if they are ever transcribed into an mRNA and translated to a protein. To better represent the active *E. coli* transcriptome, an additional dataset was created, representing mRNAs that have been found through RNA sequencing (RNASeq). Here the gene annotations from GenBank were fitted into the annotated borders of RNASeq confirmed operons reported by Conway et al. After eliminating non-protein coding genes and exceptionally small genes not suitable for subsequent analysis, a set of 1249 terminal genes, from monocistronic operons as well as the last genes of polycistronic operons, with their corresponding 3'-environments were created for subsequent analysis. For comparison, the 3'-regions of 1450 non-terminal genes of polycistronic operons, as well as 1000 random DNA sequences were also analyzed. For the analysis of the 3'-regions, the terminal 200 nts including the stop codon and the 200 nts after the stop codon were extracted from the *E. coli* genome. Due to exceptionally short ORFs, some genes had to be excluded from analysis. The folding properties of

the operons 3'-environments were analyzed with the program RNALfold (Lorenz *et al.*, 2011). The RNALfold algorithm was used to screen the 3'-environments for hairpin structures in 50 nts windows. The RNALfold output was reimported into the data-pipeline for further analysis (Fig. 14).

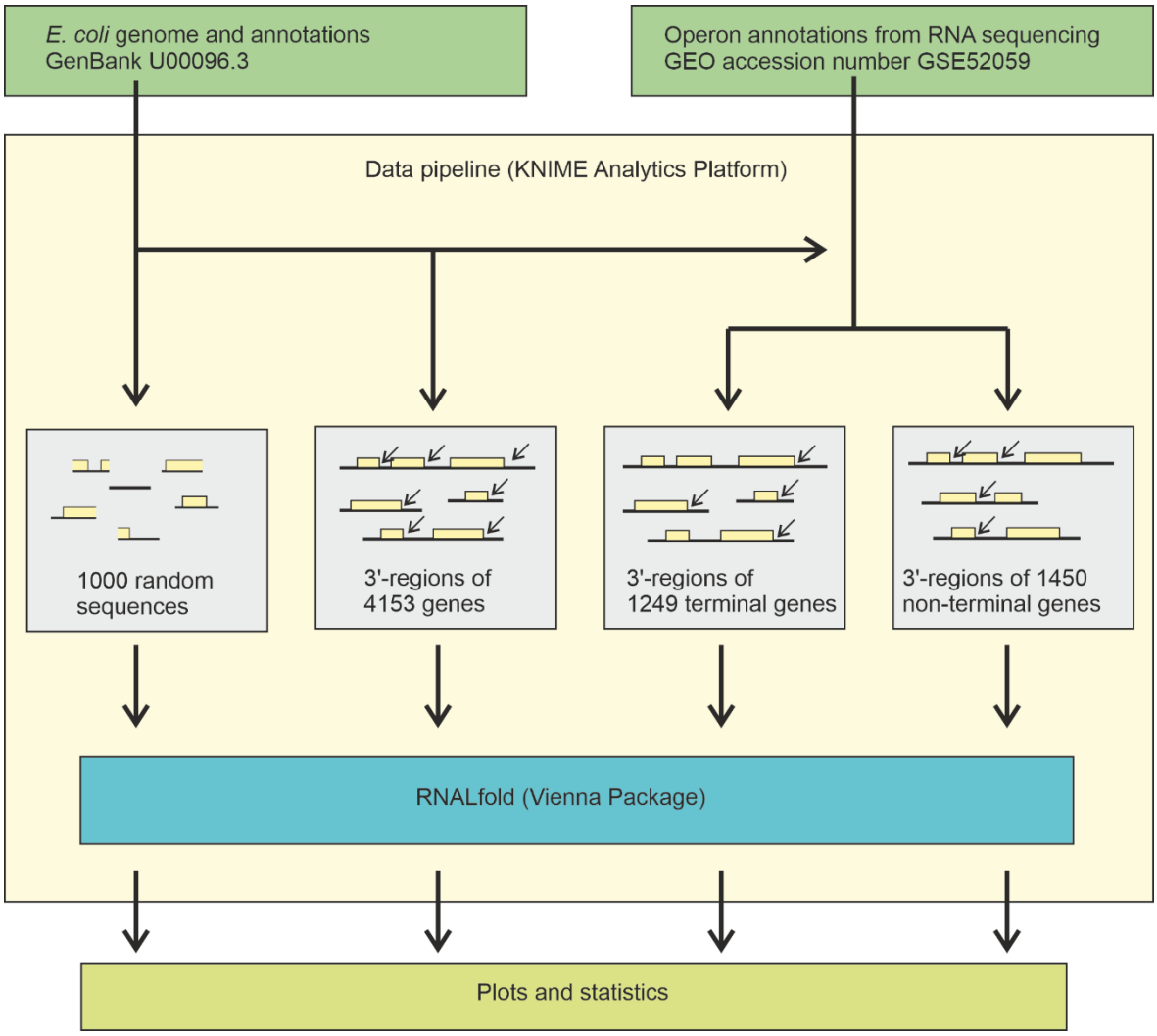

Figure 14. Computational analysis. *E. coli* genome and gene annotations from GenBank entry U00096.3 were used to list all 3'-regions of 4153 *E. coli* genes. Additional, 1000 random sequences were extracted for analysis. Merging with the GSE52059 dataset containing RNASeq confirmed operon annotations (Conway *et al.*, 2014), allowed the differentiation of terminal (1249) and non-terminal genes (1450) of confirmed operons. The 200 last nts of an ORF and the 200 nts after the stop codon were then screened for local RNA hairpin structures using RNALfold in 50 nt windows.

In total, 170 110 individual local hairpins have been found by RNALfold for all 4153 protein coding genes of *E. coli* (49 037 hairpins for the 1249 terminal genes). To better describe the characteristics of the identified hairpins, the central position of each hairpin was calculated. E.g. a hairpin stretching 11 nts from position 10 to 20 has its center in position 15. In total 85 172 hairpins were found by the RNALfold algorithm to center within the 200 nts around the stop codon (last 100 nts of the ORF and 100 nts of the 3'-region, 24 562 hairpins for the 1249 terminal genes). On average, each gene exhibited ca. 20 hairpins in that region. 18 hairpins were found in that region for the *lpp* gene (Fig. 15). Here, 11 of these hairpins center in the last 100 nts of the ORF, while only the transcription terminator and 6 additional hairpins center in the 3'-region after the stop codon. Aside from the strong transcription terminator (< -20 kcal/mol), the other structures in the 3'-region were rather weak (> -10 kcal/mol) whereas the majority of possible structures centering within the ORF is stronger (< -10 kcal/mol). Analysis of further examples highlight the diversity of the 3'-regions of different genes (Fig. 16). As for *lpp*, hairpin structures can be found both within the ORF and in the 3'-region. In the 3'-region after the stop codon, some hairpins can be found that are considerable stronger than other hairpin structures nearby. These often function as transcription terminators. Within the ORF there are generally slightly more possibilities for hairpins with a folding energy between -5 and -15 kcal/mol to form. Hairpins with a folding energy of more than -20 kcal/mol however are rare.

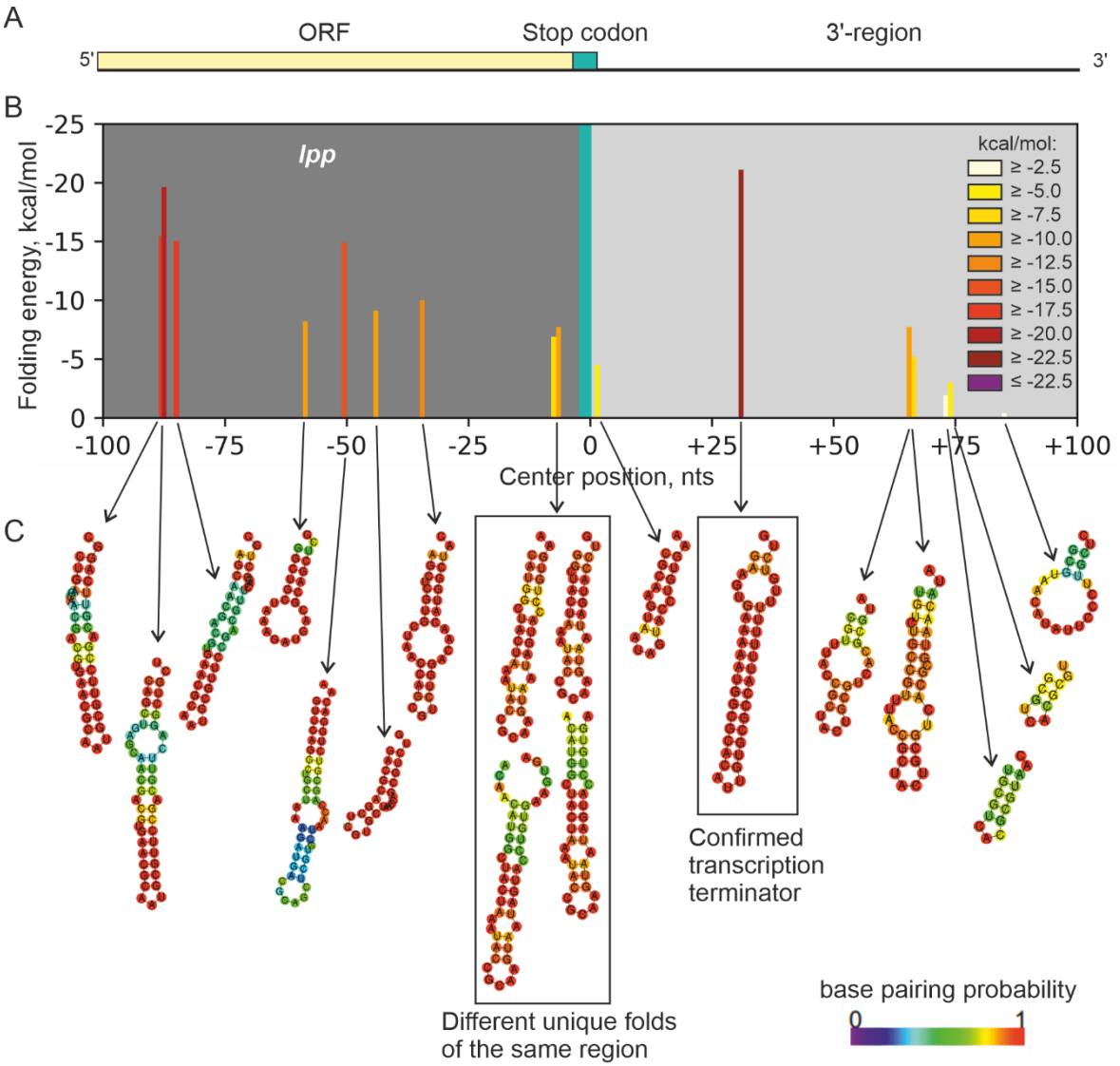

Figure 15. Local folds of the *lpp* gene. (A) The 100 last nts of the *lpp* ORF including the stop codon (teal) and the 100 nts after the stop codon (3'-region). (B) Local RNA hairpins found in the region around the *lpp* stop codon. Each bar represents a local hairpin structure with its height and color depicting the folding energy. Background color highlights the end region of the ORF (dark grey) and the 3'-region (light grey). (C) Structure of the hairpins from (B). Base pairing probability is indicated by color. The scheme was created using the RNAfold web server (Gruber et al., 2008; Lorenz *et al.*, 2011).

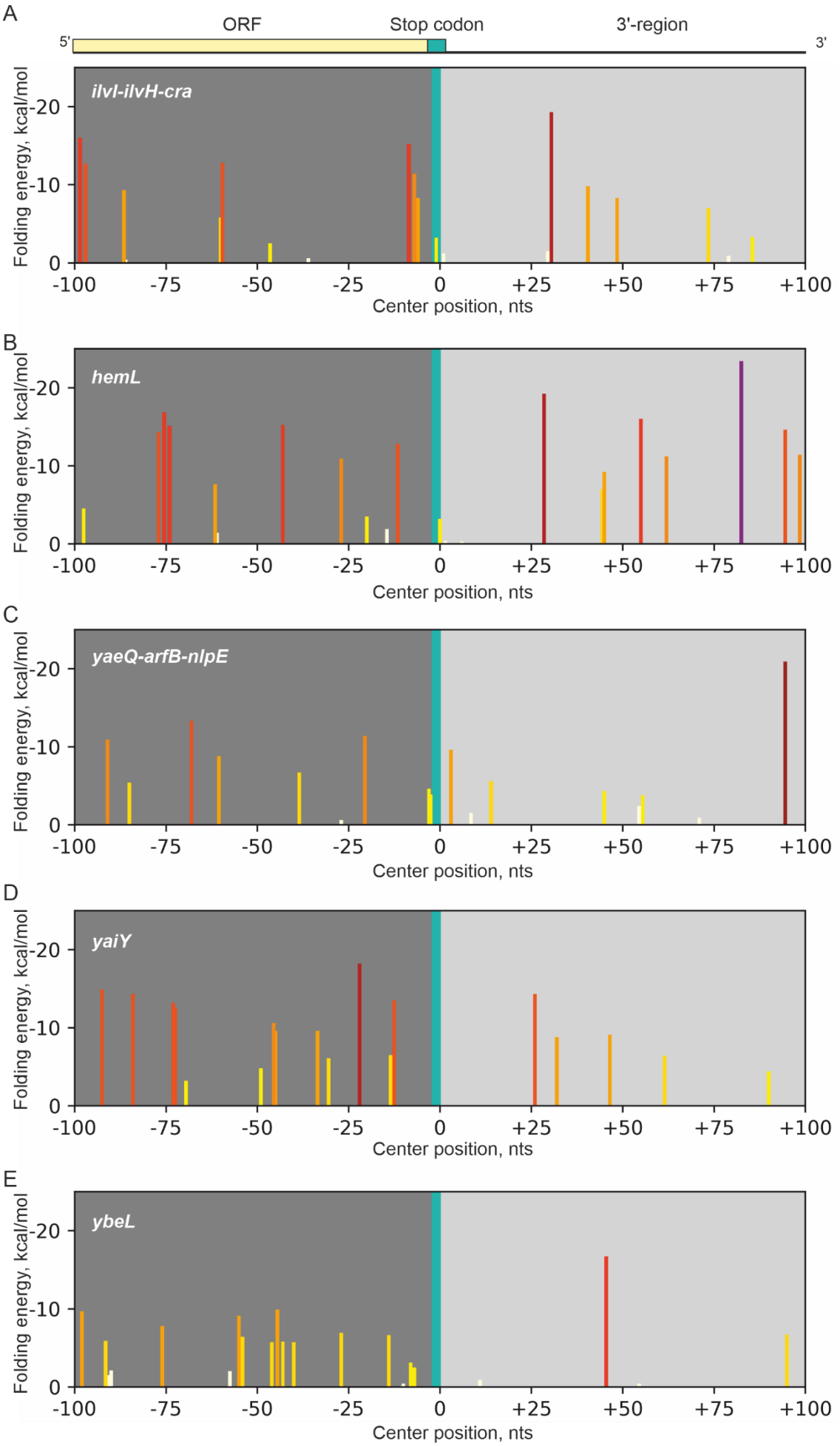
A
ORF
Stop codon
3'-region
5'
3'
ilvI-ilvH-cra
B
hemL
C
yaeQ-arfB-nlpE
D
yaiY
E
ybeL
Folding energy, kcal/mol
0
-10
-20
-100
-75
-50
-25
0
+25
+50
+75
+100
Center position, nts

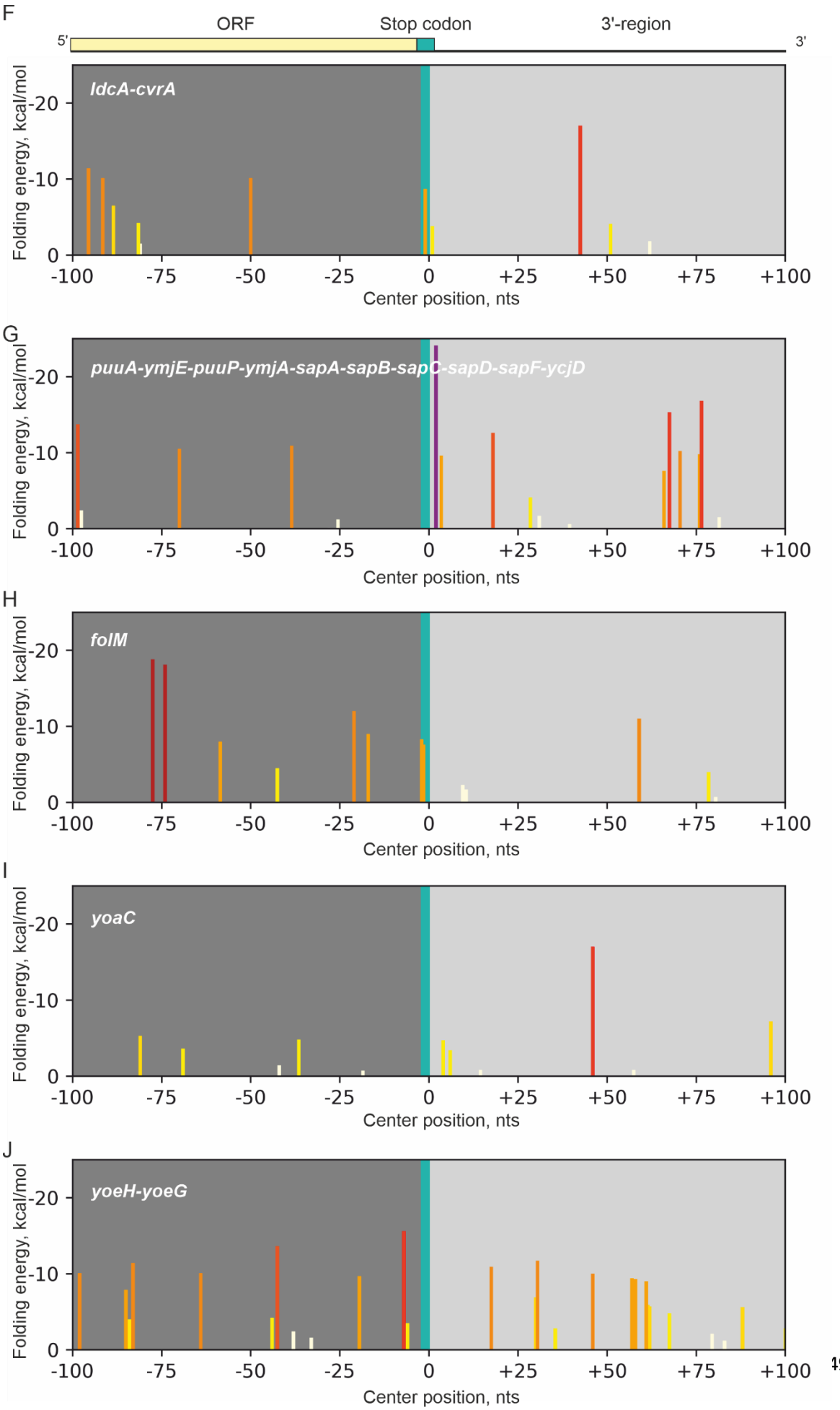
F
ORF
Stop codon
3'-region
5'
3'
ldcA-cvrA
G
puuA-ymjE-puuP-ymjA-sapA-sapB-sapC-sapD-sapF-ycjD
H
folM
I
yoaC
J
yoeH-yoeG
Folding energy, kcal/mol
0
-10
-20
-100
-75
-50
-25
0
+25
+50
+75
+100
Center position, nts

Figure 16. Local folds of terminal genes. Further examples showing the hairpins found in the 100 last nts of the ORF (dark grey) including the stop codon (teal) and the 100 nts after the stop codon (3'-region, light grey) as shown in Figure 15 for (A) *ilvI-ilvH-cra* (B) *hemL* (C) *yaeQ-arfB-nlpE* (D) *yaiY* (E) *ybeL* (F) *IdcA-cvrA* (G) *puuA-ymjE-puuP-ymjA-sapA-sapB-sapC-sapD-sapF-ycjD* (H) *folM* (I) *yoaC* (J) *yoeH-yoeG*.

To gain a comprehensive understanding, a representative subset of all hairpins from 1000 randomly selected genes was chosen from the datasets encompassing all genes, respectively terminal and non-terminal genes of RNASeq confirmed operons. The hairpins within these datasets were then aggregated and visualized using histograms, allowing for a more detailed analysis of their distribution and characteristics (Fig. 17). With color indicating folding energy, each bar represents the number of folds found for these 1000 genes centering on the position shown as the x-axis. As shown in the previous examples (Fig. 15, 16), folds occur both before and after the stop codon. It appears that there are slightly more folds inside the ORF than in the 3'-region. It is rather uncommon for mRNAs to form structures that center around the stop codon itself. The occurrence of hairpin structures between the stop codon and the subsequent 20 nts was found to be considerably low, indicating a notable scarcity of such structural elements in this specific region. Exceptionally strong RNA hairpins can be found in the 3'-region 10 nts after the stop codon. There is a clear accumulation of strong hairpins at around 25 nts after the stop codon. These strong hairpins might function as transcription terminators. The distribution of hairpins relative to the stop codon was even stronger when only the RNASeq confirmed terminal genes were observed (Fig. 17B). 65% of all genes and 83% of terminal genes have a hairpin stronger than -15 kcal/mol centered within 100 nucleotides after the stop codon that potentially serves as a transcription terminator (Tab. 1). In randomly selected RNA regions (Fig. 17D), only 47% of regions have such a hairpin within 100 nts.

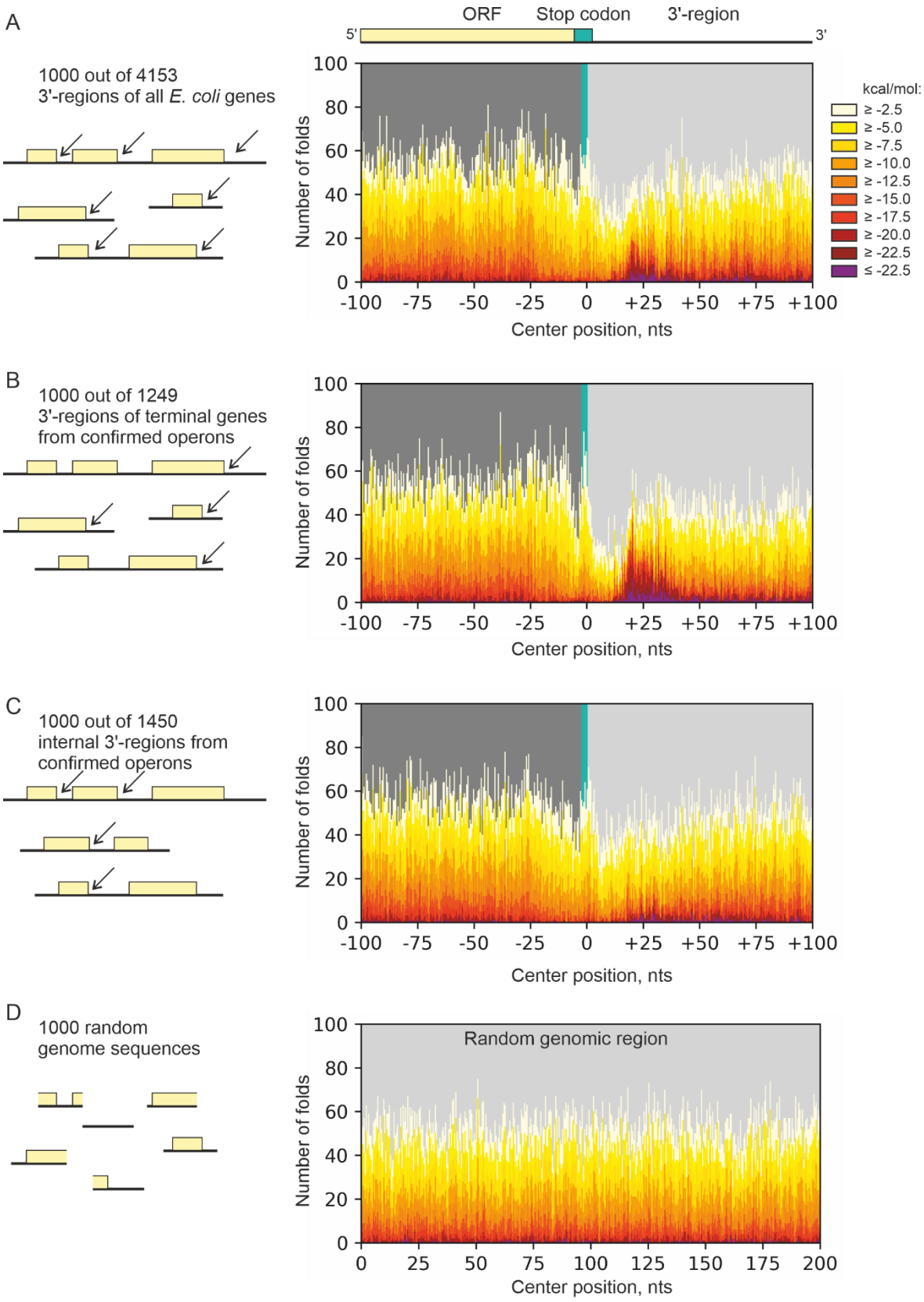

Figure 17. mRNA folding energy histograms. Hairpins from (A) 1000 randomly selected *E. coli* genes, (B) terminal genes of RNASeq confirmed operons, (C) non-terminal genes of polycistronic, RNASeq confirmed operons and (D) random DNA regions summarized as histograms. Left panels show exemplary schemes of operons (bold lines) picked for analysis. Genes are pictured as yellow

boxes with arrows highlighting the 3'-regions analyzed. Right panels show histograms of RNALfold detected local RNA folds stacked at their center position. Y-axis shows the number of folds. Color describes the folding energy.

Table 1. Prevalence of possible transcription terminators.

	% of genes/sequences that contains a hairpin stronger than -x kcal/mol within 100 nts after the stop codon		
Dataset	≤ -10 kcal/mol	≤ -15 kcal/mol	≤ -20 kcal/mol
All *E. coli* genes	92%	65%	31%
Terminal genes	97%	83%	45%
Non-terminal genes	92%	58%	24%
Random DNA regions	88%	47%	12%

A more comprehensive examination of all terminal genes provided further insights into the distribution of hairpin structures relative to the stop codon, particularly in terms of their folding energy (Fig. 18A, B). A pervasive background of small hairpins (with a folding energy smaller than -5 kcal/mol) was observed throughout the genome, irrespective of their genomic location. When compared to a region further downstream from the stop codon, the region within the ORF displayed a slightly higher prevalence of hairpins, primarily characterized by folding energies ranging between -15 and -5 kcal/mol. Notably, the region immediately adjacent to the stop codon (0 to 20 nucleotides downstream) exhibited a lower occurrence of such structures. A distinct population of remarkably strong hairpins (ranging from -10 to -30 kcal/mol) was observed in the region spanning 20 to 40 nucleotides after the stop codon. Analyzing the energy distribution of hairpin structures using a sliding-window analysis revealed the prevalence of these highly stable hairpins among terminal genes (Fig. 18C). Nearly 60% of all terminal genes exhibited a hairpin structure with a folding energy stronger than -15 kcal/mol, specifically centered within a 21-nucleotide window positioned 25 nts after the stop codon (15 to 35 nucleotides downstream from the stop codon). Moreover, hairpins with folding energies surpassing -20 kcal/mol were predominantly confined to this region, with few occurrences elsewhere apart from the subsequent 3'-region.

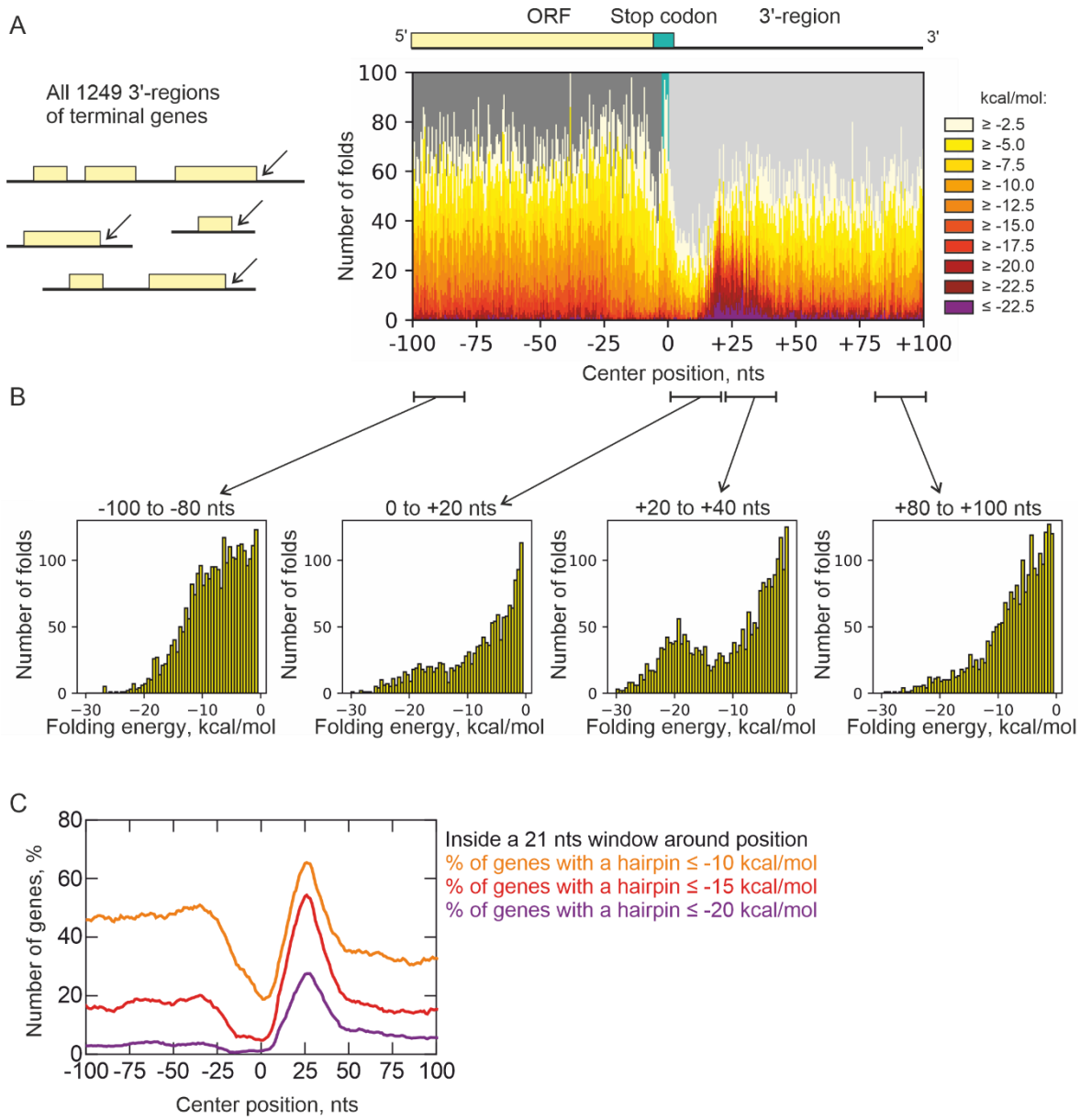

Figure 18. Folding energy distribution of hairpins at the stop codon of terminal genes. (A) All hairpins from 1249 terminal genes of RNASeq confirmed operons summarized as a histogram. (B) Folding energy distribution of hairpins inside the ORF, subsequent to the stop codon, between 20 and 40 nts after the stop codon and further downstream in the 3'-region. (C) A sliding-window analysis of the energy distribution of the data shown in (A) describes the percentage (y-axis) of terminal genes that have a hairpin stronger than a certain folding energy within a 21 nts window around the position relative to the stop codon (x-axis).

To summarize, it can be confirmed that *E. coli* mRNAs typically feature a structured 3'-UTR of at least 30 nts length that features a TTS or similar hairpin structures. Transcription terminators or similar strong hairpin structures are most common in the region 20 to 40 nts downstream of the stop codon. Terminal genes of RNASeq confirmed operons highlight these characteristics. The data indicate that mRNAs from highly expressed, well translated genes produced by intrinsic termination on the first TTS feature a rather accessible unstructured ORF end and a stop codon soon followed by a strong hairpin structure ending the 3'-UTR. 3'-UTRs that are shorter than 30 nts or do not form any structures are rather uncommon and do not represent the usual native termination context in *E. coli*.

3.2 Lpp mRNA as a Natural Model mRNA

To study ribosome recycling on a native mRNA *in vitro*, the natural mRNA of the major outer membrane prolipoprotein Lpp was chosen (Nakamura and Inouye, 1979). Lpp is one of the most abundant proteins in *E. coli* (Li et al., 2014). While the 324 nts long monocistronic lpp mRNA is among the smallest natural mRNAs in total size, its 47 nts 3'-UTR is of average length and complexity. It features a prominent transcription terminator hairpin with 14 base pairs (21.1 kcal/mol), 3 nts in the loop centering 31 nts after the stop codon (Fig. 19) (Nakamura and Inouye, 1979). The 78 aa ORF ends with AAG coding for lysine before the UAA stop codon. Lysine is the most common last codon of the RNASeq confirmed terminal genes present in 12.1% of terminal genes. The AAG codon being second most abundant with 5%. Lysine is reported to positively influence translation termination (Bjornsson et al., 1996). The efficient UAA stop codon is used in 72.6% of terminal genes. The UAAU termination signal has been reported to be the most efficient (Cridge et al., 2006; Major et al., 2002).

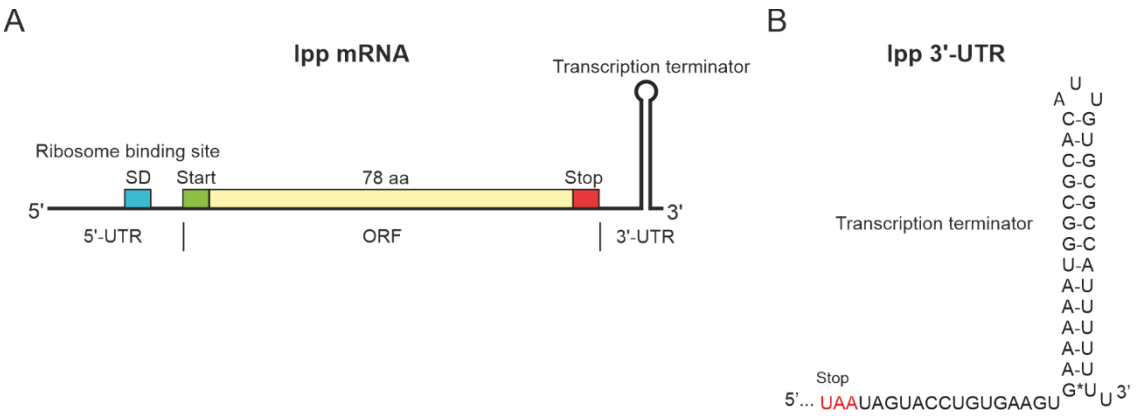

Figure 19. lpp mRNA. (A) Scheme of the lpp mRNA with its 78 aa long ORF, its 5'-UTR and the 3'-UTR with the transcription hairpin (Nakamura and Inouye, 1979). (B) Detailed sequence of the 47 nts long lpp 3'-UTR with the 14-base pair transcription terminator hairpin.

Recycling should happen at the stop codon of an mRNA after translation of the ORF. To study recycling of ribosomes on this native recycling position *in vitro*, those ribosomes must successfully perform the prior reactions. Ribosomes need to first initiate on the mRNA and secondly translate the ORF to the stop codon, producing the full-length peptide. The 5'-UTR of lpp offers several ribosome binding possibilities (Andreeva et al., 2018) enabling very efficient initiation. An initiation efficiency of >90% was determined by nitrocellulose filtration and scintillation counting. Translation was performed by reacting ICs (0.1 µM) containing lpp mRNA and labeled fMet-tRNA^{fMet} with TC containing EF-Tu, EF-G, total aa-tRNA and RF1 to prevent stop-codon-read-through. The emerging peptides have been separated by gel electrophoresis (Schagger and von Jagow, 1987) and the BODIPY-labeled products were visualized by fluorescence scanning of the gel (Fig. 20A). First peptides emerged almost immediately. Larger intermediate translation products are formed as early as 4 s after the reaction start. First 78 aa full-length peptides emerged as early as around 10 s after the reaction start and at 30 s the reaction reached a plateau. The intensities of the full-length product bands were quantified using imageJ (Schneider *et al.*, 2012) and plotted (Fig. 20B). The increasing quantity of full-length peptide was fitted with a delay phase followed by a single exponential equation (Eq. 6).

$$Y = IF\ (X < X_0, Y_0\ , Y_0 + (Amp - Y_0) * (1\ -\ exp(-k * (X - X_0)))) \qquad (6)$$

Here, X_0 describes the delay time of the exponential phase and the relative amount of translation products Y equals Y_0 for the duration of the delay. The amplitude is denoted by Amp. The delay

phase is followed by a one phase exponential association where k is the rate constant. The standard deviation is derived from biological replicates. The plotted data was obtained from the translation gel (Fig. 20A). Fitting of biological replicates calculates a length of the delay phase (X_0) of 13.7 ± 2.6 s. The rate constant k was calculated to be 0.26 ± 0.07 s^{-1}. An average translation speed τ_{total} of 17.9 ± 2.0 s can be calculated for the full-length protein with the equation $\tau_{total} = X_0 + (1/k)$. This corresponds to a ribosomal progression rate of 4.4 aa/s for the 78 amino acids protein. Up to 60% (Amp) of translating ribosomes finish the full-length peptide in the *in-vitro* translation system (Fig. 20B). The rate and the efficiency of the lpp-mRNA translation in the *in-vitro* system is within the reported range for translation *in vitro* (Wohlgemuth et al., 2010). This shows that the lpp-mRNA-based translation system is suitable as a model system for further studies.

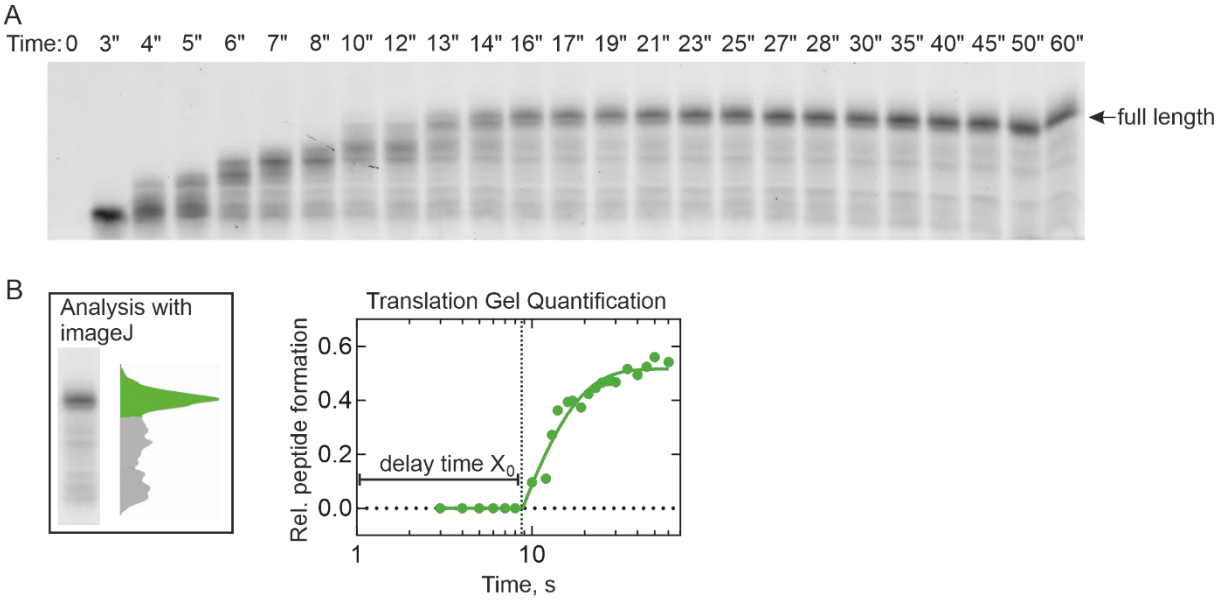

Figure 20. Translation of lpp mRNA. (A) Translation time course of lpp mRNA. (B) Quantification of the translation time course from (A). The 25 s lane is shown as an example. The full-length peptide (green) was quantified using ImageJ and plotted. The y-axis displays the peptide formation of the full-length protein relative to all visible peptide bands combined. Fitting of the full-length peptide quantification from this experiment and 4 additional biological replicates calculated a τ_{total} of 17.9 ± 2.0 s.

3.3 mRNA-Ribosome Dissociation Assay

The main goal of this work was to measure the release of an mRNA from the ribosome during recycling in a native termination context. This means that recycling happens at the stop codon of a translated ORF on a natural mRNA that has a common 3'-UTR. To measure release of the mRNA from the ribosome, an assay utilizing Förster resonance energy transfer (FRET) was established, using one fluorescence label on the small ribosomal subunit and one on the 3'-end of the mRNA. The efficiency of energy transfer from an excited donor fluorophore to a suitable acceptor fluorophore depends on the distance between the fluorophores. The smaller the distance is, the higher is the FRET efficiency. This allows FRET to be used to observe a biological reaction where the distance between two fluorescent labeled components change during the course of the reaction. FRET can be observed at a distance of up to 100 Å (Stryer, 1978). To optimize for a high amplitude and sharp signal easy to discriminate from the background noise during observation, it is beneficial that the fluorophores get close together during the cause of the reaction and are otherwise separated beyond the threshold of 100 Å. This limits the possible labeling positions on the 30S subunit as the mRNA was labeled at the 3'-end. 3'-end labeling of the mRNA was necessary for multiple reasons. While it is not impossible to chemically synthesize mRNAs as long as the native 324 nts long lpp mRNA, *in vitro* transcription appears to be cheaper and generally more practical. While an internal label can be introduced during chemical synthesis of small RNAs at any position, labeling of the 3'-end after *in vitro* transcription was the straightforward approach. Additionally, a label at the 3'-end is believed to less likely interfere with the recycling reaction as it should not enter the ribosome at any point.

3.3.1 Labeling Positions on the 30S Subunit

To establish FRET between a fluorophore on the 3'-end of the mRNA and a fluorophore on the 30S subunit, it was necessary to find a labeling position on the 30S subunit in close proximity to the mRNA tunnel entry site (Fig. 21). The ribosomal helicases S3, S4, and S5 surround the mRNA entrance side forming a tunnel like structure. As these ribosomal proteins help unwinding the mRNA, many parts of them are in direct contact with the mRNA. Notably, the flexible C-terminus of S3 and the N-terminus of S5 are very close to the mRNA. Other ribosomal proteins are located on the surface of the 30S subunit in proximity to the mRNA entry tunnel, such as S2, S8, S9, S10, S14

and S16. Unfortunately, all ribosomal proteins in this area aside from S9 are essential to the function of the ribosome and do not allow the creation of knock-out strains (Shoji et al., 2011) that would enable the purification of ribosomes from such strains and subsequent reconstitution with separately purified and labeled proteins as previously described (Belardinelli *et al.*, 2016a; Ermolenko *et al.*, 2007). To circumvent this problem, a different method had to be adapted to site-specifically label the proteins closer to the mRNA entry site.

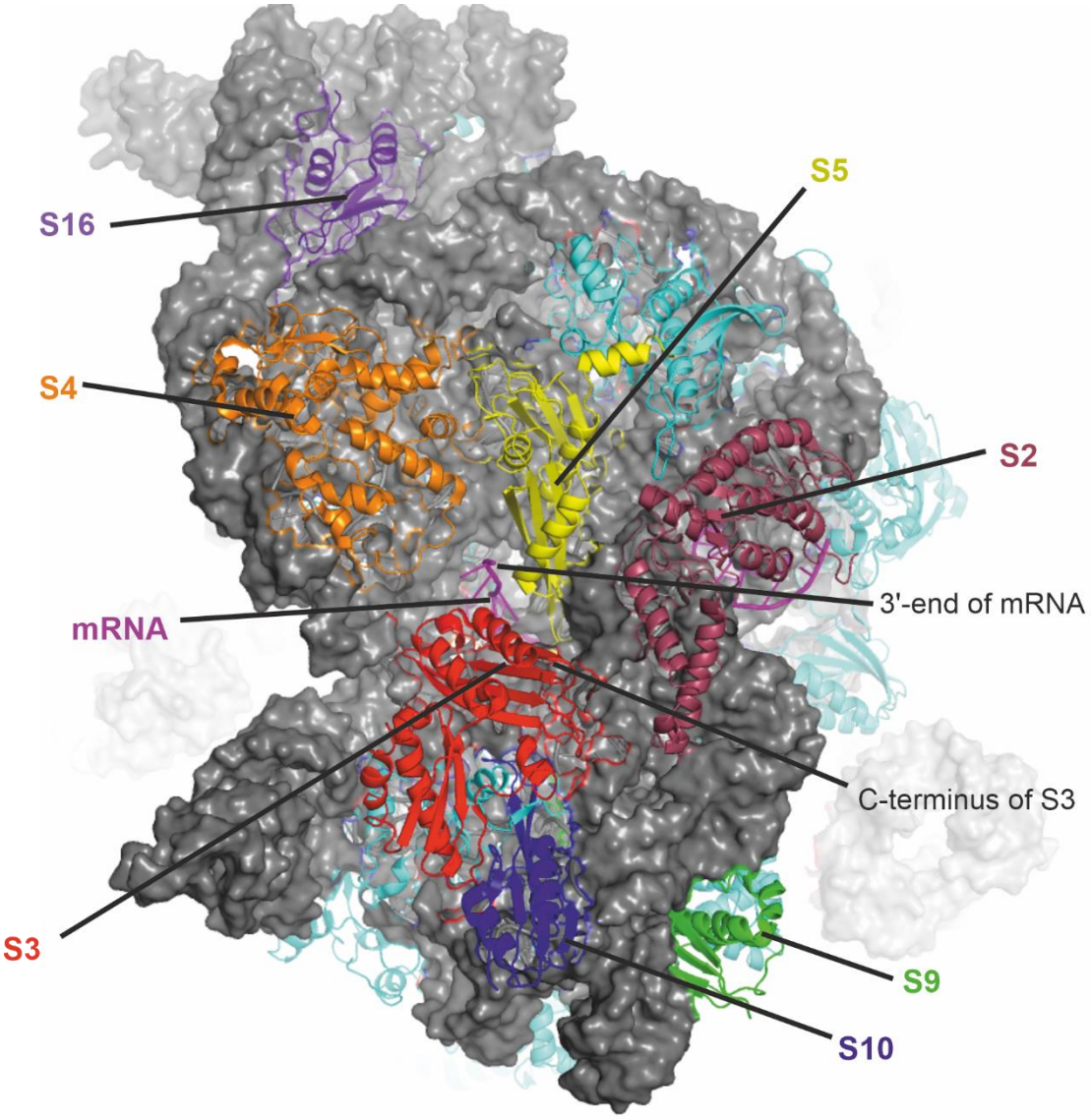

Figure 21. The 30S subunit and mRNA 3'-end. The entry site of the mRNA tunnel with the 3'-end of the mRNA (purple) is in the center. Ribosomal helicases S3 (red), S4 (orange) and S5 (yellow) surround the mRNA. The flexible C-terminus of protein S3 is close to the mRNA. Other ribosomal proteins in close proximity, S2 (pink), S9 (green), S10 (blue) and S16 (violet) are also highlighted. Image based on PDB files 6QNR (Rozov *et al.*, 2019).

3.3.2 Labeling of Ribosomal Proteins on the 30S Subunit with LplA

Most proteins of interest on the 30S subunit are essential for the cell, therefore, the creation of knock-out strains for later *in vitro* reconstitution was not possible. Instead, a method was needed to site-specifically label whole ribosomes. For this, an enzyme-supported, tag-based bioconjugation technique was adapted to introduce a fluorescent dye onto the 30S subunit. The technique functionalizes the mutant lipoic acid ligase $LplA^{W37V}$ that can introduce a functional group onto the lysine residue of the LplA acceptor peptide (LAP). Subsequently, a fluorophore can react with the functionalized lysine residue (Fig. 22A). The 13 amino acids LAP sequence has been designed to be introduced into proteins as a terminal or internal tag (Puthenveetil et al., 2009). In a two-step reaction the LAP-tag can first be functionalized with a norbornene moiety enzymatically via $LplA^{W37V}$ supported by ATP conversion (Fig. 22B). In a second step, the norbornene moiety can react with a Me-tetrazine conjugation via inverse-electron demand Diels-Alder reaction (Fig. 22C). This two-step reaction has been previously described (Baalmann *et al.*, 2018), but significant adaptations had to be made to the original protocol to suit the needs of big multimolecular complexes such as the ribosome.

The LAP-tagged proteins were overexpressed in BW25113 to out-compete the non-labeled chromosomal encoded wild type proteins *in vivo*. Overexpression of LAP-tagged proteins was necessary as ribosomal proteins appear in big polycistronic operons that are transcribed to some of the largest bacterial mRNAs. This complex operon structure makes genomic manipulations that interfere with expression of other essential downstream genes highly problematic. Overexpression bypasses these problems and adds flexibility as changing a plasmid-encoded gene is disproportionally easier than creating a new genome-manipulated strain. Overexpression of ribosomal proteins was monitored via SDS-PAGE, but in some cases there was no distinct band visible. Ribosomes were then purified from the overexpression cell lines in an analytical scale. Labeling was tested with Me-tetrazine conjugated Cy3 as previously described. Many LAP-tag positions were tested for labeling efficiency, notable proteins S3, S5, S9, S10 and S16 were successfully labeled as determined via fluorescence scanning and quantification of SDS-PAGE separated samples and spectrophotometrical measurement (Fig. 23).

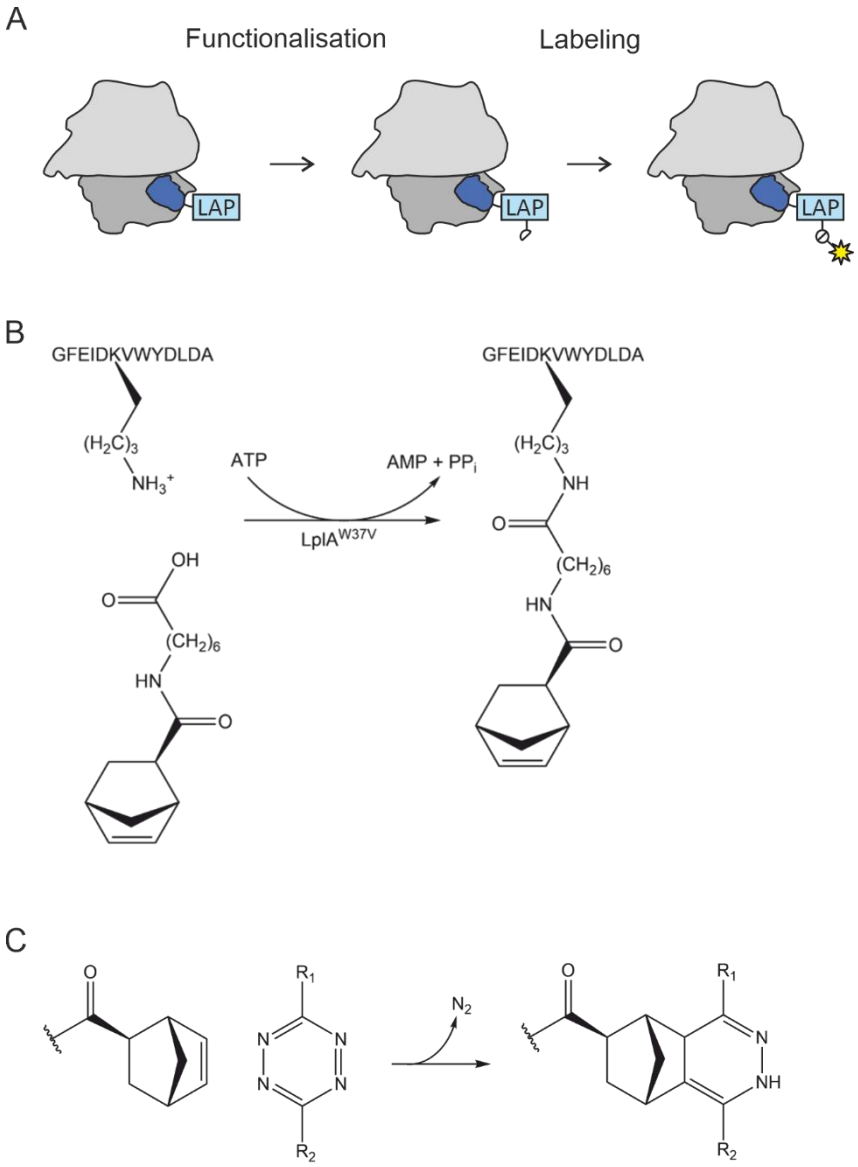

Figure 22. Ribosome labeling using the LAP-tag chemistry. (A) Scheme of the two-step labeling reaction used for ribosomal proteins. In the first step, the LAP-tagged ribosomal proteins are functionalized with a reactive norbornene group using the lipoic acid ligase mutant LplA^{W37V} (detail in B). In the second step, a fluorophore can couple with the lipoic acid group via a bio-orthogonal reaction (detail in C). (B) Reaction scheme shows the functionalization of the lysine residue in the 13-aa LAP-tag with a norbornene moiety via LplA^{W37V} supported by ATP conversion (Best et al., 2015). (C) Scheme of the norbornene moiety reacting with the Me-tetrazine conjugation via inverse-electron demand Diels-Alder reaction (Baalmann *et al.*, 2018).

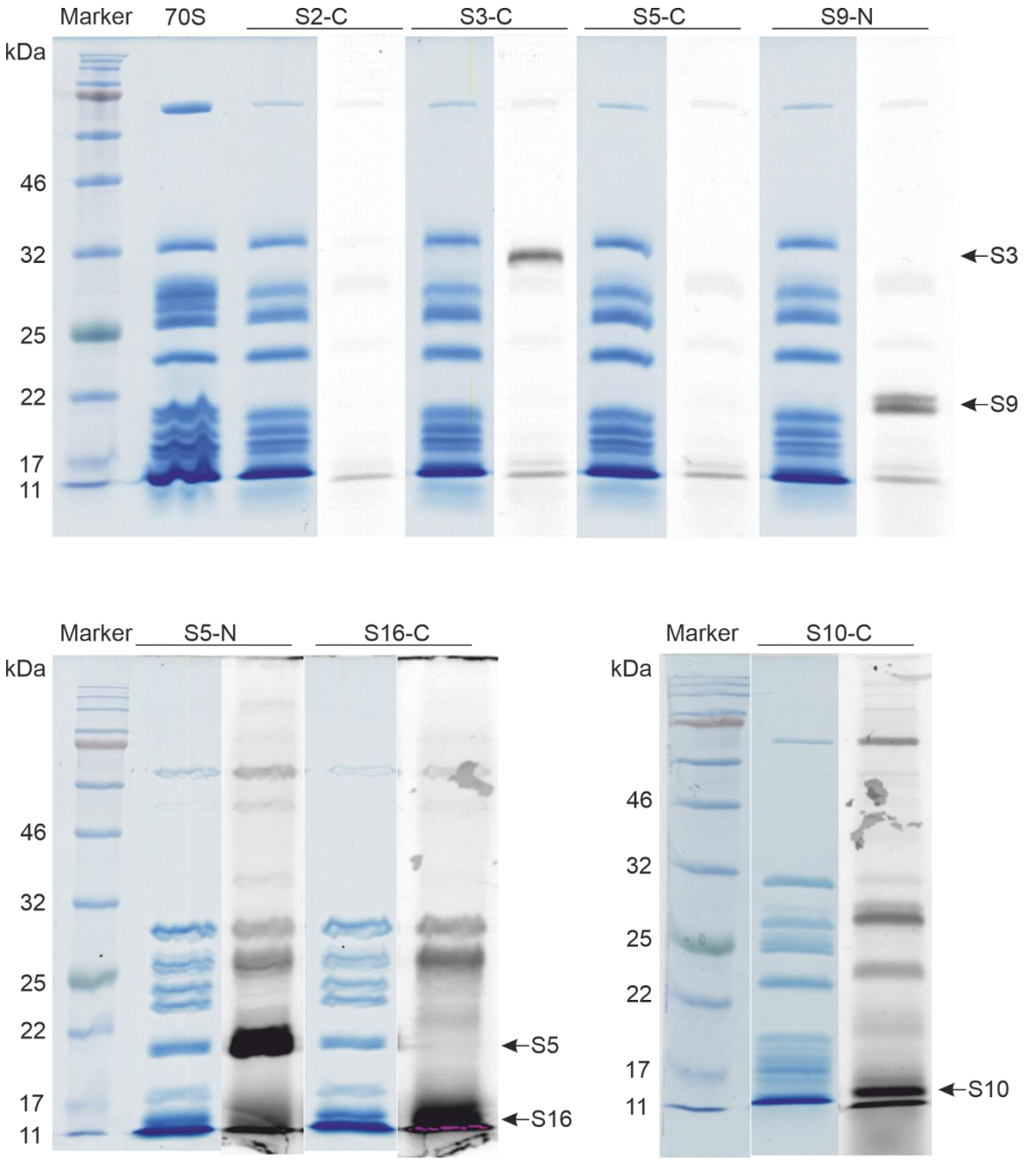

Figure 23. Labeling of ribosomal proteins. Coomassie stains (blue, left) and fluorescence scans (black, right) of SDS-PAGE of purified and Cy3-Me-tetrazine-labeled ribosomes from BW25113 overexpressing the plasmids pMW2d-S2C, pMW2-S3C, pMW2d-S5C, pMW2d-S5N, pMW2d-S9N, pMW2c-S10C, pMW2c-S16C. Bands of labeled proteins are marked.

From the pool of prospective labeling positions, S3C and S9N were selected. S9N was preferred due to the non-essential nature of the S9 gene, allowing a S9-knockout cell line to survive(Shoji *et al.*, 2011). This made it unlikely that the LAP-tag on S9 would interfere with the activity of ribosomes. On the other hand, S3C was chosen because it is structurally closest to the 3'-end of mRNA. Active ribosomes were then prepared from both variants at a large scale and labeled with Cy3-Me-tetrazine (Fig. 24A). To evaluate their performance, the active ribosome labeled with Cy3-Me-tetrazine were used in a rapid kinetic assay. The complexes programmed with a fluorescein marked mlpp-test mRNA were mixed rapidly with elongation, release, and recycling factors using a stopped-flow apparatus (Fig. 24B, C). The signal to noise ratio was found to be superior for the S3C-mRNA pair. However, fluorescein was intrinsically sensitive to the reaction and fluorescence changes from fluorescein-labeled mRNAs could not be attributed to specific reaction steps (Fig. 24D).

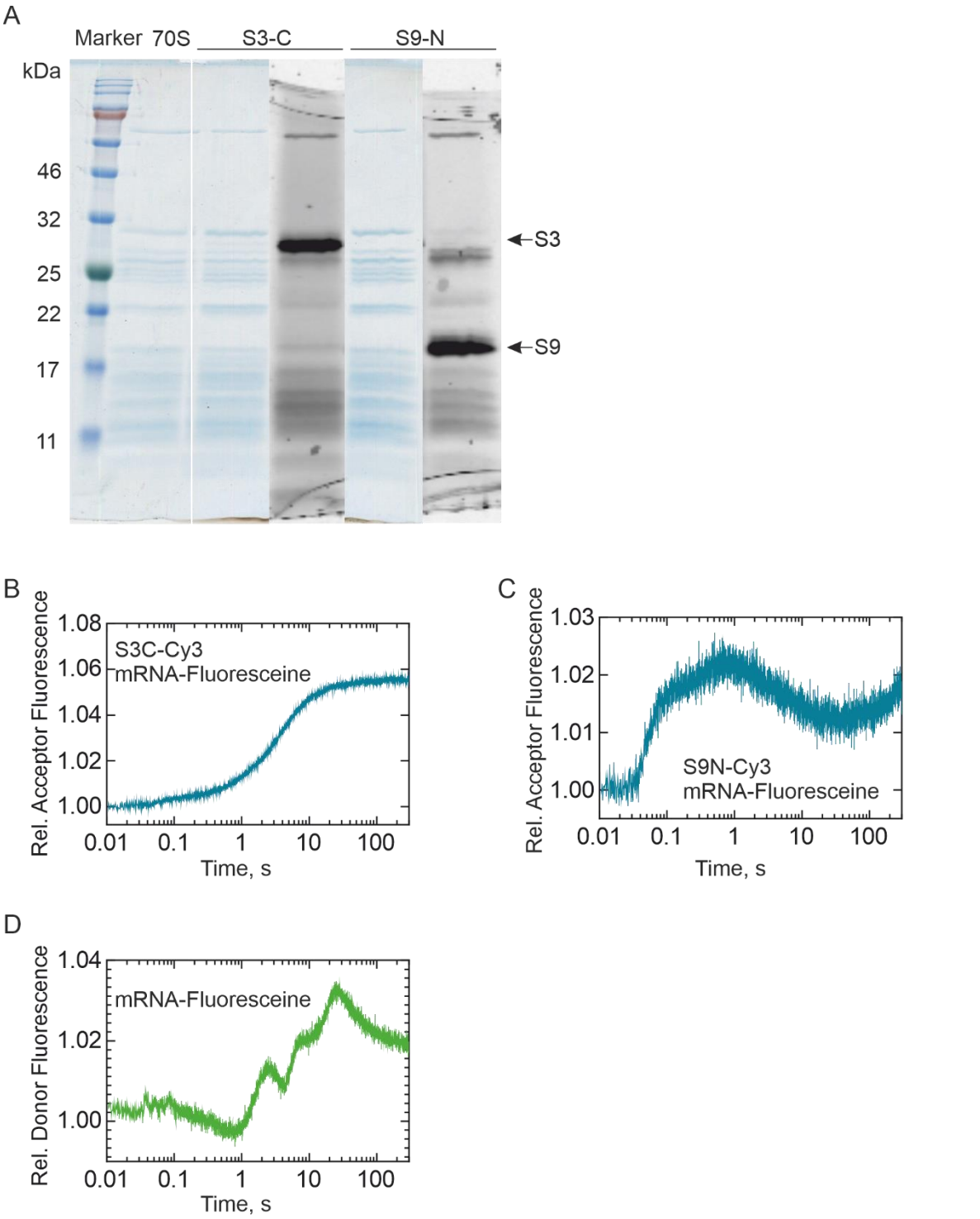

Figure 24. Testing of labeling positions S3-C and S9-N. (A) Coomassie stains (blue, left) and fluorescence scans (black, right) of SDS-PAGE of preparative scale purified and Cy3-Me-tetrazine-labeled ribosomes. (B) Performance of the S3-mRNA FRET pair. Purified ICs (0.1 µM) from S3-C-Cy3 labeled ribosomes programmed with mlpp-test mRNA labeled at the 3'-end with fluorescein were mixed in the stopped-flow apparatus with the full set of elongation, release and recycling components (4.5 µM aa-tRNA, 5 µM EF-Tu, 4 µM EF-G, 0.5 µM RF1, 0.5 µM RF3, 5 µM RRF, 1 µM IF3 and 1 mM GTP) and an unlabeled chaser mRNA (1 µM). To measure the fluorescence emission, a LED emitting at a wavelength of 470 nm was employed. The acceptor fluorescence signal was then

measured using a KV550 filter. (C) Performance of the S9-mRNA FRET pair. Experiment was carried out as in (A) but with S9-N-Cy3 labeled ribosomes. (D) Intrinsic fluorescence changes of a fluorescein labeled mRNA. Experiment as in (A) but with purified ICs (50 nM) from unlabeled ribosomes programmed with fluoresceine labeled lpp-no-Pin mRNA mixed with the full set of elongation, release and recycling components (25 µM aa-tRNA, 10 µM EF-Tu, 1 µM EF-G, 0.5 µM RF1, 0.5 µM RF3, 0.5 µM RRF, 1 µM IF3 and 1 mM GTP) and an unlabeled chaser mRNA (1 µM). To measure the fluorescence emission, a LED emitting at a wavelength of 470 nm was employed. The fluorescence signal was then measured using a KV500 filter.

The C-terminal position of S3 was finally chosen for preparative scale purification and those ribosomes were used for further experiments. S3 is amongst the proteins close around the mRNA entry tunnel, with the C-terminus pointing towards the cytosol. However, labeling with the LAP/LplA method exhibited some degree of non-specific labeling background. In particular, other ribosomal proteins were labeled, albeit to a lesser extent. This unspecific labeling may arise from either the acceptance of alternative peptide sequences by LplA or the reactivity of the anhydride intermediate generated by the norbornene substrate and AMP (Baalmann *et al.*, 2018). Reduction of the functionalization step to only 30 min improved the site specificity of the labeling (Fig. 25).

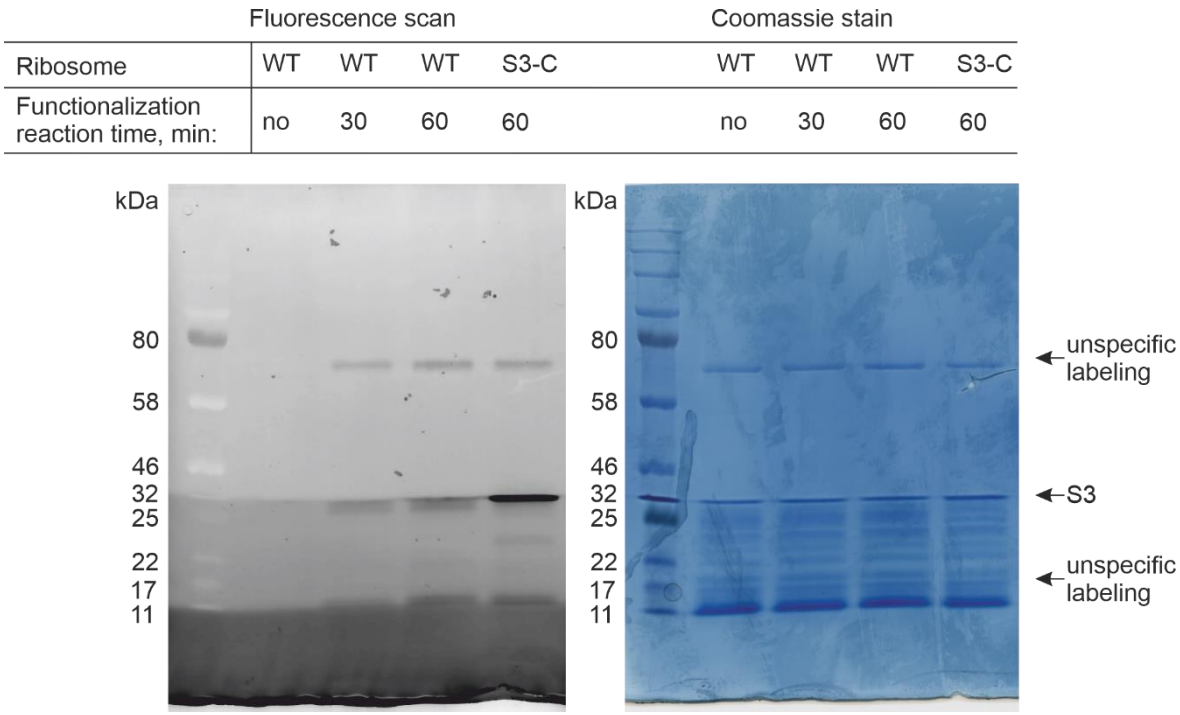

Figure 25. Optimization of labeling protocol. Fluorescence scans (black, right) and coomassie stains (blue, left) of SDS-PAGE separated S3-C-LAP tagged and untagged (WT) ribosomes after labeling reaction with Cy-3-Me-tetrazine. Unspecific labeling background is absent when the functionalization reaction with LplA has not been carried out. Labeling background is weaker for shorter functionalization incubation time. Efficient and site specific labeling requires the LAP-tag.

While Cy3 was used for the initial labeling test, the modular and scalable two-step reaction of the LAP/LplA method made it easy to label ribosomes with various Me-tetrazine conjugated dyes. As fluorescein was found to be suboptimal as a donor fluorophore (Fig. 24D) different dye pairs had to be used for different experiments. For rapid kinetic experiments, the ATTO488 to ATTO647N FRET-pair proved most suitable for demonstrating the release of the mRNA from the 30S subunit during recycling. For single molecule experiments, Cy5-labeled ribosomes were used in combination with Cy3-labeled mRNAs. With the optimized labeling protocol, which involves a 30-minute functionalization step, the proportion of unspecific labeled ribosomes was found to be only 2.5%. The reduced overall labeling efficiency of 50 to 60% for Cy5 and ATTO488 labeled ribosomes (Fig. 26) was sufficient for the following experiments.

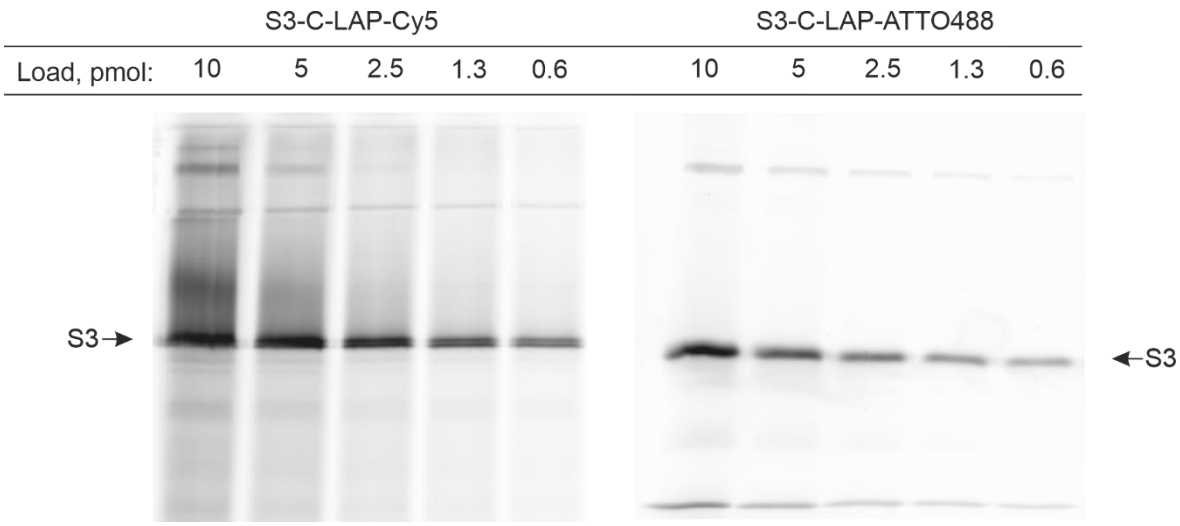

Figure 26. S3 labeled ribosomes. Fluorescence scans (black, right) of SDS-PAGE separated S3-C-LAP ribosomes after labeling reaction with Cy5 (left) and ATTO488 (right). For better visual assessment of the labeling efficiency and background, varying quantities of ribosomes were loaded into each lane.

To compare the activity of tagged and labeled ribosomes with unmodified wild-type ribosomes, initiation complexes programmed with lpp mRNA were created and translation was carried out as previously described. Translation products were separated on a gel (Fig. 27). The quantity of full-length protein was quantified, plotted, and fitted to assess the translation rate. Notably, there were no significant differences in translation speed observed among the various ribosome variants, indicating that the labeling and tagging modifications did not significantly impact the overall translation activity of the ribosomes.

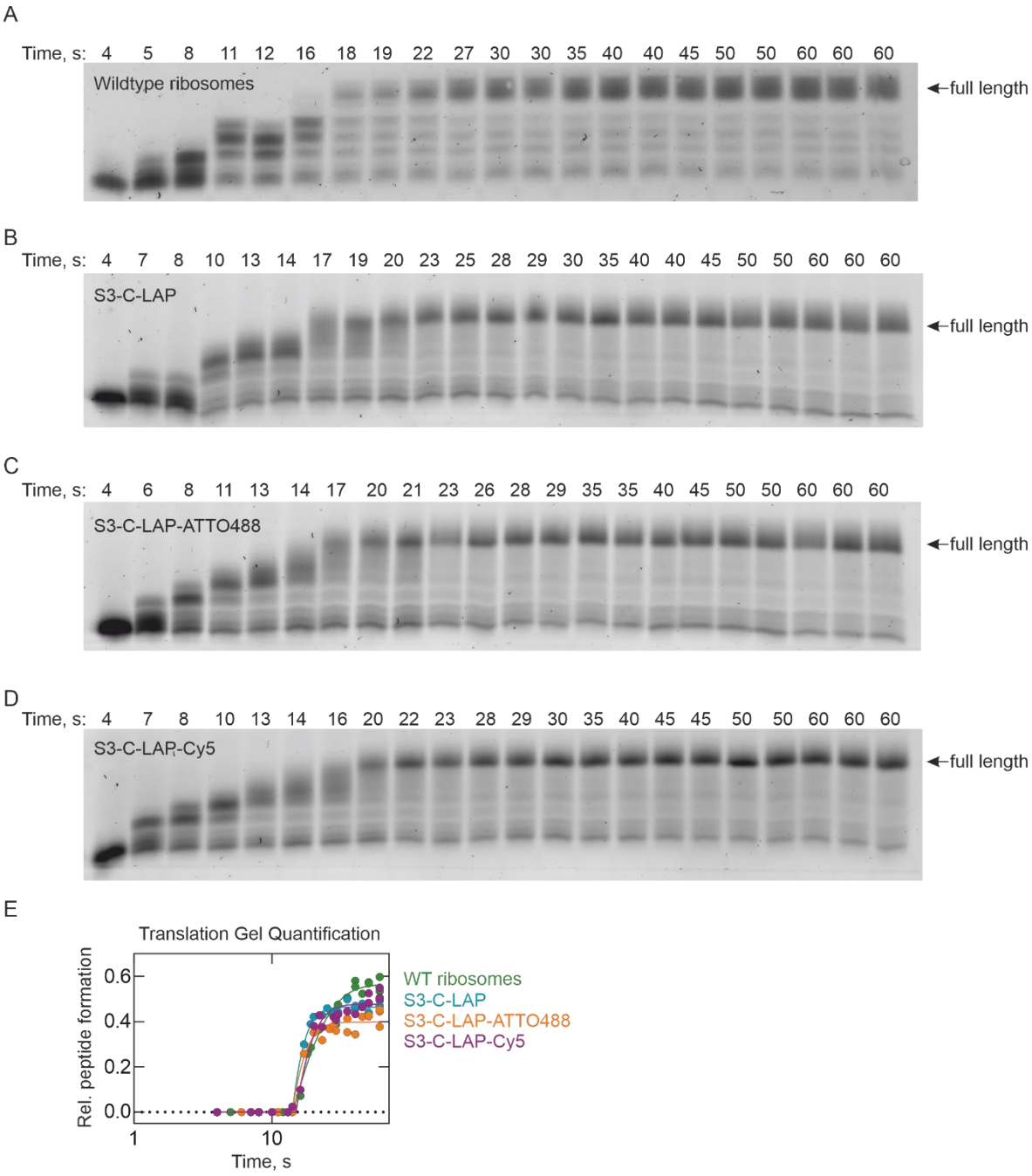

Figure 27. Activity of mutant and modified ribosomes. Translation time courses of lpp mRNA with (A) wild-type ribosomes, (B) S3 C-terminal LAP-tagged ribosomes, (C) S3-C-LAP-tag ATTO488 labeled ribosomes and (D) S3-C-LAP-tag Cy5 labeled ribosomes. (E) Quantification of the translation time course from (A-D).

3.3.3 The mRNA-S3 FRET Pair in Rapid Kinetic Experiments

For rapid kinetic experiments, the stopped-flow apparatus was used. The apparatus contains two syringes to separately load the reactants. In the following experiments, the first syringe always contains the ribosome complex, the second syringe contains translation factors and components. By applying pressured air, the stopped-flow apparatus flushes a portion of both samples into the measurement cell. Here, a light source illuminates the sample while a perpendicular photomultiplier detects light emission from the sample. The donor fluorophore ATTO488 (Fig. 28A) was excited at 470 nm with an LED light source. The maximum emission wavelength of ATTO488 is at 520 nm (Fig. 28B). Although the maximum excitation wavelength of ATTO647N (Fig. 28A) is at 646 nm, the spectra have sufficient overlap between 520 nm and 640 nm to enable energy transfer (Fig. 28B). The distance difference between the emission spectra of the two dyes made it possible to measure the acceptor fluorescence with a red sensitive photomultiplier after passing an RG 665 nm filter without interference of the donor fluorescence. For the experiment, ICs (50 nM) that contain the 3'-ATTO647N labeled *in-vitro* transcribed native lpp mRNA and ribosomes labeled on the C-terminal LAP-tag of S3 were loaded into the first syringe of the stopped flow apparatus (Fig. 28C). Elongation components, release and recycling factors (50 µM aa-tRNA, 50 µM EF-Tu, 2.5 µM EF-G, 1 µM RF1, 1 µM RF3, 5 µM RRF, 1 µM IF3, 1 mM GTP) and unlabeled chaser mRNA (0.25 µM) were loaded into the second syringe (Fig. 28C); the concentrations are final concentrations in the measurement cell after mixing. Rapid mixing in the measurement cell now allows observation of fluorescence signal changes during elongation, termination and recycling (Fig. 28D). Initiation complexes (ICs) started with high initial acceptor fluorescence (5 V) (Fig. 28D). During the reaction, the acceptor fluorescence signal decreased to a lower level (3.8 V). After stabilization of the signal at medium fluorescence, the signal dropped to a low value (2.3 V) and plateaued.

It was necessary to characterize and assign all the observed FRET signals to determine whether full dissociation of the mRNA is reached at the end of the measurement. Although a 665 nm filter was used, bleed through is possible for the excitation light as well as some partial excitation of the acceptor fluorophore at the donor excitation wavelength (470 nm). Thus, it was necessary to compare the FRET related acceptor fluorescence signal with the background fluorescence of the single fluorophores (Fig. 28D). The mRNA-release experiment was repeated with purified ICs that contain only the ATTO647N labeled mRNA and unlabeled ribosomes (acceptor control), or labeled ribosomes and unlabeled mRNA (donor control) and an additional buffer control shows the background signal without fluorophores in the sample. Donor, acceptor and buffer controls remain

at relatively constant values (acceptor at 2 V, donor at 1.1 V and buffer at 0.7 V) throughout the experiment. In the experiment with both fluorophores, the acceptor fluorescence drops to 2.3 V at the end of the reaction. After subtracting the buffer background from the single fluorophore controls, a donor background of 0.4 V and an acceptor background of 1.3 V is calculated. The sum of the single fluorophore backgrounds added to the buffer background is 2.4 V which matches the end level of the experiment with both fluorophores (2.3 V).This means that no FRET between donor and acceptor fluorophores takes place at the end of the reaction and indicates a full separation of ribosomes and mRNA (Fig. 28D).

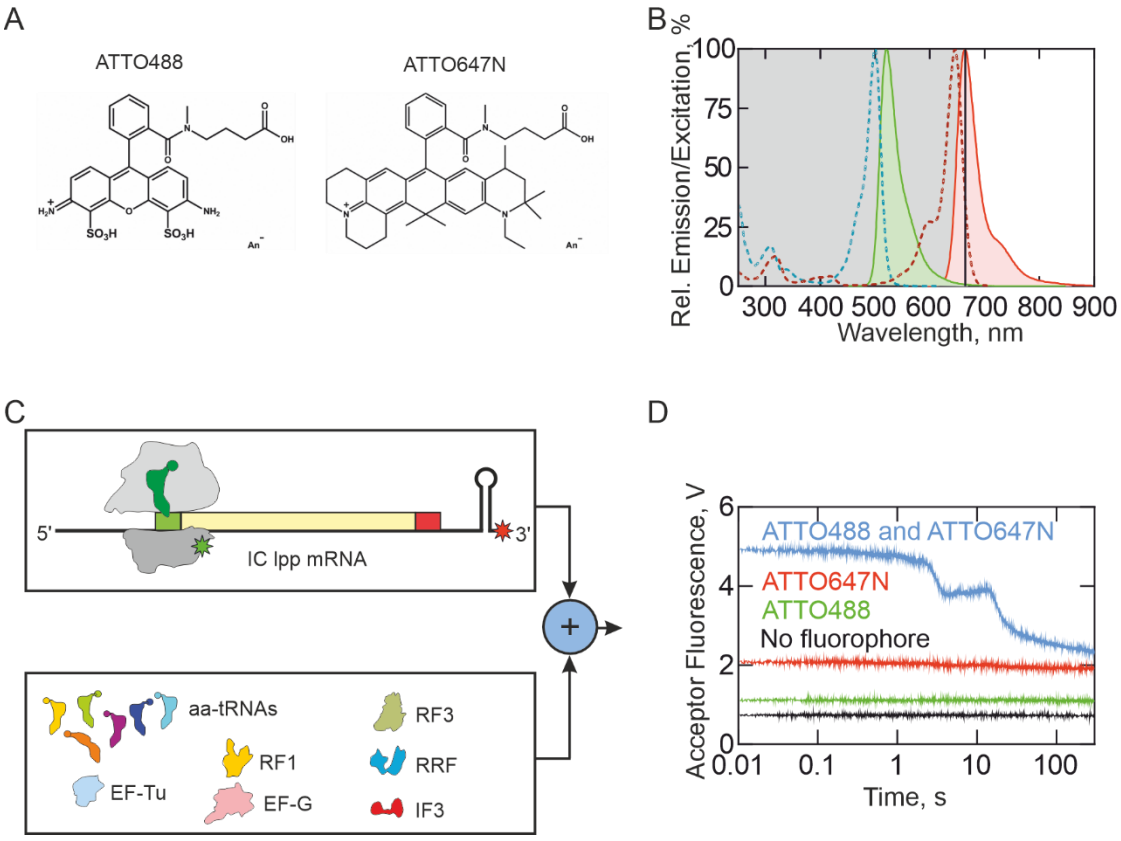

Figure 28. mRNA-ribosome dissociation assay. (A) Structure of the used fluorophores ATTO488 and ATTO647N. (B) Emission (filled) and absorption (dotted) spectra of ATTO488 (green) and ATTO647N (red). In all following acceptor fluorescence experiments with the ATTO488 and ATTO647N FRET pair, a LED light source emitting at 470 nm was used. Emission was measured with a red sensitive photomultiplier after a RG665 high-pass filter (indicated by the grey box). (C) Scheme of the reaction in the stopped flow apparatus. Purified ICs (50 nM) labeled with ATTO488 (green) at protein S3, lpp mRNA labeled at the 3'-end with ATTO647N (red) and initiator tRNA (green) were mixed with the full set of elongation, release and recycling components (50 µM aa-tRNA, 50 µM EF-Tu, 2.5 µM EF-G, 1 µM RF1, 1 µM RF3, 5 µM RRF, 1µM IF3 and 1 mM GTP) and an unlabeled chaser mRNA (0.25 µM). (D) The reaction described in (C) results in translation of the

lpp protein followed by termination and finally recycling. The reaction was performed either with the S3-mRNA FRET pair (blue), with only ATTO488-labeled IC and no label at the mRNA (donor control, green) or with unlabeled ribosomes and the ATTO647N-labeled lpp mRNA (acceptor control, red). Black Trace shows the background fluorescence if no fluorophores were present in the experiment. Traces shown are averages of 8 technical replicates and were recorded using the experimental setup described in (B).

3.3.4 Phase Assignment for the S3-mRNA FRET Pair

The initial decrease of the acceptor fluorescence in the mRNA-dissociation experiment was unexpected (Fig. 28B). It was assumed that ICs with S3-ATTO488 labeled complexes with 3'-ATTO647N labeled lpp mRNA would have a low FRET efficiency due to the length of the mRNA creating a significant distance between the fluorophores. The FRET efficiency was expected to increase during elongation because the ribosomes move towards the labeled 3'-end of the mRNA before mRNA release during recycling would disrupt FRET. Instead, the signal starts high, descends to a medium level where it remains constant for about 12 s before falling to the expected end level. The decrease of the fluorescence signal to the end level begins with the appearance of the full-length protein observed in the translation experiments (Fig. 29A) and serves as a marker to confirm phase assignment. Recycling should only happen after translation and release of the full-length protein at the stop codon. This means that the signal changes observed before the protein is fully synthesized must occur during the elongation phase. The initial decrease of the fluorescence signal must be related to some significant conformation change of the complex during translation. To test whether this conformation change is related to the mRNA, the same mRNA-release experiment was repeated with lpp mRNA variants lpp58, lpp38 and lpp18 that have shortened ORFs coding for the first 58, 38 and 18 amino acids, respectively (Fig. 29B); full length lpp has 78 amino acids. With the lpp58 mRNA, where the 20 C-terminal amino acids have been deleted, an initial decrease of the fluorescence signal is also observed but it is less pronounced compared to the experiment with the full-length lpp mRNA. The sharp decrease of the signal to the fluorescence end level begins earlier. When the shorter mRNAs lpp38 and lpp18 were used, no initial decrease of the acceptor fluorescence was observed but the signal remained constant during the entire elongation phase (Fig. 29B). Upon reaching the recycling phase, all mRNAs showed a similar loss of acceptor fluorescence intensity explained by the disruption of FRET through release of the mRNAs from the complexes. This indicates that the initial change of acceptor fluorescence observed during the elongation phase with the full-length lpp mRNA and similar but less pronounced with the lpp58 mRNA, indeed represents conformational changes of the mRNA.

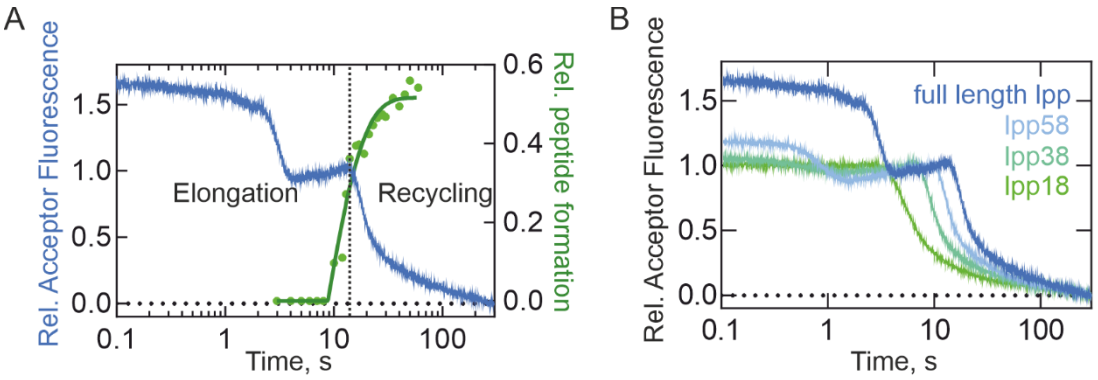

Figure 29. Assignment of the elongation phase of the mRNA-dissociation experiments. (A) Overlay of the fluorescence signal (blue, from Fig. 28D) with the formation of the full length lpp protein measured with translation gel quantification (green, from Fig. 20). (B) Translation of lpp variants with full length or shorter ORFs (number of amino acids is indicated) in the stopped-flow apparatus. The reactions were started by mixing labeled IC with the full set of elongation, release and recycling components (conditions as described in Fig. 28). Traces shown for the kinetic experiments are averages of 8 technical replicates and were normalized on the recycling phase.

To test if the structure of the mRNA causes the high initial FRET, the lpp mRNA structure can be analyzed using an *in silico* folding algorithm. Analysis of the lpp mRNA with the RNAfold program (Gruber *et al.*, 2008; Lorenz *et al.*, 2011) (Fig. 30A) showed that the lpp mRNA has a very high probability to be in a compact conformation with the 3'-end pairing to the 5'-region. In the IC the ribosome occupies the 5'-region of the mRNA at the start codon and due to the compact conformation of the mRNA, the 3'-end with the fluorophore is close to the FRET partner on the 30S subunit. During translation, the acceptor fluorescence signal drops as the mRNA structure is melted due to ribosomal progression on the ORF (Fig. 30B). In order to translate the ORF, the ribosome unwinds mRNA structures with the help of the ribosomal proteins S3, S4 and S5. Opening of the compact mRNA fold causes the 3'-end of the mRNA to be more flexible and to move further away from the ribosome. The larger distance lowers the FRET efficiency and is reflected by a lower overall acceptor fluorescence measured. For the shorter mRNAs lpp38 and lpp18, missing 40, and 60 C-terminal amino acids (120, 180 nts), respectively, the mRNA does not form such a compact conformation leaving the 3'-end more flexible in the IC. These mRNAs show a constant acceptor fluorescence during the elongation phase indicating a constant FRET efficiency throughout the reaction. The sharp drop in acceptor fluorescence at the end of the translation phase that is observed for all mRNAs (Fig. 29B) is the result of full separation of the labeled components in the recycling step FRET (Fig. 30B). The remaining acceptor fluorescence measured accounts for only the intrinsic bleed through of the fluorophores as previously shown (Fig. 28D).

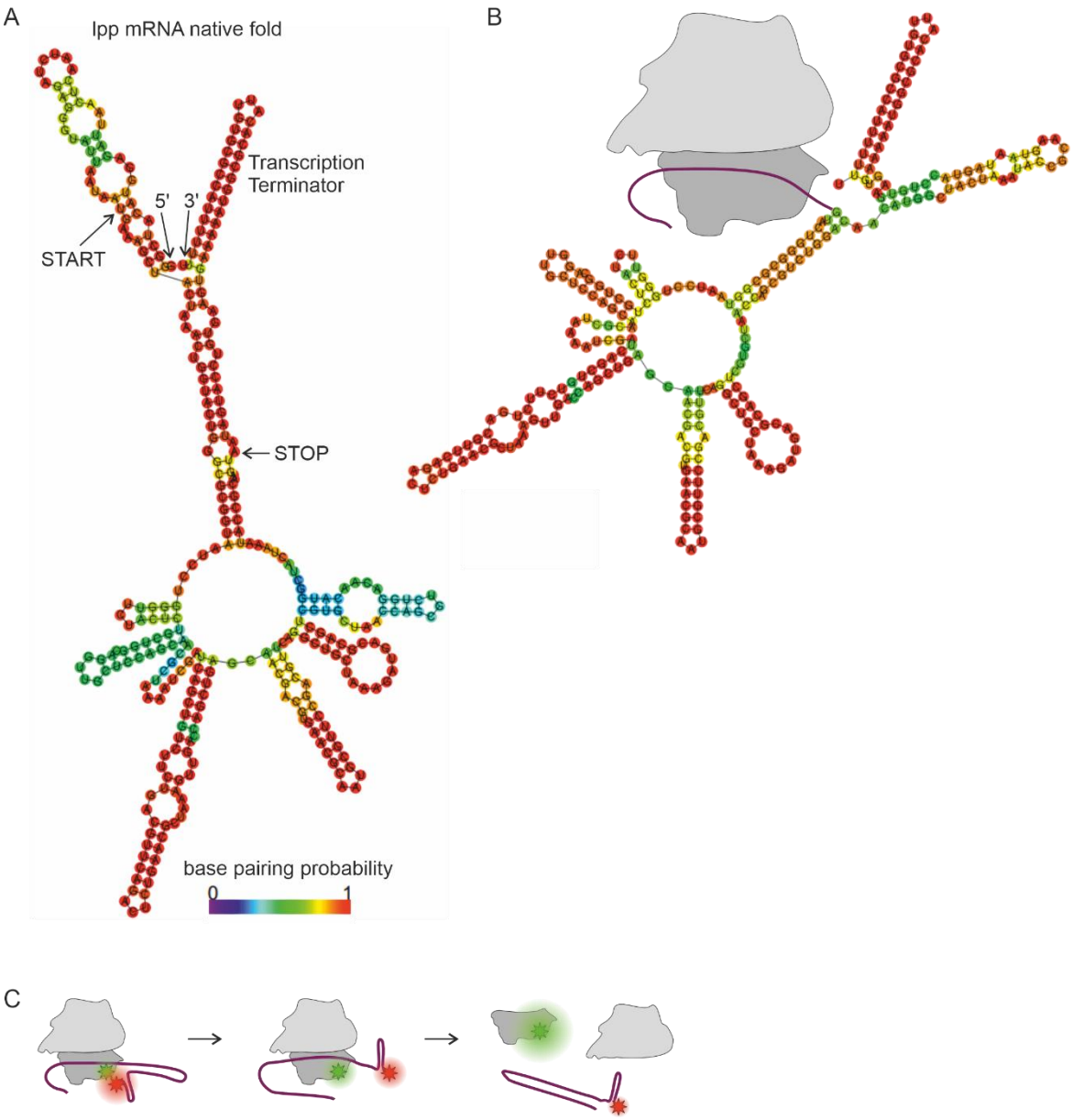

Figure 30. mRNA conformation. (A) Predicted fold of the full-length lpp mRNA. The compact super hairpin structure brings the 5'- and the 3'-end with the transcription terminator hairpin into close proximity. Base pairing probability is indicated by color. The scheme was created using the RNAfold web server (Gruber *et al.*, 2008; Lorenz *et al.*, 2011). (B) Predicted fold with the first 15 nts after the start codon occupied by the ribosome. (C) Model of mRNA structural changes during translation. Initially, in the folded conformation of the mRNA the fluorophores are in close proximity. During translation, the mRNA structure is melted by the ribosome, causing the 3'-end to move away from the ribosome, before the mRNA is finally released during recycling.

3.4 Recycling of Translating Ribosomes

3.4.1 Kinetics of mRNA Release upon Ribosome Recycling

The phase assignment of the mRNA-release experiment (Fig. 28) identifies the last phase of the reaction as the mRNA release. The stopped-flow trace obtained in this experiment with the full-length lpp mRNA can be fitted (Fig. 31A) with a delay followed by two exponential phases (decay) equation (Eq. 7):

$$Y = IF(X < X_0, Y_0, Y_0 + Amp_1 * (1 - exp(-k_1 * (X - X_0))) + Amp_2 * (1 - exp(-k_2 * (X - X_0)))) \quad (7)$$

As for equation (6), X_0 describes the delay time of the exponential phase and Y equals Y_0 for the duration of the delay. The amplitudes Amp_1 and Amp_2 are corresponding to the two rate constants k_1 and k_2. Fitting of 4 independent experiments determines a X_0 of 15.7 ± 0.8 s, a k_1 of 0.15 ± 0.2 s^{-1} and a k_2 of 0.014 ± 0.001 s^{-1}; Amp_1 is 62.5 ± 2.4 % of the total amplitude. The stopped-flow traces obtained with the mRNAs with shortened lpp ORFs, lpp58, lpp38 and lpp18, were also analyzed by fitting with equation (7) (Fig. 31B). Calculated delay phase duration X_0, rate constants k1 and k2 and the relative amplitudes of the two phases for the lpp mRNA variants are summarized in Table 1. Plotting of the calculated delay times X_0 revealed a linear dependence on the length of the OFRs (Fig. 31C). From the slope of the linear fit, it can be calculated that the delay phase X_0 increases by 1 s per 4.9 amino acids (aa). The inverse value of 4.9 aa/s fits to the translation speed of 4.4 aa/s that was calculated from the gel quantification (Fig. 20). The linear fit of the delay times for the different ORF lengths (Fig. 31C) intercepts the axes near the origin, confirming the linear dependence of the delay time on the length of the ORF.

The mRNA release signal during the recycling phase showed two distinct phases. This can either indicate a two-step reaction mechanism where a fluorescence change, e.g. caused by conformational change of the ribosome or the mRNA precedes or follows the actual mRNA release reaction, or the two phases are caused by two different populations in a heterogenous sample that perform the same reaction but at a different speed. In the first case, the relative amplitudes of the two connected reactions should remain constant throughout all experiments while heterogenous populations may differ in their relative proportion and causing different amplitudes. While for the lpp18 mRNA the amplitude Amp_2 of the slow rate k_2 accounts for only 20.3 ± 0.2 % of the total amplitude, Amp2 increases with the length of the ORF and for the full-length mRNA Amp_2 makes up 37.5 ± 2.4 % of the total amplitude (Fig. 31D; Tab. 2). As shown with the translation gel, only up to 60% of translating ribosomes finish the full-length lpp protein (Fig. 20). This matches with the Amp_1 of 62.5 ± 2.4 % of the fast rate k_1 for the full length lpp mRNA. This indicates that the two-

phasic signal may indeed be caused by two distinct populations of ribosome complexes. This, and the comparison with the proportion of ribosomes that finish the full-length translation product for the full-length lpp mRNA, indicate that the fast rate likely accounts for the fully translating ribosomes, which upon reaching the stop codon, are quickly recycled, leading to mRNA release. For shorter mRNAs the population of ribosomes translation the full ORF is higher, because on a shorter ORF with fewer elongation steps the heterogeneity, which increases with every step, is lower (Tab. 2). The slow rate k_2 and amplitude Amp_2 likely show the slow dissociation of the ribosome population in the heterogenous sample that did not finish the full-length protein.

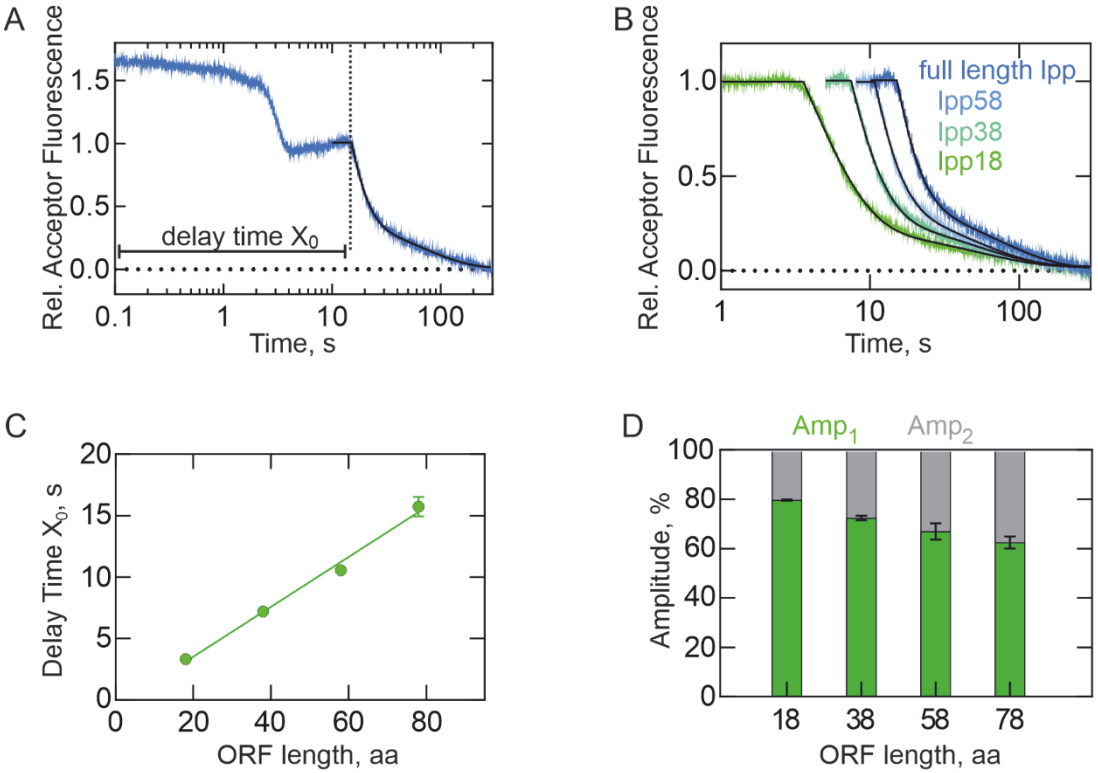

Figure 31. Analysis of the mRNA-release experiments. (A) Acceptor fluorescence signal of the full-length mRNA-release experiment (from Fig. 28B). The mRNA release phase is fitted with a delay phase (delay time X_0) followed by a double exponential phase (Eq. 7). For data fitting the initial 10 s of the signal were removed. (B) Fitting of the mRNA release traced obtained in Fig. 29B. For data fitting of the recycling phases, the initial 10 (lpp full length), 8 (lpp58), 5 (lpp38) or 0.1 s (lpp18) were removed. Fitting parameters are shown in Table 2 and are from 3 to 4 independent experiments. (C) Delay phase duration X_0 of the mRNA variants from (B) reveal a linear correlation with ORF length and a rate of translation of 4.9 aa/s. (D) Bar chart of fast (Amp1, green) and slow (Amp2, grey) amplitudes for the mRNA variants. Data shown in Table 2.

Table 2. Fitting parameters of lpp ORF variants.

ORF length, aa	Delay time (X_0), s	k_1, s^{-1}	k_2, s^{-1}	Amp_1, %	Amp_2, %
78	15.7 ± 0.8	0.15 ± 0.2	0.014 ± 0.001	62.5 ± 2.4	37.5 ± 2.4
58	10.6 ± 0.2	0.21 ± 0.01	0.018 ± 0.002	66.9 ± 3.4	33.1 ± 3.4
38	7.2 ± 0.2	0.26 ± 0.02	0.019 ± 0.001	72.4 ± 0.9	27.6 ± 0.9
18	3.3 ± 0.2	0.26 ± 0.02	0.018 ± 0.001	79.7 ± 0.2	20.3 ± 0.2

All values are mean ± standard deviation from 3 to 4 independent experiments.

3.4.2 mRNA Release and Subunit Splitting

The order of events during recycling is controversially discussed. While the splitting of the 70S ribosome into subunits has been in detail studied (Borg *et al.*, 2016; Fu *et al.*, 2016; Peske *et al.*, 2005; Savelsbergh *et al.*, 2009), the mechanism of the release of natural mRNAs from the ribosome remains unclear. The kinetics of mRNA release from translating ribosomes measured with the here established assay can now be compared to the kinetics of subunit splitting. Subunit splitting and the dissociation of the mRNA from the ribosome can be measured in rapid kinetic experiments with the same fluorescence-labeled ribosome complexes, albeit in separate experiments. Splitting of the ribosomal subunits can be measured using light scattering because the 70S ribosome scatters a higher proportion of low wavelength light than the separated 50S and 30S subunits (Savelsbergh *et al.*, 2009). Subunit splitting was measured using a wavelength of 350 nm and detection of the scattered light at a 90° angle without using a filter (Fig. 32A). The fluorescent dyes, ATTO488 and ATTO647N, used for the mRNA release assay do not interfere with the light scattering measurements at 350 nm (Fig. 32B).

Purified ICs containing the ATTO647N-labeled lpp mRNA and the S3-LAP-ATTO488-labeled ribosomes were rapidly mixed with the full set of elongation, release and recycling components (aa-tRNAs, EF-Tu, EF-G, RF1, RF3, RRF, IF3, GTP, unlabeled chaser mRNA) in a stopped-flow apparatus. The light scattering signal showed a continuous but small decrease followed by a steep and sudden signal drop (Fig. 32B). The initial signal decrease is likely due to spontaneous degradation of stalled ribosome complexes during the elongation phase. The signal drop after the elongation phase can be fitted with the same double exponential equation after a delay phase as used for the mRNA release phase previously described (Eq. 7). Fitting of the displayed trace determines a delay phase

X_0 of 13.5 ± 0.6 s, a k_1 of 0.19 ± 0.05 s^{-1} and a k_2 of 0.032 ± 0.013 s^{-1}. Amp_1 is 49.6 ± 8.7 % of the total amplitude. As for the mRNA release, for the subunit splitting the full elongation phase (the first 10 s of the shown trace) had to be excluded prior to the fitting otherwise the algorithm from the GraphPad Prism software could not find X_0. The subunit splitting and the mRNA release traces can be compared to each other (Fig. 32C). The delay times X_0 (15.7 ± 0.8 s and 13.5 ± 0.6 s) and the faster rate k_1 (0.15 ± 0.2 and 0.19 ± 0.05 s^{-1}) measured for mRNA release and subunit splitting suggest that both reactions happen at about the same time. Subunit splitting and mRNA release appear dependent on each other, as both happen with a similar rate. The temporal resolution of the experiments does not allow to determine a clear order of the events if there even is an order.

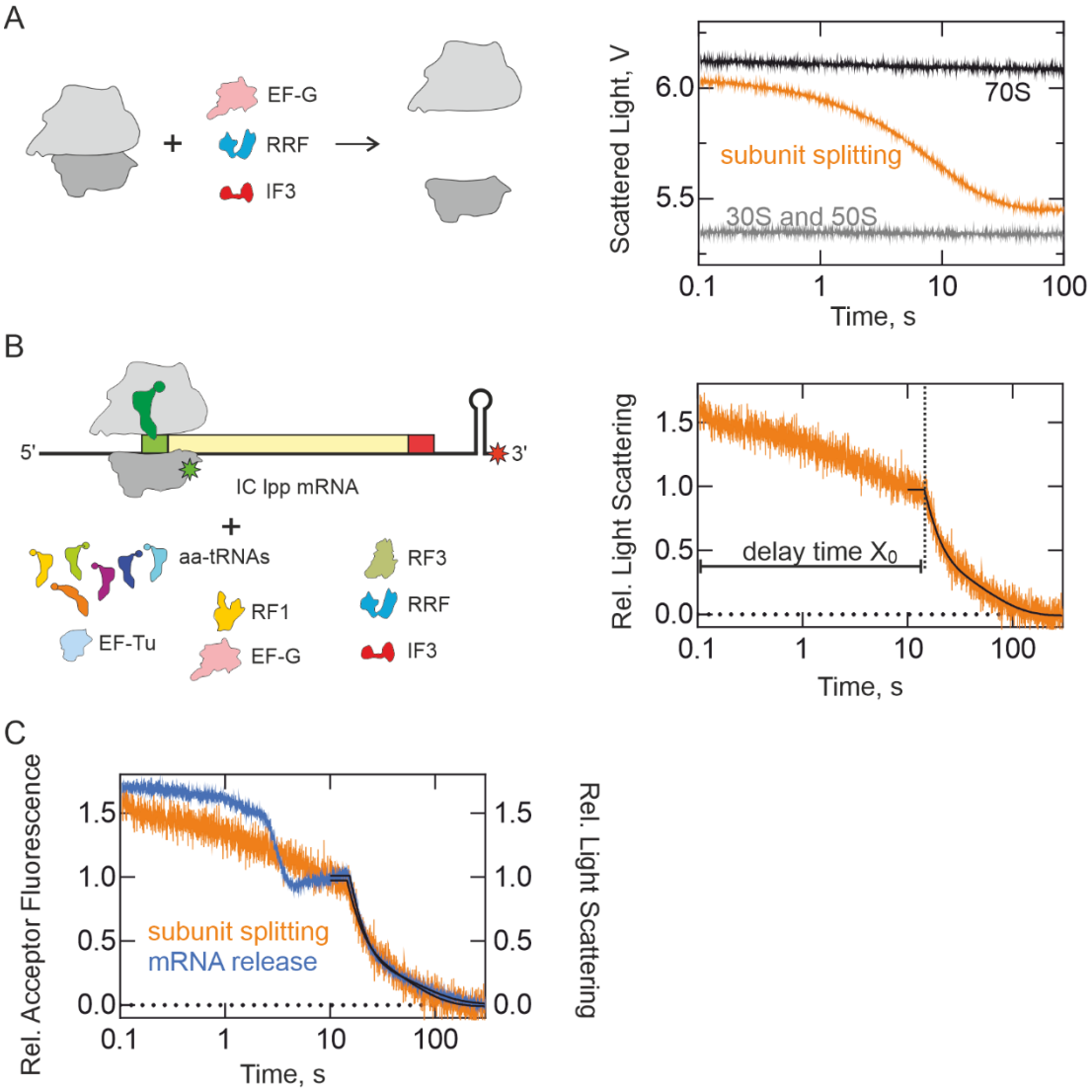

Figure 32. Dissociation of ribosomal subunits. (A) The experimental setup for the light scattering assay demonstrated with vacant 70S ribosomes. Scattered light measured for 0.2 µM vacant 70S ribosomes (black) and separated 30S and 50S subunits (grey, with 1 µM IF3) is shown. Light scattering experiments were measured using a Xenon light source with a monochromator passing light at 350 nm. Scattered light was measured without a filter at an 90° angle. Vacant ribosomes that were rapid mixed with EF-G (2.5 µM), RRF (5 µM) and IF3 (1 µM) demonstrate the subunit splitting reaction (orange). (B) Purified ICs (0.05 µM) containing the full length lpp mRNA were rapid mixed with the full set elongation, release and recycling components (aa-tRNAs, EF-Tu, EF-G, RF1, RF3, RRF, IF3, GTP) and unlabeled chaser mRNA. The experimental conditions were the same as for the mRNA-dissociation assay (Fig. 28). Traces shown are averages of 4 technical replicates. The recycling phase is fitted with a delay phase (delay time X_0) followed by a double exponential phase (Eq. 7). For data fitting the initial 10 s were removed. Fitting determined a delay phase X_0 of 13.5 ± 0.6 s, a k_1 of 0.19 ± 0.05 s^{-1} and a k_2 of 0.032 ± 0.013 s^{-1}. Amp_1 is 49.6 ± 8.7 % of the total amplitude. Fits are derived from 4 independent experiments. (C) Overlay of the subunit splitting trace (orange, from B) with the mRNA-release trace (blue, from Fig. 28B).

3.4.3 mRNA Dissociation in the Absence of RRF

While it has been shown that RRF is the key component needed for subunit splitting (Borg *et al.*, 2016; Karimi *et al.*, 1999), it is unclear how mRNA release depends on RRF (Chen *et al.*, 2017). Is the mRNA only weakly bound and dissociates after nascent protein release spontaneously or does it require subunit splitting for subsequent dissociation, i.e. the activity of RRF and EF-G? To assess these questions, mRNA release and subunit splitting were measured in the absence of RRF, IF3 and RF3. Purified ICs (50 nM) containing the full-length lpp mRNA were rapidly mixed with only elongation factors (50 µM aa-tRNAs, 50 µM EF-Tu, 2.5 µM EF-G), 1 µM RF1, 1 mM GTP and 0.25 µM unlabeled chaser mRNA (Fig 33A). RF1 catalyzes nascent protein release but was also necessary to prevent stop codon read through and it should stall the complexes in a pre-recycling state (PRC). The mRNA-release trace shows a very similar signal change during the elongation phase with the characteristic initial signal decrease that was previously observed in the presents of all factors (Fig. 33C). The slight fluorescence increase during the elongation phase between 5 and 11 s in this complex indicates that the ATTO488 label on the small subunit and the ATTO647N label at the 3'-end of the mRNA are in close proximity prior to the recycling reaction. This increase of the signal is followed by a very slow decrease, which starts at about the same time as measured in the presents of all factors (Fig. 33C). This mRNA release phase can be fitted with a delay phase (delay time X_0) followed by a single exponential phase (Eq. 6). For data fitting the initial 10 s were removed. Additionally, the delay phase X_0 was constrained to 15.7 s as the algorithm could not determine it independently. Fitting determined a rate k_1 of 0.0060 ± 0.0002 s^{-1}. Fits are derived from 3 independent experiments. The corresponding light scattering signal indicating subunit splitting shows only a marginal decrease in intensity (Fig. 33B). In the absence of RF3, RRF and IF3, the PRC is not recycled but slowly degrades. The rate of the mRNA release is too slow to be biologically relevant (Fig. 33C). The experiment shows that, albeit subunit splitting requires the action of RRF, the PRC with the natural lpp mRNA has a reduced stability that allows spontaneous dissociation of the mRNA without the recycling reaction performed by the combined action of RRF and EF-G. This indicates that mRNA release can happen independently. However, drastic changes to the complex architecture such as splitting of the subunits is necessary to remove a native mRNA with a 3'-UTR from the ribosome in a biological relevant time frame.

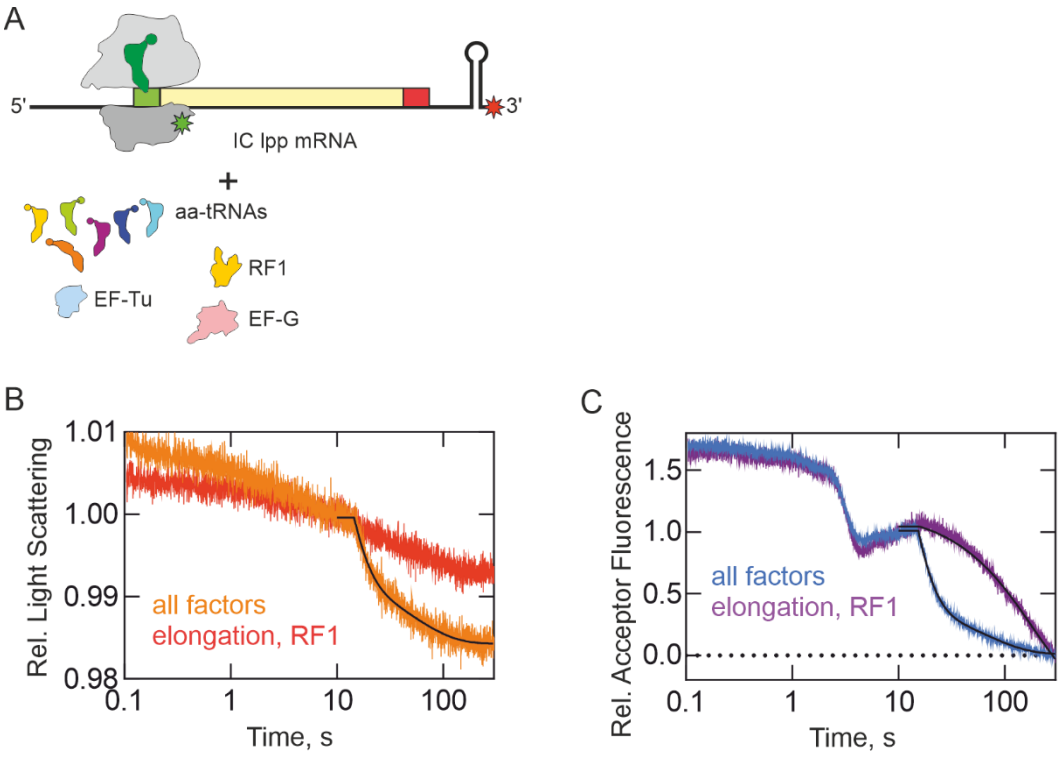

Figure 33. mRNA dissociation without RRF. (A) Experimental setup to measure mRNA release and subunit splitting in the absence of recycling factors. ICs featuring the 3'-ATTO647N-labeled full length lpp mRNA and S3-ATTO488-labeled 30S were rapidly mixed with elongation factors (aa-tRNAs, EF-Tu, EF-G), RF1, GTP and unlabeled chaser mRNA. Subunit splitting was measured via light scattering (red) and mRNA release was measured via acceptor fluorescence of the S3-mRNA FRET pair (violet). Traces shown are averages of 4 technical replicates. (B) Overlay of the subunit splitting traces with all factors (orange, from Fig. 32) with the subunit splitting traces without RF3, RRF and IF3 (red). Traces were normalized on the end of the elongation phase to highlight the amplitudes and the progression of the traces during the recycling phase. (C) Overlay of the mRNA release experiment with all factors (blue, from Fig. 28) with the mRNA release experiment without RF3, RRF and IF3 (violet). Traces were normalized on the recycling phase. The data from acceptor fluorescence experiments without recycling factors is fitted with a delay phase (delay time X_0) followed by a single exponential phase (Eq. 6). For data fitting the initial 10 s were removed. Additionally, the delay phase X_0 was constrained to 15.7 s as the algorithm could not determine it independently. Fitting determined a rate k_1 of 0.0060 ± 0.0002 s^{-1}. Fits are derived from 3 independent experiments.

3.5 Influence of the 3’-UTR on mRNA Release

3.5.1 Release of mRNAs with Truncated 3’-UTRs

The fact that native mRNAs have structured 3’-UTRs has so far not been considered in studies about ribosome recycling and instead short unstructured model mRNAs or undefined mRNA fragments as in polysome breakdown assays were used (Chen *et al.*, 2017; Iwakura *et al.*, 2017; Peske *et al.*, 2005). The dissociation of a natural mRNA with a hairpin in the 3’-UTR might be sterically less favorable than dissociation of shorter mRNAs, as used previously, or of mRNAs with a short and unstructured 3’-UTR. Using the lpp-mRNA-based translation allows studying the contribution of the 3’-UTR to mRNA dissociation in a native termination context and e.g. without possible effects of a SD sequence. Two truncated lpp-mRNA variants were used, one with a truncation of the hairpin leaving only of 8 nts after the stop codon (lpp-no-Pin mRNA) and one ending with the stop codon (lpp-stop mRNA) (Fig. 34A). mRNA release and subunit splitting were measured with purified ICs programmed with those mRNAs (Fig. 34) with the full set of elongation, release and recycling components (aa-tRNAs, EF-Tu, EF-G, RF1, RF3, RRF, IF3, GTP, unlabeled mRNA) under the previously described conditions (Fig. 28, 32). In comparison to mRNA release and subunit splitting measured with the full-length lpp mRNA (Fig. 32C), the signal changes in the elongation phase showed some differences which are likely caused by different conformations of the truncated mRNAs. Subunit splitting and mRNA release during the recycling phase for both the lpp-no-Pin mRNA (Fig. 34B) and the lpp-stop mRNA (Fig. 34C) resembled that measured with the full length lpp mRNA (Fig. 32B). Similar as observed with the native lpp mRNA, subunit splitting and mRNA release happens simultaneously. The recycling phases were fitted as previously described with a double exponential phase after a delay phase (Tab. 3). The numbers from the fitting of independent experiments (Tab. 3) and the visual overlay of the traces (Fig. 34) show that also for the mRNAs with truncated 3’-UTRs, a clear order of events cannot be determined. The mRNA release happens simultaneously to the subunit splitting.

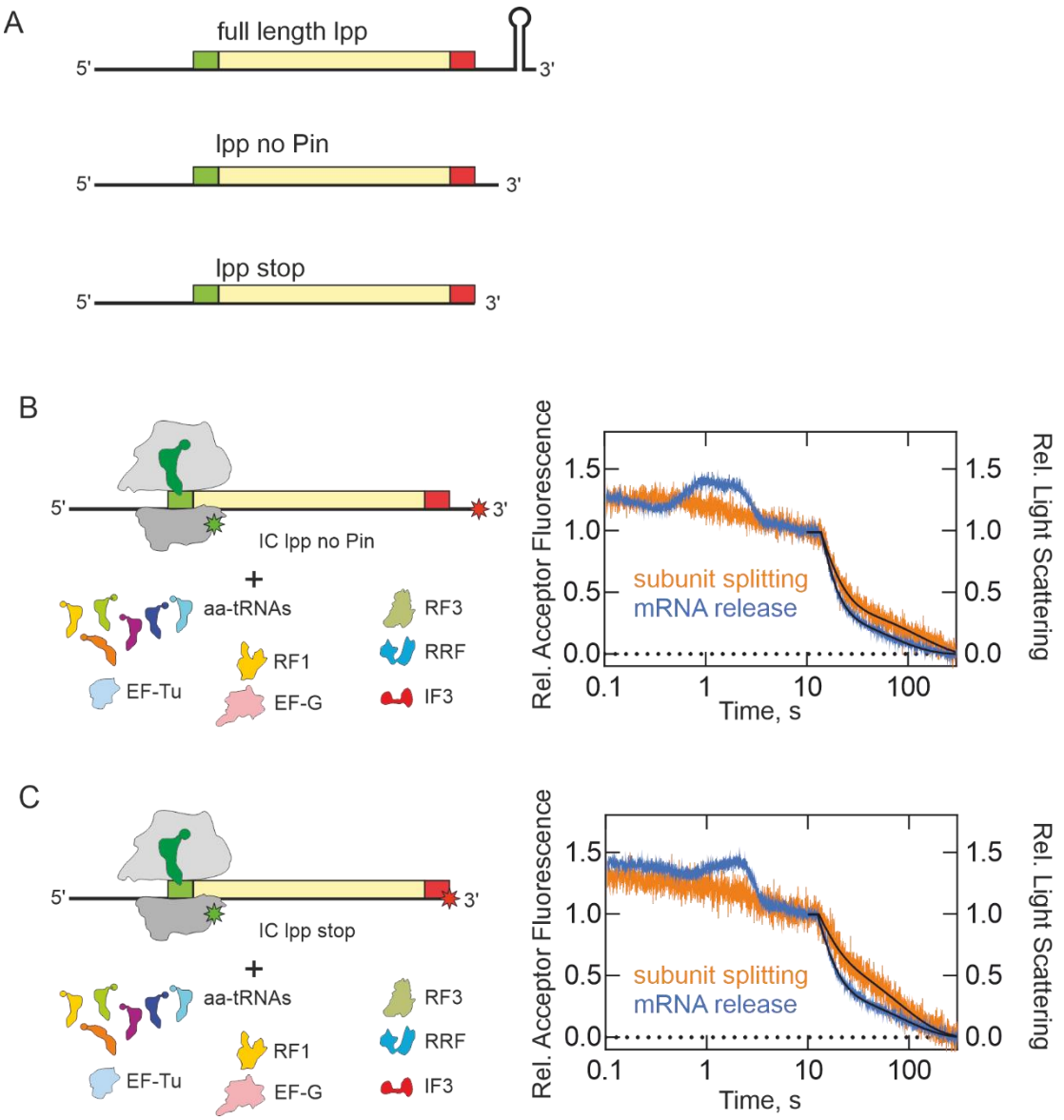

Figure 34. Recycling of mRNAs with truncated 3'-UTR. (A) Scheme of the used mRNAs: the natural full-length lpp mRNA with hairpin, the lpp-no-Pin mRNA without the hairpin and 8 nts after the stop codon and the lpp-stop mRNA that ends with the stop codon and has no 3'-UTR. (B) Purified ICs containing the lpp-no-Pin mRNA were rapid mixed with the full set elongation, release and recycling components (aa-tRNAs, EF-Tu, EF-G, RF1, RF3, RRF, IF3, GTP) and unlabeled chaser mRNA (as in Fig. 28). Overlay of the subunit splitting traces (orange) and the mRNA-release traces (blue). Traces shown are averages of 4 technical replicates. The recycling phase is fitted with a delay phase (delay time X_0) followed by a double exponential phase (Eq. 7). For data fitting the initial 10 s of the signal were removed. Fits are derived from 3 independent experiments (Table 3). (C) Same experiment as in (B) but with the lpp-stop mRNA.

Table 3. Fitting parameters of lpp 3'-UTR variants in the presence of all factors.

Experiment	Delay time (X_0), s	k_1, s^{-1}	k_2, s^{-1}	Amp_1, %	Amp_2, %
Full-length lpp mRNA:					
mRNA release	15.7 ± 0.8	0.15 ± 0.02	0.014 ± 0.001	62.5 ± 2.4	37.5 ± 2.4
Subunit splitting	13.5 ± 0.6	0.19 ± 0.05	0.032 ± 0.013	49.6 ± 8.7	50.4 ± 8.7
lpp-no-Pin mRNA:					
mRNA release	14.7 ± 0.6	0.18 ± 0.01	0.013 ± 0.003	68.9 ± 2.9	31.1 ± 2.9
Subunit splitting	13.9 ± 1.1	0.15 ± 0.02	0.011 ± 0.003	57.7 ± 2.3	42.3 ± 2.3
lpp-stop mRNA:					
mRNA release	13.5 ± 1.1	0.17 ± 0.01	0.015 ± 0.006	63.9 ± 4.4	36.1 ± 4.4
Subunit splitting	12.1 ± 1.3	0.15 ± 0.05	0.034 ± 0.017	22.0 ± 10.0	78.0 ± 10.0

All values are mean ± standard deviation from 3 to 4 independent experiments.

3.5.2 Dissociation of mRNAs with Truncated 3'-UTRs without Recycling

The next question was if the truncated mRNA requires also RRF and subunit splitting for efficient release, as previously shown for the full length lpp mRNA or if they can spontaneously dissociate from ribosome complexes after translation and release of the protein. To test this the previously described ICs with the truncate mRNAs (Fig. 34A) were mixed only with elongation components (aa-tRNAs, EF-Tu, EF-G, GTP), RF1 and unlabeled mRNA but without RF3, RRF and IF3 (Fig. 35A). Overlaying the mRNA release signal for the three different mRNAs (Fig. 35A) shows that the mRNAs with truncated or lacking 3'-UTR dissociate after the elongation phase at a much faster rate than the full length lpp mRNA with its native structured 3'-UTR. The mRNA release traces of the lpp-no-Pin and lpp-stop mRNA could be fitted with the equation used previously (Eq. 7). For the lpp-no-Pin mRNA a delay of 13.8 ± 0.4 s, a fast rate k_1 of 0.078 ± 0.008 s^{-1} and a slow rate of 0.013 ± 0.001s^{-1} was calculated. The fast rate accounts for 35.9 ± 3.9 % of the total amplitude. For the lpp-stop mRNA, a delay of 12.7 ± 0.4 s, fast rate k_1 of 0.17 ± 0.01 s^{-1} and a slow rate of 0.013 ± 0.001 s^{-1} was calculated. The fast rate accounts for 51.0 ± 3.9 % of the total amplitude. When plotted together (Fig. 35A) the dependence of mRNA release on the 3'-UTR is immediately visible, the smaller the 3'-UTR the faster mRNA release in the absence of RRF, RF3 and IF3. The lpp-no-Pin mRNA with the short 8 nts 3'-UTR dissociated much faster from the PRC than the lpp mRNA with the full native 3'-UTR. But recycling factors enhance the release of this mRNA (Fig. 35B). For the lpp-stop mRNA, which has no 3'-UTR, there is almost no difference in dissociation between the experiments with and without RRF, RF3 and IF3 (Fig. 35D).

The light scattering traces for both experiments with the truncated mRNAs (Fig. 35C, E) are very similar to the traces obtained in the subunit splitting experiment with the full-length lpp mRNA (Fig. 33B) in the presence and absence of recycling factors. In the absence of RF3, RRF and IF3, amplitude of the signal change is smaller than in the presence of all factors. Ribosome subunit splitting does not depend on the 3'-UTR of the mRNA, but it requires recycling factors. It however appears that the mRNA significantly contributes to the overall complex stability as complex degradation can be seen in the light scattering experiments with truncated mRNAs. mRNA release appears to be context dependent on the 3'-UTR. mRNAs lacking the native structured 3'-UTR can dissociate spontaneously when the ribosome reaches the end of the mRNA, but mRNAs with a native 3'-UTR require subunit splitting for efficient release.

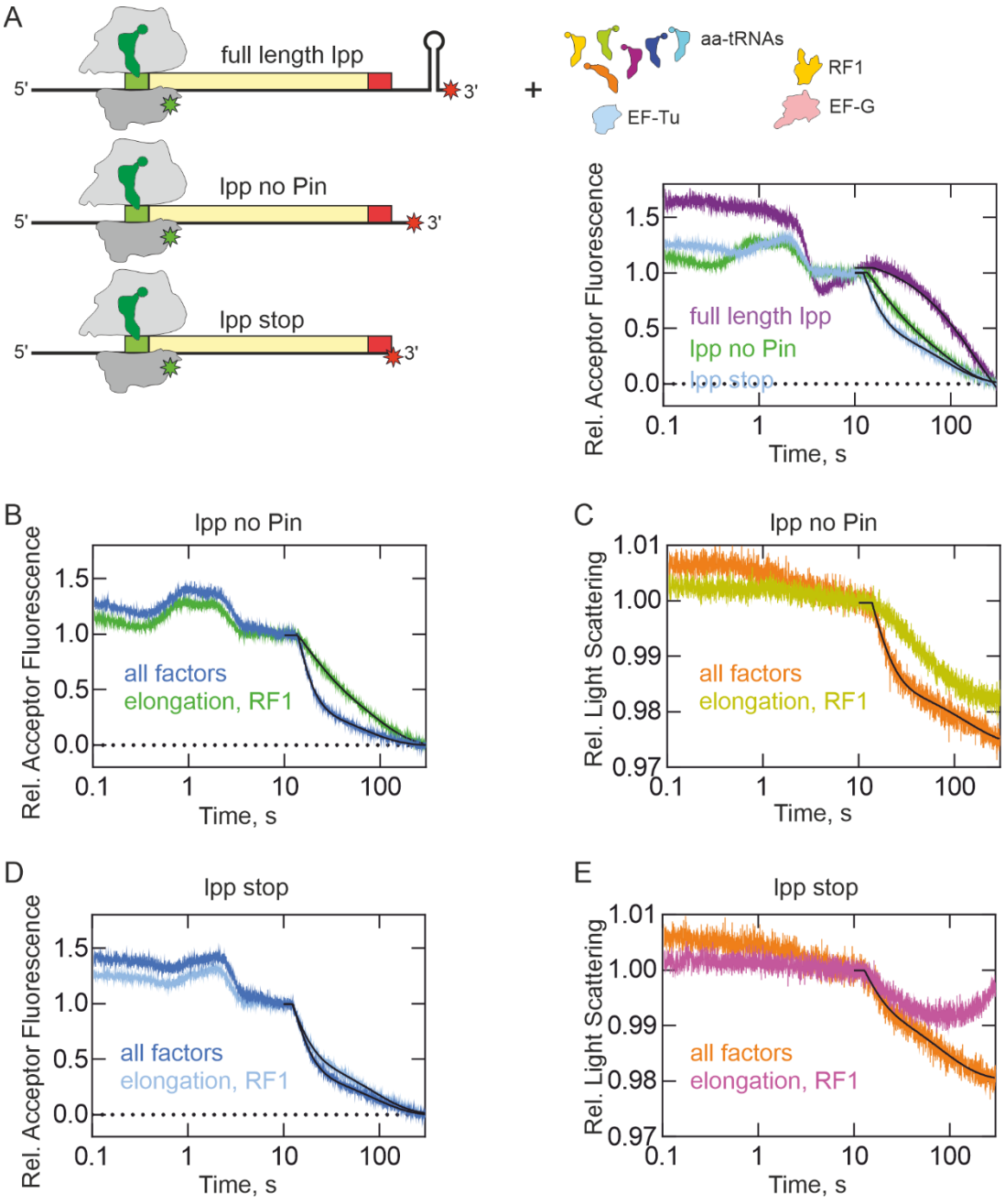

Figure 35. Dissociation of mRNAs with truncated 3'-UTRs without recycling. (A) Purified complexes programmed with the three mRNAs were rapid mixed with elongation factors (aa-tRNAs, EF-Tu, EF-G, GTP), RF1 and unlabeled chaser mRNA. An overlay of the resulting mRNA release traces for the full length lpp mRNA (violet), the lpp-no-Pin mRNA (green) and the lpp-stop mRNA (light blue) is shown. Traces are averages of 4 technical replicates. The recycling phase is fitted with a delay phase (delay time X_0) followed by a double exponential phase (Eq. 7). Results are summarized in Table 4. For data fitting the initial 10 s were removed. (B) Overlay of the mRNA-release trace for the lpp-no-Pin mRNA from the experiment with all factors (blue, from Fig. 34B) and from the experiment with only elongation components and RF1 (green, from A). (C) Overlay of the subunit splitting trace for the lpp-no-Pin mRNA from the experiment with all factors (orange, from Fig. 34B) and from the experiment with only elongation components and RF1 (yellow). (D) Overlay of the mRNA-release trace for the lpp-stop mRNA from the experiment with all factors (blue, from

Fig. 34C) and from the experiment with only elongation components and RF1 (light blue, from A). (E) Overlay of the subunit splitting trace for the lpp-stop mRNA from the experiment with all factors (orange, from Fig. 34C) and from the experiment with only elongation components and RF1 (pink).

Table 4. Fitting of mRNA release of lpp 3'-UTR variants.

Experiment	Delay time (X_0), s	k_1, s^{-1}	k_2, s^{-1}	Amp_1, %	Amp_2, %
mRNA release of full-length lpp mRNA:					
All factors	15.7 ± 0.8	0.15 ± 0.02	0.014 ± 0.001	62.5 ± 2.4	37.5 ± 2.4
Elongation, RF1	= 15.7*[1]	0.0060 ± 0.0002*[1]	n.d.*[1]	100*[1]	n.d.*[1]
lpp-no-Pin mRNA:					
All factors	14.7 ± 0.6	0.18 ± 0.01	0.013 ± 0.003	68.9 ± 2.9	31.1 ± 2.9
Elongation, RF1	13.8 ± 0.4	0.078 ± 0.008	0.013 ± 0.001	35.9 ± 3.9	64.1 ± 3.9
lpp-stop mRNA:					
All factors	13.5 ± 1.1	0.17 ± 0.01	0.015 ± 0.006	63.9 ± 4.4	36.1 ± 4.4
Elongation, RF1	12.7 ± 0.4	0.17 ± 0.01	0.013 ± 0.001	51.0 ± 3.9	49.0 ± 3.9

All values are mean ± standard deviation from 3 to 4 independent experiments.
*[1] Single exponential fit after a delay constrained to 15.7 s.

3.6 Recycling Studied Using Single Molecule TIRF

The stopped-flow technique used for the bulk kinetic experiments has strengths and weaknesses. It is possible to study very fast reactions with excellent temporal resolution but it is also very material consuming and samples with mixed populations will give a mixed result that can be difficult to interpret. Here, the main challenge was complex heterogeneity. In order to start the recycling reactions, ribosomes had to initiate on the mRNA and translate the mRNA. Not all ribosomes show full activity in these processes. *In vitro* 90% of ribosomes initiate on an mRNA and 60% of translating ribosomes complete the synthesis of the full-length lpp protein (Fig. 20). The ribosomes, which do not finish translation, also contributed to the bulk fluorescence signals, making the signal more complex. To fit the results, a two-exponential equation was needed to describe the resulting two phases seen in the recycling reaction. It can be assumed that the first, faster phase represents the recycling of ribosome complexes at the stop codon, whereas the slower phase likely results from the fraction of ribosomes, which do not show full translation of the lpp protein.

As a result of the bulk kinetic experiments, the hypothesis was formed that subunit splitting happens first but is immediately followed by mRNA release from the 30S subunit because for the release of the native lpp mRNA, subunit splitting is a prerequisite for fast mRNA release. To investigate this further, it was decided to use a different experimental approach. In single molecule FRET (smFRET) experiments it is possible to observe single ribosomal complexes performing the recycling reaction. Complexes can be characterized on their FRET efficiencies and individual populations of molecules can be sorted for the analysis. For these experiments, total internal reflection fluorescence (TIRF) microscopy is used. In TIRF microscopy, the excitation beam is shot from below towards a transparent objective slide at an angle that allows full reflection of the beam on the slide-water interface above. This creates an evanescent wave selectively exciting fluorophores immobilized on the slide. Low concentration and spatial separation of immobilized molecules enables the observation of single isolated fluorophores. Double-labeled samples allow observation of FRET between fluorescent dye molecules. For the smFRET experiments, it was necessary to change the fluorophores to the established and widely used Cy3-Cy5-FRET pair as the ATTO dyes showed photoblinking events that would have complicated the analysis. To study mRNA release, hydrazide conjugated Cy3 was attached to the 3'-end of the mRNA and the 30S subunit was labeled with Me-tetrazine conjugated Cy5 at the C-terminal LAP-tag of S3 via LplA. The Cy5-labeled ribosomes showed the same catalytic activity as all other ribosome types used in this work (Fig. 27). To study subunit splitting in TIRF microscopy, ribosomes with S6-Cy3 labeled 30S and L9-Cy5 labeled 50S subunits were used. These labeling positions were prepared via knock-out and

reconstitution as previously described and have been established for the measurement of subunit rotation (Sharma *et al.*, 2016). Here, smFRET TIRF microscopy was used to first assess the distribution of FRET populations in the heterogenous samples and further to observe subunit splitting and mRNA release of individual ribosomes. The analysis allows the fitting of combined selected FRET trajectories to determine rate constants for the reactions of interest.

3.6.1 Characterization of Ribosome Complexes

Characterizing different populations within a sample is a core strength of the smFRET technique. Here, single molecules can be observed and grouped by their characteristics such as their FRET efficiency. Initiation complexes were investigated for comparison with PRCs, which were then used in the following experiments. Initiation complexes were prepared as described with S6-Cy3 and L9-Cy5 labeled subunits and native lpp mRNA, S3-Cy5 labeled ribosomes and 3'-Cy3 labeled lpp mRNA. PRCs were formed by short incubation of ICs with elongation factors, aa-tRNAs and RF1, which stabilizes the complex on the stop codon. Ribosome complexes were diluted to 0.5 to 1 nM concentration and were anchored on neutravidin coated biotin-PEG quartz slides through a biotinylated DNA oligo annealed to the lpp mRNAs 5'-end. Slides were flushed with imaging buffer prior to measurement. Flushing with imaging buffer and the low concentration of the sample were sufficient to ensure that factors used for complex preparation and the small fraction of non-initiated ribosomes would not interfere with the experiments. Movies of single molecules were recorded using TIRF microscopy. Experiments were performed at 20 °C. Observation period was 100 s with 100 ms per time point (1000 points). Fluorescence traces of single molecules were extracted and FRET efficiency was calculated. For every trace, a mean FRET efficiency was calculated for the duration in which the molecules showed FRET. These FRET values were summarized in FRET distribution histograms (Fig. 36). FRET distributions were fitted with a gaussian function to quantify the subpopulation inside the samples (Tab. 5).

The S6-Cy3 and L9-Cy5 IC had a high population of traces (90%) showing FRET values of 0.73 (Fig. 36A) characteristic for the non-rotated state (Sharma *et al.*, 2016). A small population representing 10% of traces showed the lower FRET efficiency of 0.51 characteristic for the rotated state. The pre-recycling-complex (PRC) featuring the S6-Cy3 and L9-Cy5-labeled ribosome at the stop codon of the native lpp mRNA with a deacylated tRNA in the P site and RF1 in the A site, the substrate for recycling by RF3, RRF and EF-G, was also mainly found in the high FRET non-rotated

state (83%, Fig. 36B, Tab. 5). In subsequent, separately performed experiments, only the high FRET traces were analyzed. Low FRET traces characteristic for the rotated state were not further analyzed.

For complexes with the S3-Cy5 and mRNA-Cy3 FRET pair, designated to investigate the release of mRNA from the 30S subunit, the main populations show high FRET values of 0.77. High FRET efficiency indicates very close proximity of the dyes in both IC (Fig. 36C) and PRC (Fig. 36D). For the PRC, this agrees with the predicted small distance between the fluorophores (Fig. 30). In ICs, the full-length lpp mRNA supposedly adopts a compact conformation where its 3' end is localized near the ribosome. In the PRC, the ribosome has traveled towards the stop codon and occupies parts of the 3'-UTR. Because of the 3'-UTR hairpin structure, the 3' Cy3 is again in close proximity to the S3-Cy5. Small populations with medium FRET values, at FRET efficiencies of 0.53, exist for both complexes. For the PRC, a small population showing a low FRET efficiency of 0.33 appears. This low FRET efficiency might be caused by ribosomes that did not finish translating the full-length peptide and are stalled with the mRNA in an elongated conformation.

In bulk kinetic experiments (Fig. 29B) complexes formed with the lpp18 mRNA, which has a shortened ORF coding only for the first 18 aa of lpp, showed constant acceptor fluorescence throughout the elongation phase whereas ribosomes programmed with the full-length lpp mRNA and to a lesser extend with the lpp58 mRNA showed a decrease of acceptor fluorescence during the elongation phase. This was likely due to conformational changes of the hairpin structure that is formed by the longer lpp mRNAs. Here, the lpp18 mRNA was included as a control to assess whether the different FRET populations seen for the full-length lpp mRNA might be related to different mRNA conformations (Fig. 36E, F). The PRC with the lpp18 mRNA showed the same main populations with FRET efficiencies of 0.77, 0.55 and 0.33 as the PRC with full-length lpp mRNA. But unlike the IC programmed with full-length lpp mRNA, also the IC formed on the shorter mRNA showed the low FRET population at 0.33.

Taking these results together, it is not entirely clear whether the medium and low FRET populations of the mRNA-S3 FRET pair only represent mRNAs in a different conformation, or if these complexes belong to a separate population of ribosomes that differ from the main population, such as complexes stalled during the elongation. It is also possible that both effects contribute to these lower FRET populations. In the following experiments, only the main populations were further analyzed.

Table 5. smFRET characterization of pre-formed ribosome complexes.

Complex	N *[1]	FRET efficiency of populations (Relative size of populations)		
		$FRET_{high}$	$FRET_{medium}$	$FRET_{low}$
IC S6-Cy3 L9-Cy5	663	0.74 ± 0.01 (90 ± 3%)	0.51 ± 0.01 (10 ± 3%)	
PRC S6-Cy3 L9-Cy5	589	0.73 ± 0.01 (83 ± 6%)	0.50 ± 0.01 (17 ± 6%)	
IC lpp-Cy3 S3-Cy5	340	0.77 ± 0.01 (87 ± 3%)	0.53 ± 0.02 (13 ± 3%)	
PRC lpp-Cy3 S3-Cy5	544	0.77 ± 0.01 (62 ± 2%)	0.52 ± 0.01 (26 ± 3%)	0.33± 0.02 (12 ± 3%)
IC lpp18-Cy3 S3-Cy5	318	0.77 ± 0.01 (59 ± 5%)	0.53 ± 0.01 (32 ± 6%)	0.32 ± 0.01 (9 ± 6%)
PRC lpp18-Cy3 S3-Cy5	513	0.77 ± 0.01 (59 ± 4%)	0.55 ± 0.01 (31 ± 4%)	0.33 ± 0.01 (10 ± 2%)

Single molecule experiments and analysis was performed by Dr. Tamara Senyushkina. All values are mean ± standard deviation from 3 to 4 independent datasets. *[1] N = Number of traces in combined datasets.

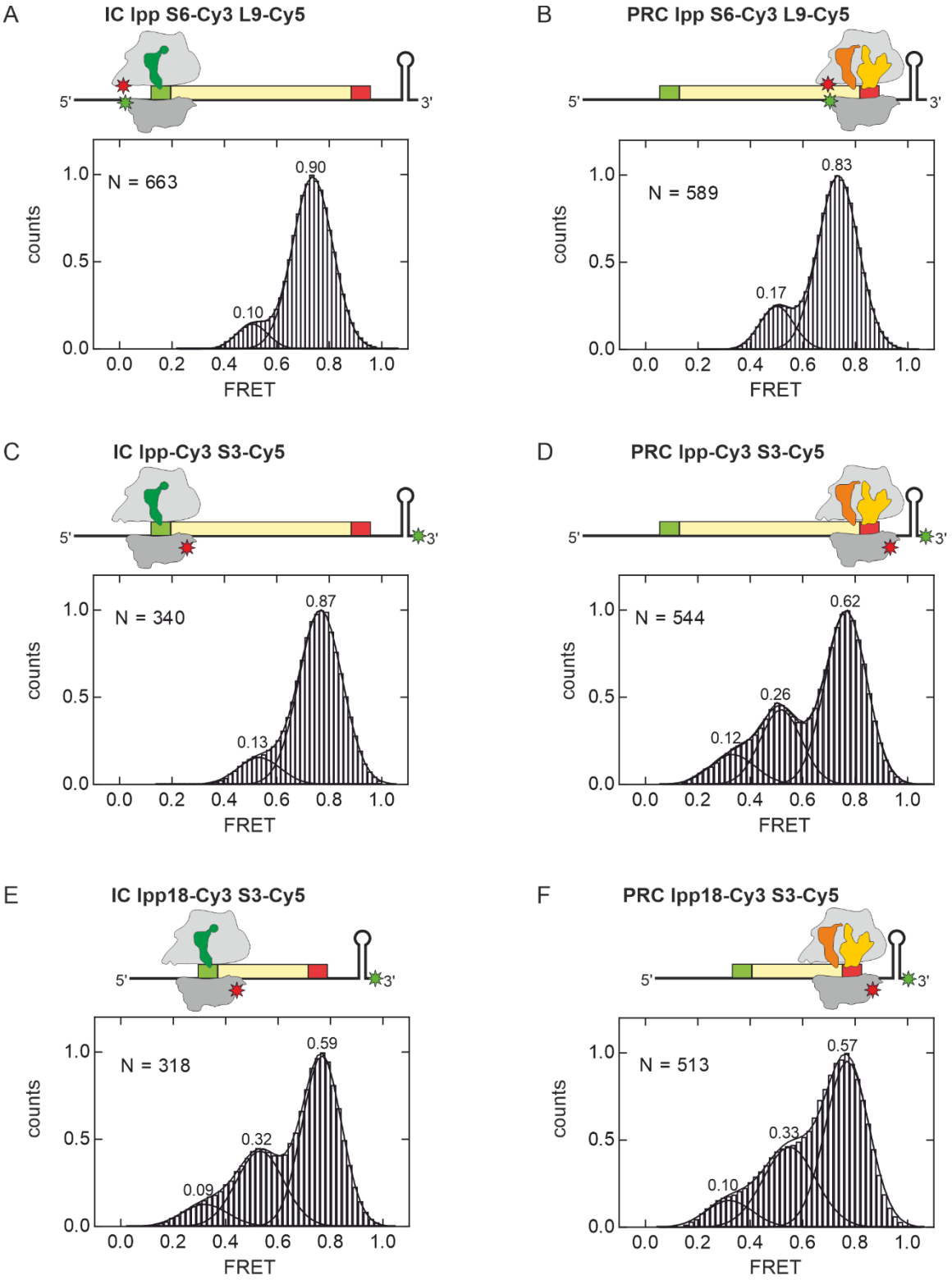

Figure 36. smFRET characterization of pre-formed ribosome complexes. FRET populations of used traces are shown as histograms. N is the number of traces from 3 to 4 independent datasets. Schemes above the histograms describe the complexes. The mRNA with the structured 3'-UTR is shown as the bold black line with start codon (green), ORF (yellow) and stop codon (red) as boxes on the mRNA. 50S (light grey) and 30S (dark grey) subunits are positioned at the start codon (IC) or at the stop codon (PRC). ICs contain initiator tRNA in the P site (green). PRCs have a tRNA (orange)

bound in the P site and RF1 (yellow) bound in the A site. Positions of fluorophore Cy5 (red) and Cy3 (green) are indicated by stars. Single molecule experiments and analysis was performed by Dr. Tamara Senyushkina. (A) IC with full length lpp mRNA and S6-Cy3 and L9-Cy5 labeled ribosomes, (B) PRC with full length lpp mRNA and S6-Cy3 and L9-Cy5 labeled ribosomes, (C) IC with Cy3-labeled full length lpp mRNA and S3-Cy5 labeled ribosomes, (D) PRC with Cy3-labeled full length lpp mRNA and S3-Cy5 labeled ribosomes, (E) IC with Cy3-labeled lpp18 mRNA and S3-Cy5 labeled ribosomes, (F) PRC with Cy3-labeled lpp18 mRNA and S3-Cy5 labeled ribosomes.

3.6.2 Observation of the Recycling Reaction via smFRET

The initial characterization of the PRCs gave an overview on the different populations within the sample. In separate experiments, PRCs with the S6-L9 FRET pair and with the mRNA-S3 FRET pair were immobilized on biotin-PEG slides as described above. Imaging buffer with different concentrations of RRF (0, 1, or 5 µM) and RF3 (1 µM), EF-G (1 µM) and GTP (1 mM) or without recycling factors was applied to the slides. IF3 was omitted because at the low concentration of ribosomes used in the single molecule experiments subunit reassociation events can be disregarded. The time between the application of the imaging buffer and the beginning of the measurement, the delay time t_{delay}, was recorded for the later analysis and data fitting. In the observed traces, donor and acceptor usually keep their fluorescence intensities until one of the dyes signals vanishes. The control experiments performed in imaging buffer without any release and recycling factors were needed to distinguish between a recycling driven dissociation event and photobleaching or spontaneous complex disintegration, as signal disappearance of one fluorophore can mean either the dissociation of the labeled factor or bleaching of the fluorophore. As observed in the stopped-flow experiments, mRNA release and subunit splitting can happen without recycling by EF-G and RRF, but to a different extend and speed.

For the S6-Cy3 and L9-Cy5 FRET pair, only traces that show the non-rotated state, which should be characteristic for the binding of RF1 in the A site (Adio *et al.*, 2015), were analyzed. A simultaneous disappearance of donor and acceptor signals indicates photobleaching of the donor fluorophore or can in principle be caused by dissociation of the 70S ribosome from the anchored mRNA, i.e. by mRNA dissociation from the ribosome, or by dissociation of the mRNA from the biotinylated anchor oligonucleotide. 1464 (N) traces of PRC in imaging buffer without factors were manually screened for such events. The simultaneous disappearance of donor and acceptor signals was observed in 4.2 % of traces (N = 64). For 1452 traces of PRC in the presence of release and recycling components (1 µM RF3, 1 µM RRF, 1 µM EF-G and 1 mM GTP), it was only observed in 3.7% (N = 54) of traces

(Fig. 37A). All other traces showed prior disappearance of the acceptor fluorescence under both experimental conditions, but with different trajectory time distributions as will be explained later. Because simultaneous signal loss events are as infrequent in the presence of recycling factors as they are in the absence, it can be concluded that recycling factors do not promote mRNA release from the ribosome prior to the subunits splitting. The infrequency of such events strongly suggests that the simultaneous signal loss can be attributed to photobleaching of the donor fluorophore. In the majority of traces, a loss of the acceptor fluorescence is observed before the disappearance of the donor fluorescence (Fig. 37A). The acceptor dye Cy5 is attached to protein L9 of the 50S subunit and the donor dye Cy3 is attached to protein S3 of the 30S subunit. This means that the 50S subunit leaves the complex with the 30S subunit and the mRNA before the 30S subunit dissociates form the mRNA, which itself is attached to the cover slip. Hence, subunit splitting must proceed the dissociation of the mRNA from the 30S subunit. For the analysis of the 70S splitting experiments only the FRET traces where acceptor fluorescence disappeared first were used for the subsequent fitting and calculation of rate constants.

The same experiment was also performed for the S3-mRNA FRET pair. Also here, only the main population, which showed high FRET efficiency, was further analyzed, as the nature of the low FRET states remains unclear. The Cy3-labeled mRNAs were anchored on the slides while the acceptor fluorophore Cy5 was on the ribosome. Therefore, vanishing of Cy5 fluorescence indicates either photobleaching or the release of the S3-Cy5 labeled 30S subunit from the mRNA. Vanishing of the donor signal exclusively means photobleaching of the dye. Disappearance of both signals simultaneously indicates the disruption of the immobilization of the complex. Therefore, only traces where the Cy5 signal disappeared first were used for subsequent analysis to determine the rate constants of the mRNA release (Fig. 37B).

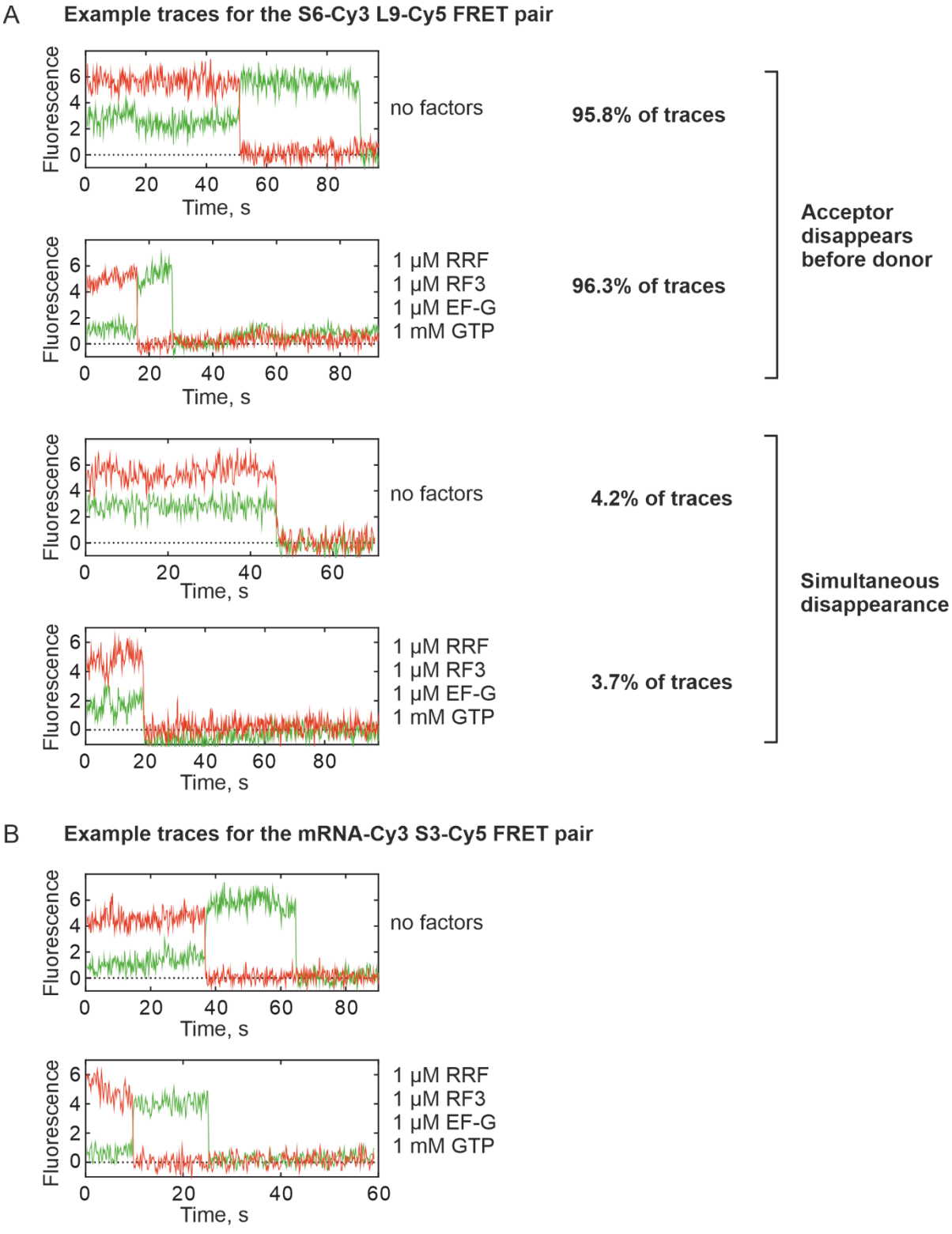

Figure 37. Example traces from smFRET experiments. Donor fluorescence is shown in green (Cy3) and acceptor fluorescence in red (Cy5). Single molecule experiments and analysis was performed by Dr. Tamara Senyushkina. (A) Example traces are shown for PRC complexes with the S6-Cy3 and L9-Cy5 label. Traces show either an acceptor signal drop before a donor signal drop or a simultaneous drop of both. In experiments without recycling factors 95.8% of traces show acceptor before donor signal disappearance. Only 4.2% show a simultaneous loss of both fluorophores'

fluorescence. The numbers are 96.3% and 3.7%, respectively, for experiments with recycling factors. (B) Example traces are shown for PRC complexes with 3'-Cy3 labeled mRNAs and the S3-Cy5 label on the ribosome. For this FRET pair, only traces with the acceptor signal disappearing before the donor signal were observed.

3.6.3 Analysis and Data Fitting of the smFRET Results

Because for the PRC featuring the S6-Cy3 and L9-Cy5 double labeled ribosomes it cannot be distinguished between 50S release and photobleaching of the Cy5 dye, the FRET traces' lengths of complexes observed in imaging buffer without factors had to be compared to the FRET traces' lengths of complexes observed in the presence of factors (1 µM RF3, 1 µM EF-G, 1 mM GTP) with different concentrations of RRF (0, 1 µM, or 5 µM). Experiments were performed with PRCs programmed with the native full-length lpp mRNA as previously described. Only high FRET traces (83% of all traces) that show vanishing of the acceptor fluorophore prior to vanishing of the donor fluorophore (96% of high FRET traces) were used for the analysis. The time between the application of the imaging buffer and the start of the measurement was recorded as the delay time of the experiment (t_{delay}). The numbers of light-emitting particles (N) included in the analysis at each time were counted from the data. Dependencies of non-recycled complexes on the time (example traces in Fig. 38A, B, C) were single exponential fitted with the following equation (Eq. 8):

$$y = A\, exp(-k_{obs}) \tag{8}$$

to obtain rate of the observed decay k_{obs}. The photobleaching correction rate k_{ph}, which accounts for photobleaching and spontaneous complex degradation, was calculated from the experiments without factors with the equation (Eq. 9):

$$\mathrm{k}_{ph} = \frac{1}{t_{delay} + \frac{1}{k_{obs}}} \tag{9}$$

With the rate of photobleaching k_{ph} and the delay time t_{delay} and the observed rates k_{obs}, the corrected rates constants k_{cor} were calculated according to equation (Eq. 10):

$$\mathrm{k}_{cor} = \frac{1}{t_{delay} + \frac{1}{k_{obs} - k_{ph}}} \tag{10}$$

For the S6-Cy3 and L9-Cy5 PRC, a correction rate k_{ph} of 0.029 ± 0.006 s^{-1} was determined. The numbers determined for N, t_{delay}, k_{obs} and k_{cor} for all experiments can be found in Table 6. Experiments were repeated 3 to 4 times. Corrected rates of 0.016 ± 0.001, 0.019 ± 0.0004 and 0.027 ± 0.0007 were calculated for the subunit splitting at 0, 1 and 5 µM RRF, respectively, showing a concentration dependency on RRF (Fig. 38D).

Release of mRNAs from the 30S subunit or 30S subunit dissociation from the mRNA was tested with PRCs featuring 3'-Cy3-labeled mRNAs and S3-Cy5 labeled 30S subunits. With the Cy3-labeled mRNA anchored on the slides, the vanishing of the Cy5 signal indicates either photobleaching or the release of the S3-Cy5 labeled 30S subunit from the mRNA. Both the full length lpp mRNA and the shorter lpp18 mRNA were used. Experiments were performed as described for the S6-L9 FRET pair. Only high FRET traces that show vanishing of the acceptor fluorophore prior to vanishing of the donor fluorophore were used for the analysis. Correction rates k_{ph} of 0.025 ± 0.004 s^{-1} and 0.033 ± 0.005 s^{-1} were determined for the lpp18-Cy3 and full-length lpp-Cy3 PRC, respectively. All parameters are presented in Table 5, showing a concentration dependency on RRF.

The rates for the 30S subunit release from the mRNA determined with the mRNA-Cy3 and S3-Cy5 FRET pair for both full length lpp and lpp18 mRNA are very similar to the rates determined for the 70S ribosome splitting with the S6-Cy3 and L9-Cy5 FRET pair (Fig. 38D). Variations are within the standard deviations indicating that the two reactions happen almost simultaneously at each RRF concentration. The measured rates show a dependence on the RRF concentration and appear to have plateaued at 5 µM RRF with the same rates for subunit splitting and mRNA release. These findings are in agreement with the bulk kinetic experiments measured with the stopped-flow technique. In the bulk kinetic experiments, it was also shown that mRNA release and subunit splitting happen simultaneously. However, for the full-length lpp mRNA it was shown that subunit splitting is necessary for the rapid release of the mRNA. This was also indicated by analysis of the S6-L9 FRET traces where the acceptor fluorophore on the 50S subunit disappeared prior to the donor fluorophore on the 30S subunit in 96% of cases. The inverted order of events, where the mRNA release would precede the subunit splitting, was only supported by 4% of the recorded traces. Further it is expected that all these 4% of traces actually show photobleaching of the donor fluorophore instead of the release of the mRNA from the 70S ribosome. From both bulk and single molecule experiments it can be concluded that subunit splitting and mRNA release happen simultaneously for mRNAs with a native structured 3'-UTR, but subunit splitting needs to precede to allow rapid mRNA release. mRNAs with truncated 3'-UTRs were shown in bulk kinetic experiments to rapidly dissociate from the ribosome after translation of the full-length protein even without recycling factors. For this reason, it was not possible to use these mRNAs in smFRET

experiments as PRCs programmed with mRNAs with truncated 3'-UTRs would lose their mRNAs already prior to the measurement.

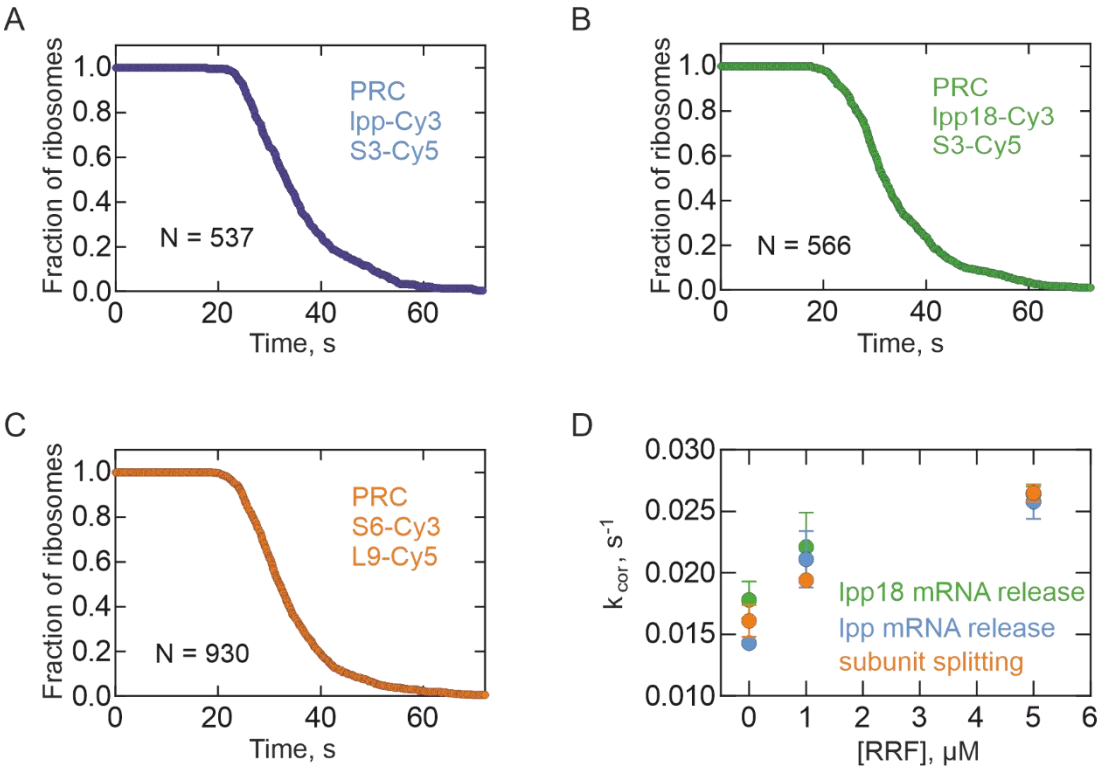

Figure 38. Dependence of mRNA release and subunit splitting on the RRF concentration. Examples of the kinetic analysis of the smFRET traces, shown are experiments at 5 μM RRF. The fraction of ribosomes that show acceptor fluorescence is plotted over time. PRCs with the full-length lpp-Cy3 mRNA (A) or lpp18-Cy3 mRNA (B) and S3-Cy5, and with S6-Cy3 and L9-Cy5 (C) are shown. The resulting FRET trajectories were fitted and corrected for photobleaching. (D) Concentration dependence of the corrected rates k_{cor} for mRNA release of full-length mRNA (blue) and lpp18 (green) and for subunit splitting (orange). Rates were calculated as described (Eq. 8, 9, 10). Error bars show the standard deviation from 3 or 4 independent datasets (Table 6). Single molecule experiments and analysis was performed by Dr. Tamara Senyushkina.

Table 6. Rate constants determined by smFRET.

Complex		N	[RRF], µM	t_{delay}, s	k_{obs}, s^{-1}	k_{cor}, s^{-1}
PRC S3-Cy5 lpp18-Cy3		264	0	24.7	0.054	0.017
		164	0	22.7	0.052	0.016
		152	0	27.5	0.065	0.019
	Mean ± StD			**25.0 ± 2.4**	**0.057 ± 0.007**	**0.018 ± 0.002**
		108	1	29.2	0.095	0.023
		108	1	33.2	0.070	0.018
		162	1	26.4	0.087	0.024
		137	1	26.8	0.093	0.024
	Mean ± StD			**28.9 ± 3.1**	**0.086 ± 0.011**	**0.022 ± 0.003**
		145	5	26.4	0.110	0.026
		199	5	23.9	0.100	0.027
		222	5	23.3	0.089	0.026
	Mean ± StD			**24.5 ± 1.6**	**0.100 ± 0.011**	**0.026 ± 0.0006**
PRC S3-Cy5 full-length lpp-Cy3		191	0	23.3	0.053	0.014
		166	0	24.9	0.055	0.014
		197	0	25.4	0.057	0.015
	Mean ± StD			**24.5 ± 1.1**	**0.055 ± 0.002**	**0.014 ± 0.0006**
		71	1	26.9	0.091	0.023
		99	1	28.7	0.072	0.018
		114	1	28.6	0.091	0.022
	Mean ± StD			**28.1 ± 1.0**	**0.085 ± 0.011**	**0.021 ± 0.002**
		207	5	23.1	0.091	0.025
		132	5	23.4	0.093	0.025
		198	5	23.6	0.110	0.027
	Mean ± StD			**23.3 ± 0.2**	**0.098 ± 0.010**	**0.026 ± 0.001**
PRC S6-Cy3 L9-Cy5 full-length lpp		168	0	24.9	0.056	0.016
		262	0	24.5	0.061	0.018
		259	0	23.9	0.055	0.016
		206	0	26.3	0.053	0.015
	Mean ± StD			**24.9 ± 1.0**	**0.056 ± 0.003**	**0.016 ± 0.001**
		152	1	25.2	0.069	0.020
		277	1	24.7	0.065	0.019
		115	1	25.2	0.067	0.019
		125	1	25.8	0.068	0.020
	Mean ± StD			**25.2 ± 0.4**	**0.067 ± 0.002**	**0.019 ± 0.0004**
		261	5	22.9	0.102	0.027
		201	5	26.4	0.110	0.026
		200	5	22.7	0.093	0.026
		268	5	22.8	0.098	0.027
	Mean ± StD			**23.7 ± 1.8**	**0.100 ± 0.007**	**0.027 ± 0.001**

Single molecule experiments and analysis was performed by Dr. Tamara Senyushkina.

4 Discussion

4.1 Ribosome Recycling in a Physiological Context

The first goal of this thesis was to identify a natural mRNA as a model mRNA for ribosome recycling studies that represents the physiological termination and recycling situation. This was necessary because previous studies on recycling relied on small model mRNAs or mRNA fragments (Chen *et al.*, 2017; Iwakura *et al.*, 2017; Peske *et al.*, 2005). The results were in part contradictory and likely influenced by the unphysiological nature of the model mRNAs used. To find a suitable mRNA, it was firstly necessary to obtain an overview of the bacterial transcriptome. The bacterial transcriptome is highly dynamic and complex. While early studies, for example on the *trp* operon (Platt, 1981; Wu and Platt, 1978), identified the basic rules of bacterial operon structure, the technological advances of whole mRNA sequencing (Conway *et al.*, 2014; Yan *et al.*, 2018) were needed to understand the full complexity. While Rho dependent transcription termination can be disregarded as being too situational and unpredictable, Rho-independent intrinsic termination sufficiently creates varying sets of mRNAs from seemingly static operons (Yan *et al.*, 2018). While it is generally known that mRNAs have 3'-UTRs and often end with a transcription terminator hairpin, the prevalence of these and similar structures within the 3'-regions of genes was not well investigated. Studies on hairpin structures in the 3'-regions of genes have often not sufficiently considered the operon organization of prokaryotes (Chemla et al., 2020; Miura et al., 2018). For this reason, a detailed analysis of the *E. coli* transcriptome was performed in this study to characterize the native termination context in *E. coli* mRNA. The classification of terminal or internal genes of RNASeq confirmed operons (Fig. 14) allowed to differentiate between two different translation termination situations.

In the first situation, termination occurs in the intercistronic space of polycistronic operons, after translation of an ORF that is not the terminal ORF of an operon (Fig. 17C). In bacteria, ORFs of polycistronic operons are relatively compact (Kushner, 2018). ORFs can even overlap (Salgado *et al.*, 2000). In this case, it is unclear if a ribosome that has completed translation of an ORF is recycled after peptide release, i.e. if subunits and mRNA fully dissociate. In principle, the ribosome might be able to re-initiate on the downstream ORF as a non-recycled 70S ribosome (Yamamoto et al., 2016), or as a partially recycled 30S pre-initiation complex (Milon and Rodnina, 2012). In the latter case, the action of EF-G and RRF would cause subunit splitting resulting in the loss of the 50S subunit. The 30S subunit would stay attached to the mRNA and can find the next start codon with the help of initiation factors. It appears possible that re-initiation might be highly context dependent and carefully modulated by the distance between ORFs and appearance and strengths of an SD

sequence nearby (Huber et al., 2019; Yoo and RajBhandary, 2008). Internal regions of polycistronic operons were also analyzed with the previously described data pipeline (Fig. 17C) but were not considered in further experiments because it is unclear if mRNA release is a biologically desired step of intercistronic ribosome recycling. Nevertheless, it would be interesting to explore this relationship between recycling and re-initiation in future experiments.

While it remains unclear under which circumstances recycling and eventual re-initiation on downstream genes can happen, recycling must happen after translation of a monocistronic mRNA or of the terminal ORF of a polycistronic mRNA (Fig. 17B). The focus of this thesis is, therefore, on this native termination situation. Here, the results of the bioinformatic analysis confirmed the hypothesis that the terminal 3'-regions of genes are generally rich in hairpin structures. The overwhelming presence of strong hairpin elements centering within the first 100 nts after the stop codon of terminal genes (Fig. 16, 17B, 18) suggest that most 3'-UTRs indeed can be formed by intrinsic transcription termination on a terminator hairpin. However, classification of found hairpins is beyond the scope of this thesis. The research on what part of those hairpins are efficient transcription terminators and which are only serving as stability elements would require a more detailed analysis of the complexity hinted by full length mRNA sequencing studies (Conway *et al.*, 2014; Yan *et al.*, 2018). For a future extended analysis, several additional factors need to be considered. While it is known that a single operon usually can create multiple different mRNAs, in this study, the simplification of equaling one operon with only one mRNA was necessary to simplify the performed analysis. The reduced coverage of the GSE52059 dataset (Conway *et al.*, 2014), that included approximately two thirds of the over 4000 *E. coli* genes discovered so far, however, was considered beneficial to represent the *E. coli* transcriptome as a significant portion of GenBank annotated genes are not protein-coding, only situational or low expressed or even considered non-functional evolutionary artifacts. As only sufficiently expressed mRNAs can be found via RNA sequencing above background level, the reported operons can be considered as representatives for the bacterial transcriptome. In this thesis, the 1249 terminal genes that have been found by RNA sequencing were studied. Together with the 1450 internal genes, they account for 2699 of the 4153 protein coding genes from *E. coli* that were also analyzed. To extend this analysis in the future, the role of rho dependent transcription termination must also be considered as it may lead to different, possible shorter 3'-UTRs (Mitra *et al.*, 2017).

The transcriptome analysis confirmed that the lpp mRNA, the natural mRNA of the major outer membrane prolipoprotein Lpp (Nakamura and Inouye, 1979), was an suitable representative model mRNA for a physiological recycling situation to study the mRNA release during recycling.

4.2 Establishment of FRET Labels Using LplA

Many reactions of molecular machines such as the ribosome can be best observed when fluorophores on reaction relevant positions are directly or indirectly affected. Most fluorophores are sensitive to changes in the environment and alter their photophysical properties upon approximation to certain chemical groups. This effect can, for example, be used to observe the movement of the mRNA during translocation with a fluorophore at the 3'-end of the mRNA that is dragged closer to the ribosome during the reaction (Peske et al., 2004; Savelsbergh *et al.*, 2003). But usually, it is not desired that the used fluorophores are directly affected as it may be difficult to then assign fluorescence changes to the correct reaction (Fig. 24D). As reactions of molecular machines such as the ribosome often consist of multiple steps, this phase assignment might be problematic. To observe reactions with a pair of fluorophores suitable for FRET that are not directly affected by the reaction but are altered in their distance to each other has advantages because these signal changes can often be easier assigned to a process. Binding and release of factors, head swiveling, subunit rotation or splitting can be observed with FRET partners at different positions on the ribosome or on the interacting factors (Belardinelli *et al.*, 2016a). In this thesis, the aim was to measure subunit splitting and the release of an mRNA from the ribosome. The assay to measure subunit splitting via light scattering in bulk kinetic experiments was already established (Savelsbergh *et al.*, 2009). The established labeling positions on the protein S6 on the 30S subunit and L9 on the 50S subunit, originally designed for measuring subunit rotation (Sharma *et al.*, 2016), could be used to measure subunit splitting in smFRET experiments. A method to measure the release of a long native mRNA from the 30S subunit had to be developed. As almost all ribosomal proteins in the relevant area near the mRNA entry tunnel (Fig. 21) were essential to *E. coli*, a multi-step enzyme-supported bioconjugation technique was adapted to introduce a fluorescent dye onto the 30S subunit.

Among the rapidly expanding variety of tag-based site specific bioconjugation techniques, the LplA based method was chosen. Here, the lipoic acid ligase $LplA^{W37V}$ was used to site specifically introduce a fluorophore to the ribosome for the first time (Fig. 22). A norbornene group was introduced to the LAP-tag for subsequent inverse-electron demand Diels-Alder reaction with Me-tetrazine conjugated dyes as previously described (Baalmann *et al.*, 2018), but significant ribosome specific adaptions had to be made to the original protocol. Introduction of the LAP-tag into the genome of cell lines may be in principle possible, transient overexpression is a good alternative suitable for ribosomal proteins. Overexpression of LAP-tagged ribosomal proteins in BW25113 enabled purification of catalytically active and tagged ribosomes (Fig. 23, 24, 26). Catalytic activity

of the S3-LAP-tagged ribosomes was comparable to unmodified wild type ribosomes (Fig. 27). The LAP-tag itself is with only 13 aa amongst the smallest bioconjugation tags, especially when compared to the almost 300 aa big HALO-tag (Los et al., 2008). Modification of the LAP-tag with a norbornene moiety by LplA was optimized and in the end carried out in a way that compromised high functionalization efficiency with minimal unspecific background functionalization (Fig. 25, 26). LplA mediated LAP-tag functionalization and the subsequent labeling reaction efficiently work under mild conditions. This means the labeling steps can be performed in almost all buffer systems and even in cell lysate and only require a minimal magnesium and reactant concentrations. This enables the integration of the labeling into already established purification protocols. The flexible modularity of LAP-tag labeling allowed the test of many different commercially available Me-tetrazine conjugated fluorophores such as Cy3, Cy5 or ATTO488.

Use of LplA for site-specific labeling of ribosomes has many advantages over other labeling techniques reported. Here, also the knock-out and reconstitution path (Belardinelli *et al.*, 2016a; Ermolenko *et al.*, 2007) was used for labeling of the ribosomal proteins S6 and L9 (Sharma *et al.*, 2016). This method requires the ribosomal target proteins to be non-lethal when knocked out as ribosomes need to be purified from cultivatable knock-out strains. In addition, the target proteins must not contain functional important cysteines. To ensure site specificity of the labeling reaction with the maleimide conjugated fluorophore, typically all cysteines but the targeted one must be exchanged for other amino acids. For many ribosomal proteins such as S3 this is not possible because the knock-out is lethal (Shoji *et al.*, 2011). However, as shown here, *E. coli* tolerates the introduction of a protein tag to many essential proteins without them losing their function and activity on the ribosome (Fig. 23, 27).

Utilizing enzymes like the lipoic acid ligase LplA or the biotin ligase BirA for site specific bioconjugation is a relatively young concept with enormous potential. In *E. coli*, the function of LplA is to introduce a particular post-translational modification (lipoylation) to specific sequence of its target protein (Fujiwara et al., 2005). LplA also accepts other substrates and can be used to introduce various reactive groups (Fernández-Suárez et al., 2007). The W37V mutation of LplA allows the use of a broader variety of substrates (Baruah et al., 2008). The improved sequence of the 13 aa LAP-tag increases modification efficiency (Puthenveetil *et al.*, 2009). LplA mediated modification of LAP-tagged target proteins have been used for a large variety of subsequent bioconjugation reactions such as azide-alkyne click chemistry to introduce PEGylation (Plaks et al., 2015), Sonogashira cross-coupling (Hauke et al., 2014) or inverse-electron demand Diels-Alder reaction (Best *et al.*, 2015) to introduce fluorophores. Apart from more obvious uses of LplA like highly specific *in vitro* or cell surface fluorescence labeling (Baalmann *et al.*, 2018), rather particular

approaches have been made to utilize LplA for site specific radiofluorination (Drake et al., 2016) or to engineer antibody-drug conjugates for temporal controlled sequential release of cooperative drug combinations (Thornlow et al., 2019).

The shown experiments and applications demonstrate the benefits of the LplA mediated bioconjugation. The work described here can be adapted to establish other labeling positions on the ribosome enabling further research. The example of site-specifically labeling ribosomes may also be helpful for research on other multicomponent molecular machines such as RNA polymerases, the spliceosome, the proteasome and others.

4.3 mRNA Release in a Native Termination Context

The main goal of this study was to find out when a natural mRNA in a native termination background will be recycled from the ribosome in relation to the subunit splitting. The lpp mRNA served as a suitable and representative model mRNA. It showed a high efficiency in initiation and translation. Its maximum translation speed of 4.4 (Fig. 20) to 4.9 (Fig. 31) aa/s was in the range of 4 to 22 aa/s reported for bacterial translation (Wohlgemuth *et al.*, 2010). This was sufficient for the use in further experiments. Utilizing the LplA/LAP-tag labeling method, a FRET pair was created between the 3'-end of the mRNA and the protein S3 on the 30S subunit. This FRET pair allowed to observe the mRNA during elongation, termination and recycling and most importantly, the assay showed a distinct signal for the release of the mRNA (Fig. 28). This mRNA release phase during recycling was identified and characterized with control experiments. The phase assignment then allowed comparison with the subunit splitting reaction measured with the same complexes (Fig. 32C). For subunit splitting, a separate experimental setup measuring the light scattering of the ribosomal subunits was used (Savelsbergh *et al.*, 2009). Additionally, single molecule experiments were performed to measure mRNA release and subunit splitting. In single molecule experiments the S3-mRNA FRET pair was used to measure the mRNA release and subunit splitting was observed with the S6-L9 FRET pair (Sharma *et al.*, 2016).

The measured rates for subunit splitting from bulk and single molecule experiments can be compared to the rates measured in previous studies (Tab. 7). The different rates reported reflect the sensitivity of the subunit splitting reaction to different experimental setups, factor concentrations, buffer systems and other parameters. In the bulk kinetic experiments described

here, the translation of the ORF prior to the release and recycling reactions is clearly the rate defining step causing the subunit splitting and mRNA release to happen after a significant delay time (Fig. 32C). Nevertheless, the here reported rates determined for the subunit splitting are very close to the rates reported for experiments with similar factor concentrations and conditions (Peske *et al.*, 2005). In the single molecule experiments, pre-recycling complexes were used which are stalled with RF1 in the A site of the ribosome. Action of RF3 then enables RRF and EF-G to bind and carry out the subunit splitting. The reported rates (Tab. 7) were corrected for photobleaching and spontaneous complex degradation but the necessity to release RF1 via RF3 before RRF can bind to the ribosome still contributes to the rate. Considering the low factor concentration and temperature that slow down the reaction, the results are still comparable to similarly obtained numbers from single molecule studies (Prabhakar *et al.*, 2017), where a low RF2 concentration in the imaging buffer was used to prepare ribosome complexes for the recycling reaction. In that study, the time between RF2 dissociation and subunit splitting was measured (Tab. 7).

Table 7. Example rates (k) measured for subunit splitting from different kinetic studies.

Source	[RRF], µM	[EF-G], µM	Buffer	Temperature	k, s^{-1}
lpp mRNA*[1]	5	2.5	TAKM HiFi	37°C	0.19 ± 0.05[#]
lpp-no-Pin*[1]	5	2.5	TAKM HiFi	37°C	0.15 ± 0.02[#]
lpp-stop*[1]	5	2.5	TAKM HiFi	37°C	0.15 ± 0.05[#]
lpp mRNA*[3]	0	1	TAKM HiFi	RT	0.016 ± 0.001
lpp mRNA*[3]	1	1	TAKM HiFi	RT	0.019 ± 0.0004
lpp mRNA*[3]	5	1	TAKM HiFi	RT	0.027 ± 0.001
(Peske *et al.*, 2005)*[1]	5	2	$TAKM_7$	37°C	0.3 ± 0.1
	5	saturated	$TAKM_7$	37°C	0.7 ± 0.2
(Chen *et al.*, 2017)*[1]	2	3	$TAKM_5$	37°C	0.39 ± 0.05[a]
	2	3	$TAKM_5$	37°C	0.50 ± 0.04[b]
	2	3	$TAKM_{7.5}$	37°C	0.074 ± 0.004
	2	3	$TAKM_3$	37°C	2.8 ± 0.1
(Borg *et al.*, 2016)*[1]	40	5.1	TAKM HiFi	37°C	25
	15	4.5	TAKM HiFi	37°C	5
	5	3	TAKM HiFi	37°C	2
(Iwakura *et al.*, 2017)*[2]	5	5	$TAKM_8$	30°C	0.008 ± 0.002
(Prabhakar *et al.*, 2017)*[3]	20	50	TAKM HiFi	RT	1.5 s[†]
	20	0.05	TAKM HiFi	RT	13.9 s[†]

*[1]rapid kinetic experiment *[2]low time resolution experiment *[3]smFRET [#]full translation system [†]Mean time between RF2 dissociation and subunit splitting [a]mRNA without SD [b]mRNA with SD

While the splitting of subunits is independent of the mRNA type, the dissociation kinetics of the mRNA is notably influenced by the specific mRNA context. A 50-fold difference was previously reported for the release rates of mRNAs with and without a SD sequence (Chen *et al.*, 2017). As the subunit splitting is better understood than the mRNA release, it is beneficial not to compare the mRNA release rates between different studies but to the subunit splitting rates in those respective studies. This allows to discuss and determine the order of events and gain mechanistic insights.

The apparent rates measured for mRNA release and subunit splitting are identical within the error of the measurement (Tab. 3, 6). This is caused by the limitations in the temporal resolution of the experiments. The qualitative analysis still suggests that the subunit splitting must precede to enable the spontaneous release of the native mRNA. In single molecule experiments with the S6-L9 FRET pair, it was shown that the 50S subunit is released from the mRNA prior to the 30S subunit in most cases (Fig. 37). This shows how subunit splitting precedes the mRNA release. The results of the bulk kinetic experiments with the full-length native mRNA also indicate this order of events (Fig. 32). The mechanistic requirement of subunit splitting for mRNA release becomes clear in the experiments without recycling factors and with the 3'-UTR truncated mRNAs (Fig. 35). Whereas the 3'-truncated mRNAs can spontaneously dissociate from the ribosome after translation of the protein, the mRNA with the structured native 3'-UTR only dissociates with a very slow rate likely corresponding to complex degradation. This shows the requirement of the subunit splitting for the release of the native mRNA. In conclusion, it was shown here that with a natural mRNA with a native structured 3'-UTR, the recycling happens in the order that the mRNA dissociates rapidly after subunit splitting. As the mRNA enters the ribosome on the 30S subunit between the ribosomal proteins S3, S4 and S5 and is then located on the 50S subunit facing side between the head and body of the 30S subunit (Rozov *et al.*, 2019), it appears logical that the subunits must split before the mRNA can be released. Likely, the structured 3'-UTR makes it sterically difficult for the mRNA to spontaneously dissociate from the ribosome.

The clear order of events and requirement of the mRNA release on the subunit splitting was less pronounced for the 3'-truncated mRNAs. While for the lpp-no-Pin mRNA that ends 8 nts after the stop codon and lacks the native hairpin, the presence of recycling factors accelerated mRNA release notably, the lpp-stop mRNA that ends with the stop codon and has no 3'-UTR dissociated from the ribosome spontaneously and rapidly after translation was finished. Here, subunit splitting was not a requirement and neither the presence of recycling factors. This shows that a natural 3'-UTR is important for the complex stability. Further, the slowly decreasing light scattering signal suggests that ribosomes that have lost their mRNA might be intrinsically less stable than ribosome complexes with a bound mRNA and might therefore dissociate under the low Mg^{2+} (3.5 mM) conditions in the

experiment. Apparently, the subunits and the mRNA altogether contribute to the overall complex stability. This behavior also prohibited the creation of PRCs that contain these 3'-mutant mRNAs for smFRET experiments, as the complexes were not stable enough for the conditions of the measurements.

The destabilization resulting from the lack of a natural 3'-UTR can also explain the very rapid rates for mRNA release that have been measured in a previous study (Chen *et al.*, 2017). Small mRNAs lacking a natural 3'-UTR appear to be prone to dissociation from ribosomal complexes that have only a deacylated tRNA in the P site and lack a peptide due to peptide release by release factors or due to preparation of ribosome complexes via incubation of ribosomes, mRNA and deacylated tRNA (Chen *et al.*, 2017). Together with the intrinsic instability of ribosomes without mRNA at low Mg^{2+} concentrations, these effects need to be considered in studies on ribosome recycling that use unnatural or short mRNAs.

The findings reported here are also different from what was shown with model mRNAs that contain a SD sequence (Chen *et al.*, 2017; Peske *et al.*, 2005). When recycling is measured with mRNAs that contain an SD sequence aligned with the aSD motif of the ribosome, the mRNA stays attached to the ribosome after subunit splitting for a significant period of time (Peske *et al.*, 2005). Here, it is unclear if IF3 plays a role for the eventual release of the mRNA and the tRNA from the 30S subunit (Fu *et al.*, 2016; Karimi *et al.*, 1999; Peske *et al.*, 2005). However, in proximity of the terminal stop codon of natural mRNAs where recycling happens *in vivo*, SD sequences are usually not expected to be more frequent than in the average genome. Further, it is controversially discussed whether SD sequences alone have major implications on the ribosome or whether the integration into a proper ribosome binding site is needed for successful stabilization of the ribosome on that mRNA position (Mohammad et al., 2016).

4.4 Unifying Model of Prokaryotic Ribosome Recycling

This study shows the order of events for recycling of ribosomes in a full translation system with a natural mRNA with a native structured 3'-UTR: first the 70S ribosome is split into subunits before the mRNA dissociates. Likely, this means that subunit splitting is the rate-limiting step for the release of a natural mRNA. Additionally, the experiments with the short lpp18 mRNA show that mRNA release is independent of the ORF length. A native termination situation is critical for

studying the order of events as an unnatural situation might allow the mRNA to dissociate from the ribosome without requiring subunit splitting or it remains bound to the 30S subunit via because of SD-aSD interactions.

Different models for the mechanism of subunit splitting initially existed but the scientific consensus now favors a mechanism where RRF binding is followed by EF-G binding and GTP hydrolysis that leads to the disruption of inter-subunit bridges leading to the subunit splitting (Agrawal *et al.*, 2004; Barat *et al.*, 2007; Borg *et al.*, 2016; Dunkle *et al.*, 2011; Gao *et al.*, 2007; Gao *et al.*, 2005; Pai *et al.*, 2008; Peske *et al.*, 2005; Savelsbergh *et al.*, 2009; Yokoyama *et al.*, 2012). This disruption of subunit bridges has been shown in detail in recent structural studies (Fu *et al.*, 2016) and supported by extensive rapid kinetic and single molecule studies (Borg *et al.*, 2016; Prabhakar *et al.*, 2017).

The release of the deacylated P-site tRNA during recycling was not investigated here. In previous studies different models for tRNA release were proposed. It appears that tRNA release might also be context dependent. In studies where the mRNA persists on the 30S subunit after subunit splitting also the tRNA remains bound (Fu *et al.*, 2016; Peske *et al.*, 2005). In the case where fast mRNA release is observed with unstably bound mRNAs, usually also a fast tRNA release was observed which was either slower (Chen *et al.*, 2017) or faster than mRNA release (Iwakura *et al.*, 2017). Different tRNAs show slightly different rates, for example, a 2-fold difference was reported for Phe and Gly tRNAs (Chen *et al.*, 2017). To get a comprehensive picture of tRNA release upon recycling of ribosomes translating natural mRNAs and in a native termination background, it is therefore necessary to test at least a representative selection of tRNAs.

The role of IF3 has not been addressed in this thesis and it remains unclear if IF3 enhances the release of mRNA and tRNA from the 30S subunit after subunit splitting. Studies that used small model mRNAs with a SD sequence suggested that IF3 is needed for the release of the tRNA from the 30S subunit (Fu *et al.*, 2016; Karimi *et al.*, 1999; Peske *et al.*, 2005). In the single molecule experiments shown here, IF3 was not used, and the results did not differ from the bulk experiments which were done in the presence of IF3. The reason for adding IF3 in the bulk kinetic experiments was that IF3 was needed to prevent reassociation of the subunits. However, if IF3 influences the release of the native mRNA was not investigated and needs further experiments.

The results of this thesis and the data from previous studies such as the comprehensive analysis of subunit splitting (Borg *et al.*, 2016) can be integrated into a unifying model of ribosome recycling (Fig. 30). Here, RRF binds to the post-termination complex and is followed by EF-G binding and GTP hydrolysis which leads to the disruption of inter-subunit bridges and causes splitting of the 70S ribosome into a 50S subunit and a 30S subunit which ich still bound to the mRNA and to that likely

also the tRNA (Agrawal *et al.*, 2004; Barat *et al.*, 2007; Borg *et al.*, 2016; Dunkle *et al.*, 2011; Gao *et al.*, 2007; Gao *et al.*, 2005; Pai *et al.*, 2008; Peske *et al.*, 2005; Savelsbergh *et al.*, 2009; Yokoyama *et al.*, 2012). The mRNA dissociates immediately after splitting from the 30S subunit. RRF and EF-G dissociate from the 50S subunit (Barat *et al.*, 2007; Fu *et al.*, 2016) and IF3 binds the 30S subunit preventing re-association of the subunits (Hirokawa *et al.*, 2005). An effect of IF3 on mRNA and tRNA release is unclear. tRNA release remains controversially discussed (Chen *et al.*, 2017; Iwakura *et al.*, 2017; Peske *et al.*, 2005) and more research must be done.

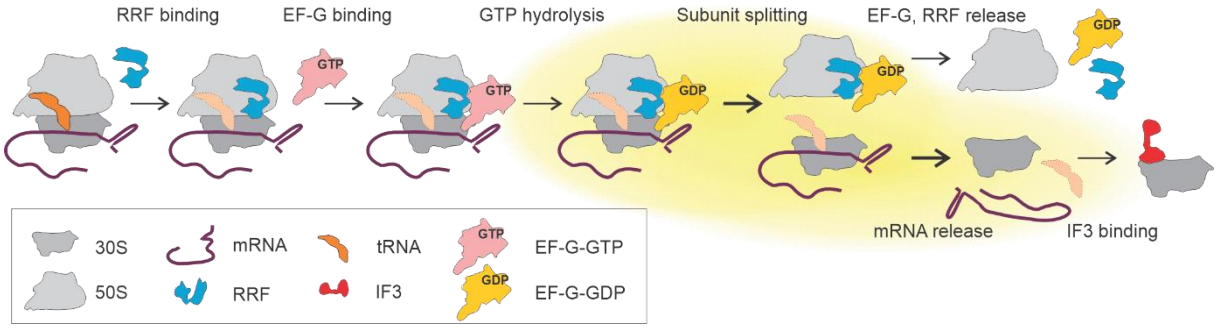

Figure 39. Unifying model of ribosome recycling. Recycling on a natural mRNA with a structured 3'-UTR. The above described results showing subunit splitting preceding the mRNA release are highlighted and integrated into the models previously summarized in other studies (Borg *et al.*, 2016). tRNA (orange) release was not addressed and is still controversially discussed (Chen *et al.*, 2017; Iwakura *et al.*, 2017; Peske *et al.*, 2005) indicated by fading color.

4.5 Conclusion and Perspective

In summary, the release of a natural mRNA with a native structured 3'-UTR from the ribosome upon recycling was observed by means of bulk kinetic and single molecule techniques. In order to find a suitable model mRNA, a transcriptome analysis was performed in this study. Establishment of a FRET pair using a sophisticated bioconjugation technique enabled to observe the release of the mRNA from the 30S subunit. The outcome of this thesis allowed to integrate the mRNA release into a unifying model of prokaryotic ribosome recycling. The main focus of future experiments will be on tRNA release during recycling and the interplay of recycling and re-initiation in intercistronic regions of the mRNA to close the remaining gaps in knowledge about prokaryotic recycling.

5 References

Adio, S., Senyushkina, T., Peske, F., Fischer, N., Wintermeyer, W., and Rodnina, M.V. (2015). Fluctuations between multiple EF-G-induced chimeric tRNA states during translocation on the ribosome. Nat Commun *6*, 7442. 10.1038/ncomms8442.

Adio, S., Sharma, H., Senyushkina, T., Karki, P., Maracci, C., Wohlgemuth, I., Holtkamp, W., Peske, F., and Rodnina, M.V. (2018). Dynamics of ribosomes and release factors during translation termination in E. coli. Elife *7*. 10.7554/eLife.34252.

AEvarsson, A., Brazhnikov, E., Garber, M., Zheltonosova, J., Chirgadze, Y., al-Karadaghi, S., Svensson, L.A., and Liljas, A. (1994). Three-dimensional structure of the ribosomal translocase: elongation factor G from Thermus thermophilus. EMBO J *13*, 3669-3677. 10.1002/j.1460-2075.1994.tb06676.x.

Agrawal, R.K., Sharma, M.R., Kiel, M.C., Hirokawa, G., Booth, T.M., Spahn, C.M., Grassucci, R.A., Kaji, A., and Frank, J. (2004). Visualization of ribosome-recycling factor on the Escherichia coli 70S ribosome: functional implications. Proc Natl Acad Sci U S A *101*, 8900-8905. 10.1073/pnas.0401904101.

Alkalaeva, E.Z., Pisarev, A.V., Frolova, L.Y., Kisselev, L.L., and Pestova, T.V. (2006). In vitro reconstitution of eukaryotic translation reveals cooperativity between release factors eRF1 and eRF3. Cell *125*, 1125-1136. 10.1016/j.cell.2006.04.035.

Andreeva, I., Belardinelli, R., and Rodnina, M.V. (2018). Translation initiation in bacterial polysomes through ribosome loading on a standby site on a highly translated mRNA. Proc Natl Acad Sci U S A *115*, 4411-4416. 10.1073/pnas.1718029115.

Baalmann, M., Best, M., and Wombacher, R. (2018). Site-Specific Protein Labeling Utilizing Lipoic Acid Ligase (LplA) and Bioorthogonal Inverse Electron Demand Diels-Alder Reaction. Methods Mol Biol *1728*, 365-387. 10.1007/978-1-4939-7574-7_23.

Ban, N., Nissen, P., Hansen, J., Moore, P.B., and Steitz, T.A. (2000). The complete atomic structure of the large ribosomal subunit at 2.4 A resolution. Science *289*, 905-920. 10.1126/science.289.5481.905.

Barat, C., Datta, P.P., Raj, V.S., Sharma, M.R., Kaji, H., Kaji, A., and Agrawal, R.K. (2007). Progression of the ribosome recycling factor through the ribosome dissociates the two ribosomal subunits. Mol Cell *27*, 250-261. 10.1016/j.molcel.2007.06.005.

Baruah, H., Puthenveetil, S., Choi, Y.-A., Shah, S., and Ting, A.Y. (2008). An Engineered Aryl Azide Ligase for Site-Specific Mapping of Protein–Protein Interactions through Photo-Cross-Linking. Angewandte Chemie International Edition *47*, 7018-7021. 10.1002/anie.200802088.

Belardinelli, R., Sharma, H., Caliskan, N., Cunha, C.E., Peske, F., Wintermeyer, W., and Rodnina, M.V. (2016a). Choreography of molecular movements during ribosome progression along mRNA. Nat Struct Mol Biol *23*, 342-348. 10.1038/nsmb.3193.

Belardinelli, R., Sharma, H., Peske, F., Wintermeyer, W., and Rodnina, M.V. (2016b). Translocation as continuous movement through the ribosome. RNA Biol *13*, 1197-1203. 10.1080/15476286.2016.1240140.

Ben-Shem, A., Garreau de Loubresse, N., Melnikov, S., Jenner, L., Yusupova, G., and Yusupov, M. (2011). The structure of the eukaryotic ribosome at 3.0 A resolution. Science *334*, 1524-1529. 10.1126/science.1212642.

Berthold, M.R., Cebron, N., Dill, F., Gabriel, T.R., Kötter, T., Meinl, T., Ohl, P., Sieb, C., Thiel, K., and Wiswedel, B. (2008). KNIME: The Konstanz Information Miner. held in Berlin, Heidelberg, 2008//. C. Preisach, H. Burkhardt, L. Schmidt-Thieme, and R. Decker, eds. (Springer Berlin Heidelberg), pp. 319-326.

Best, M., Degen, A., Baalmann, M., Schmidt, T.T., and Wombacher, R. (2015). Two-step protein labeling by using lipoic acid ligase with norbornene substrates and subsequent inverse-electron demand Diels-Alder reaction. Chembiochem *16*, 1158-1162. 10.1002/cbic.201500042.

Bieri, P., Leibundgut, M., Saurer, M., Boehringer, D., and Ban, N. (2017). The complete structure of the chloroplast 70S ribosome in complex with translation factor pY. EMBO J *36*, 475-486. 10.15252/embj.201695959.

Bjornsson, A., Mottagui-Tabar, S., and Isaksson, L.A. (1996). Structure of the C-terminal end of the nascent peptide influences translation termination. EMBO J *15*, 1696-1704.

Bock, L.V., Blau, C., Schroder, G.F., Davydov, II, Fischer, N., Stark, H., Rodnina, M.V., Vaiana, A.C., and Grubmuller, H. (2013). Energy barriers and driving forces in tRNA translocation through the ribosome. Nat Struct Mol Biol *20*, 1390-1396. 10.1038/nsmb.2690.

Borg, A., Pavlov, M., and Ehrenberg, M. (2016). Complete kinetic mechanism for recycling of the bacterial ribosome. RNA *22*, 10-21. 10.1261/rna.053157.115.

Bowman, J.C., Hud, N.V., and Williams, L.D. (2015). The Ribosome Challenge to the RNA World. Journal of Molecular Evolution *80*, 143-161. 10.1007/s00239-015-9669-9.

Bowman, J.C., Petrov, A.S., Frenkel-Pinter, M., Penev, P.I., and Williams, L.D. (2020). Root of the Tree: The Significance, Evolution, and Origins of the Ribosome. Chem Rev *120*, 4848-4878. 10.1021/acs.chemrev.9b00742.

Brilot, A.F., Korostelev, A.A., Ermolenko, D.N., and Grigorieff, N. (2013). Structure of the ribosome with elongation factor G trapped in the pretranslocation state. Proc Natl Acad Sci U S A *110*, 20994-20999. 10.1073/pnas.1311423110.

Brown, A., Shao, S., Murray, J., Hegde, R.S., and Ramakrishnan, V. (2015). Structural basis for stop codon recognition in eukaryotes. Nature *524*, 493-496. 10.1038/nature14896.

Carter, A.P., Clemons, W.M., Jr., Brodersen, D.E., Morgan-Warren, R.J., Hartsch, T., Wimberly, B.T., and Ramakrishnan, V. (2001). Crystal structure of an initiation factor bound to the 30S ribosomal subunit. Science *291*, 498-501. 10.1126/science.1057766.

Chemla, Y., Peeri, M., Heltberg, M.L., Eichler, J., Jensen, M.H., Tuller, T., and Alfonta, L. (2020). A possible universal role for mRNA secondary structure in bacterial translation revealed using a synthetic operon. Nat Commun *11*, 4827. 10.1038/s41467-020-18577-4.

Chen, Y., Kaji, A., Kaji, H., and Cooperman, B.S. (2017). The kinetic mechanism of bacterial ribosome recycling. Nucleic Acids Res *45*, 10168-10177. 10.1093/nar/gkx694.

Conway, T., Creecy, J.P., Maddox, S.M., Grissom, J.E., Conkle, T.L., Shadid, T.M., Teramoto, J., San Miguel, P., Shimada, T., Ishihama, A., et al. (2014). Unprecedented high-resolution view of bacterial operon architecture revealed by RNA sequencing. MBio *5*, e01442-01414. 10.1128/mBio.01442-14.

Creecy, J.P., and Conway, T. (2015). Quantitative bacterial transcriptomics with RNA-seq. Curr Opin Microbiol *23*, 133-140. 10.1016/j.mib.2014.11.011.

Cridge, A.G., Major, L.L., Mahagaonkar, A.A., Poole, E.S., Isaksson, L.A., and Tate, W.P. (2006). Comparison of characteristics and function of translation termination signals between and within prokaryotic and eukaryotic organisms. Nucleic Acids Res *34*, 1959-1973. 10.1093/nar/gkl074.

Cunha, C.E., Belardinelli, R., Peske, F., Holtkamp, W., Wintermeyer, W., and Rodnina, M.V. (2013). Dual use of GTP hydrolysis by elongation factor G on the ribosome. Translation (Austin) *1*, e24315. 10.4161/trla.24315.

Dallas, A., and Noller, H.F. (2001). Interaction of translation initiation factor 3 with the 30S ribosomal subunit. Mol Cell *8*, 855-864. 10.1016/s1097-2765(01)00356-2.

Diaconu, M., Kothe, U., Schlunzen, F., Fischer, N., Harms, J.M., Tonevitsky, A.G., Stark, H., Rodnina, M.V., and Wahl, M.C. (2005). Structural basis for the function of the ribosomal L7/12 stalk in factor binding and GTPase activation. Cell *121*, 991-1004. 10.1016/j.cell.2005.04.015.

Drake, C.R., Sevillano, N., Truillet, C., Craik, C.S., VanBrocklin, H.F., and Evans, M.J. (2016). Site-Specific Radiofluorination of Biomolecules with 8-[(18)F]-Fluorooctanoic Acid Catalyzed by Lipoic Acid Ligase. ACS Chem Biol *11*, 1587-1594. 10.1021/acschembio.6b00172.

Dreyfus, M. (1988). What constitutes the signal for the initiation of protein synthesis on Escherichia coli mRNAs? J Mol Biol *204*, 79-94. 10.1016/0022-2836(88)90601-8.

Dunkle, J.A., Wang, L., Feldman, M.B., Pulk, A., Chen, V.B., Kapral, G.J., Noeske, J., Richardson, J.S., Blanchard, S.C., and Cate, J.H. (2011). Structures of the bacterial ribosome in classical and hybrid states of tRNA binding. Science *332*, 981-984. 10.1126/science.1202692.

Emory, S.A., Bouvet, P., and Belasco, J.G. (1992). A 5'-terminal stem-loop structure can stabilize mRNA in Escherichia coli. Genes Dev *6*, 135-148. 10.1101/gad.6.1.135.

Ermolenko, D.N., Majumdar, Z.K., Hickerson, R.P., Spiegel, P.C., Clegg, R.M., and Noller, H.F. (2007). Observation of Intersubunit Movement of the Ribosome in Solution Using FRET. Journal of Molecular Biology *370*, 530-540. 10.1016/j.jmb.2007.04.042.

Fei, J., Kosuri, P., MacDougall, D.D., and Gonzalez, R.L., Jr. (2008). Coupling of ribosomal L1 stalk and tRNA dynamics during translation elongation. Mol Cell *30*, 348-359. 10.1016/j.molcel.2008.03.012.

Fernández-Suárez, M., Baruah, H., Martínez-Hernández, L., Xie, K.T., Baskin, J.M., Bertozzi, C.R., and Ting, A.Y. (2007). Redirecting lipoic acid ligase for cell surface protein labeling with small-molecule probes. Nat Biotechnol *25*, 1483-1487. 10.1038/nbt1355.

Fraser, C.S., Berry, K.E., Hershey, J.W., and Doudna, J.A. (2007). eIF3j is located in the decoding center of the human 40S ribosomal subunit. Mol Cell *26*, 811-819. 10.1016/j.molcel.2007.05.019.

Fu, Z., Kaledhonkar, S., Borg, A., Sun, M., Chen, B., Grassucci, R.A., Ehrenberg, M., and Frank, J. (2016). Key Intermediates in Ribosome Recycling Visualized by Time-Resolved Cryoelectron Microscopy. Structure *24*, 2092-2101. 10.1016/j.str.2016.09.014.

Fujiwara, K., Toma, S., Okamura-Ikeda, K., Motokawa, Y., Nakagawa, A., and Taniguchi, H. (2005). Crystal Structure of Lipoate-Protein Ligase A from Escherichia coli: DETERMINATION OF THE LIPOIC ACID-BINDING SITE *. Journal of Biological Chemistry *280*, 33645-33651. 10.1074/jbc.M505010200.

Fujiwara, T., Ito, K., and Nakamura, Y. (2001). Functional mapping of ribosome-contact sites in the ribosome recycling factor: a structural view from a tRNA mimic. RNA *7*, 64-70. 10.1017/s1355838201001704.

Fujiwara, T., Ito, K., Yamami, T., and Nakamura, Y. (2004). Ribosome recycling factor disassembles the post-termination ribosomal complex independent of the ribosomal translocase activity of elongation factor G. Mol Microbiol *53*, 517-528. 10.1111/j.1365-2958.2004.04156.x.

Gao, N., Zavialov, A.V., Ehrenberg, M., and Frank, J. (2007). Specific interaction between EF-G and RRF and its implication for GTP-dependent ribosome splitting into subunits. J Mol Biol *374*, 1345-1358. 10.1016/j.jmb.2007.10.021.

Gao, N., Zavialov, A.V., Li, W., Sengupta, J., Valle, M., Gursky, R.P., Ehrenberg, M., and Frank, J. (2005). Mechanism for the disassembly of the posttermination complex inferred from cryo-EM studies. Mol Cell *18*, 663-674. 10.1016/j.molcel.2005.05.005.

Goyal, A., Belardinelli, R., Maracci, C., Milon, P., and Rodnina, M.V. (2015). Directional transition from initiation to elongation in bacterial translation. Nucleic Acids Res *43*, 10700-10712. 10.1093/nar/gkv869.

Goyal, A., Belardinelli, R., and Rodnina, M.V. (2017). Non-canonical Binding Site for Bacterial Initiation Factor 3 on the Large Ribosomal Subunit. Cell Rep *20*, 3113-3122. 10.1016/j.celrep.2017.09.012.

Greber, B.J., and Ban, N. (2016). Structure and Function of the Mitochondrial Ribosome. Annu Rev Biochem *85*, 103-132. 10.1146/annurev-biochem-060815-014343.

Gruber, A.R., Lorenz, R., Bernhart, S.H., Neubock, R., and Hofacker, I.L. (2008). The Vienna RNA websuite. Nucleic Acids Res *36*, W70-74. 10.1093/nar/gkn188.

Harris, C.R., Millman, K.J., van der Walt, S.J., Gommers, R., Virtanen, P., Cournapeau, D., Wieser, E., Taylor, J., Berg, S., Smith, N.J., et al. (2020). Array programming with NumPy. Nature *585*, 357-362. 10.1038/s41586-020-2649-2.

Hauke, S., Best, M., Schmidt, T.T., Baalmann, M., Krause, A., and Wombacher, R. (2014). Two-step protein labeling utilizing lipoic acid ligase and Sonogashira cross-coupling. Bioconjug Chem *25*, 1632-1637. 10.1021/bc500349h.

Heuer, A., Gerovac, M., Schmidt, C., Trowitzsch, S., Preis, A., Kotter, P., Berninghausen, O., Becker, T., Beckmann, R., and Tampe, R. (2017). Structure of the 40S-ABCE1 post-splitting complex in ribosome recycling and translation initiation. Nat Struct Mol Biol *24*, 453-460. 10.1038/nsmb.3396.

Hickerson, R., Majumdar, Z.K., Baucom, A., Clegg, R.M., and Noller, H.F. (2005). Measurement of internal movements within the 30 S ribosomal subunit using Forster resonance energy transfer. J Mol Biol *354*, 459-472. 10.1016/j.jmb.2005.09.010.

Hirokawa, G., Demeshkina, N., Iwakura, N., Kaji, H., and Kaji, A. (2006). The ribosome-recycling step: consensus or controversy? Trends Biochem Sci *31*, 143-149. 10.1016/j.tibs.2006.01.007.

Hirokawa, G., Iwakura, N., Kaji, A., and Kaji, H. (2008). The role of GTP in transient splitting of 70S ribosomes by RRF (ribosome recycling factor) and EF-G (elongation factor G). Nucleic Acids Res *36*, 6676-6687. 10.1093/nar/gkn647.

Hirokawa, G., Kiel, M.C., Muto, A., Kawai, G., Igarashi, K., Kaji, H., and Kaji, A. (2002a). Binding of ribosome recycling factor to ribosomes, comparison with tRNA. J Biol Chem *277*, 35847-35852. 10.1074/jbc.M206295200.

Hirokawa, G., Kiel, M.C., Muto, A., Selmer, M., Raj, V.S., Liljas, A., Igarashi, K., Kaji, H., and Kaji, A. (2002b). Post-termination complex disassembly by ribosome recycling factor, a functional tRNA mimic. EMBO J *21*, 2272-2281. 10.1093/emboj/21.9.2272.

Hirokawa, G., Nijman, R.M., Raj, V.S., Kaji, H., Igarashi, K., and Kaji, A. (2005). The role of ribosome recycling factor in dissociation of 70S ribosomes into subunits. RNA *11*, 1317-1328. 10.1261/rna.2520405.

Holtkamp, W., Cunha, C.E., Peske, F., Konevega, A.L., Wintermeyer, W., and Rodnina, M.V. (2014). GTP hydrolysis by EF-G synchronizes tRNA movement on small and large ribosomal subunits. EMBO J *33*, 1073-1085. 10.1002/embj.201387465.

Huang, C., Mandava, C.S., and Sanyal, S. (2010). The ribosomal stalk plays a key role in IF2-mediated association of the ribosomal subunits. J Mol Biol *399*, 145-153. 10.1016/j.jmb.2010.04.009.

Huber, M., Faure, G., Laass, S., Kolbe, E., Seitz, K., Wehrheim, C., Wolf, Y.I., Koonin, E.V., and Soppa, J. (2019). Translational coupling via termination-reinitiation in archaea and bacteria. Nat Commun *10*, 4006. 10.1038/s41467-019-11999-9.

Hunter, J.D. (2007). Matplotlib: A 2D Graphics Environment. Computing in Science & Engineering *9*, 90-95. 10.1109/MCSE.2007.55.

Hussain, T., Llacer, J.L., Wimberly, B.T., Kieft, J.S., and Ramakrishnan, V. (2016). Large-Scale Movements of IF3 and tRNA during Bacterial Translation Initiation. Cell *167*, 133-144 e113. 10.1016/j.cell.2016.08.074.

Huvet, M., and Stumpf, M.P. (2014). Overlapping genes: a window on gene evolvability. BMC Genomics *15*, 721. 10.1186/1471-2164-15-721.

Iwakura, N., Yokoyama, T., Quaglia, F., Mitsuoka, K., Mio, K., Shigematsu, H., Shirouzu, M., Kaji, A., and Kaji, H. (2017). Chemical and structural characterization of a model Post-Termination Complex (PoTC) for the ribosome recycling reaction: Evidence for the release of the mRNA by RRF and EF-G. PLoS One *12*, e0177972. 10.1371/journal.pone.0177972.

Jackson, R.J., Hellen, C.U., and Pestova, T.V. (2012). Termination and post-termination events in eukaryotic translation. Adv Protein Chem Struct Biol *86*, 45-93. 10.1016/B978-0-12-386497-0.00002-5.

Janosi, L., Hara, H., Zhang, S., and Kaji, A. (1996). Ribosome recycling by ribosome recycling factor (RRF)--an important but overlooked step of protein biosynthesis. Adv Biophys *32*, 121-201. 10.1016/0065-227x(96)84743-5.

Julian, P., Milon, P., Agirrezabala, X., Lasso, G., Gil, D., Rodnina, M.V., and Valle, M. (2011). The Cryo-EM structure of a complete 30S translation initiation complex from Escherichia coli. PLoS Biol *9*, e1001095. 10.1371/journal.pbio.1001095.

Jumper, J., Evans, R., Pritzel, A., Green, T., Figurnov, M., Ronneberger, O., Tunyasuvunakool, K., Bates, R., Zidek, A., Potapenko, A., et al. (2021). Highly accurate protein structure prediction with AlphaFold. Nature *596*, 583-589. 10.1038/s41586-021-03819-2.

Kaji, A., Kiel, M.C., Hirokawa, G., Muto, A.R., Inokuchi, Y., and Kaji, H. (2001). The fourth step of protein synthesis: disassembly of the posttermination complex is catalyzed by elongation factor G and ribosome recycling factor, a near-perfect mimic of tRNA. Cold Spring Harb Symp Quant Biol *66*, 515-529. 10.1101/sqb.2001.66.515.

Karimi, R., Pavlov, M.Y., Buckingham, R.H., and Ehrenberg, M. (1999). Novel roles for classical factors at the interface between translation termination and initiation. Mol Cell *3*, 601-609. 10.1016/s1097-2765(00)80353-6.

Katunin, V.I., Savelsbergh, A., Rodnina, M.V., and Wintermeyer, W. (2002). Coupling of GTP hydrolysis by elongation factor G to translocation and factor recycling on the ribosome. Biochemistry *41*, 12806-12812. 10.1021/bi0264871.

Kiel, M.C., Kaji, H., and Kaji, A. (2007). Ribosome recycling: An essential process of protein synthesis. Biochem Mol Biol Educ *35*, 40-44. 10.1002/bmb.6.

Klinge, S., Voigts-Hoffmann, F., Leibundgut, M., Arpagaus, S., and Ban, N. (2011). Crystal structure of the eukaryotic 60S ribosomal subunit in complex with initiation factor 6. Science *334*, 941-948. 10.1126/science.1211204.

Korniy, N., Goyal, A., Hoffmann, M., Samatova, E., Peske, F., Pohlmann, S., and Rodnina, M.V. (2019). Modulation of HIV-1 Gag/Gag-Pol frameshifting by tRNA abundance. Nucleic Acids Res *47*, 5210-5222. 10.1093/nar/gkz202.

Kothe, U., Wieden, H.J., Mohr, D., and Rodnina, M.V. (2004). Interaction of helix D of elongation factor Tu with helices 4 and 5 of protein L7/12 on the ribosome. J Mol Biol *336*, 1011-1021. 10.1016/j.jmb.2003.12.080.

Kushner, S.R. (2018). Messenger RNA in Prokaryotes. In eLS, pp. 1-11. 10.1002/9780470015902.a0000874.pub4.

Kycia, J.H., Biou, V., Shu, F., Gerchman, S.E., Graziano, V., and Ramakrishnan, V. (1995). Prokaryotic translation initiation factor IF3 is an elongated protein consisting of two crystallizable domains. Biochemistry *34*, 6183-6187. 10.1021/bi00018a022.

Leppek, K., Das, R., and Barna, M. (2018). Functional 5' UTR mRNA structures in eukaryotic translation regulation and how to find them. Nat Rev Mol Cell Biol *19*, 158-174. 10.1038/nrm.2017.103.

Li, G.W., Burkhardt, D., Gross, C., and Weissman, J.S. (2014). Quantifying absolute protein synthesis rates reveals principles underlying allocation of cellular resources. Cell *157*, 624-635. 10.1016/j.cell.2014.02.033.

Lieberman, K.R., Firpo, M.A., Herr, A.J., Nguyenle, T., Atkins, J.F., Gesteland, R.F., and Noller, H.F. (2000). The 23 S rRNA environment of ribosomal protein L9 in the 50 S ribosomal subunit. J Mol Biol *297*, 1129-1143. 10.1006/jmbi.2000.3621.

Lorenz, R., Bernhart, S.H., Honer Zu Siederdissen, C., Tafer, H., Flamm, C., Stadler, P.F., and Hofacker, I.L. (2011). ViennaRNA Package 2.0. Algorithms Mol Biol *6*, 26. 10.1186/1748-7188-6-26.

Los, G.V., Encell, L.P., McDougall, M.G., Hartzell, D.D., Karassina, N., Zimprich, C., Wood, M.G., Learish, R., Ohana, R.F., Urh, M., et al. (2008). HaloTag: a novel protein labeling technology for cell imaging and protein analysis. ACS Chem Biol *3*, 373-382. 10.1021/cb800025k.

MacDougall, D.D., and Gonzalez, R.L., Jr. (2015). Translation initiation factor 3 regulates switching between different modes of ribosomal subunit joining. J Mol Biol *427*, 1801-1818. 10.1016/j.jmb.2014.09.024.

Major, L.L., Edgar, T.D., Yee Yip, P., Isaksson, L.A., and Tate, W.P. (2002). Tandem termination signals: myth or reality? FEBS Lett *514*, 84-89. 10.1016/s0014-5793(02)02301-3.

Maracci, C., and Rodnina, M.V. (2016). Review: Translational GTPases. Biopolymers *105*, 463-475. 10.1002/bip.22832.

McKinney, W. (2010). Data Structures for Statistical Computing in Python 10.25080/Majora-92bf1922-00a.

Melnikov, S., Ben-Shem, A., Garreau de Loubresse, N., Jenner, L., Yusupova, G., and Yusupov, M. (2012). One core, two shells: bacterial and eukaryotic ribosomes. Nat Struct Mol Biol *19*, 560-567. 10.1038/nsmb.2313.

Milon, P., Carotti, M., Konevega, A.L., Wintermeyer, W., Rodnina, M.V., and Gualerzi, C.O. (2010). The ribosome-bound initiation factor 2 recruits initiator tRNA to the 30S initiation complex. EMBO Rep *11*, 312-316. 10.1038/embor.2010.12.

Milon, P., Konevega, A.L., Gualerzi, C.O., and Rodnina, M.V. (2008). Kinetic checkpoint at a late step in translation initiation. Mol Cell *30*, 712-720. 10.1016/j.molcel.2008.04.014.

Milon, P., Konevega, A.L., Peske, F., Fabbretti, A., Gualerzi, C.O., and Rodnina, M.V. (2007). Transient kinetics, fluorescence, and FRET in studies of initiation of translation in bacteria. Methods Enzymol *430*, 1-30. 10.1016/S0076-6879(07)30001-3.

Milon, P., Maracci, C., Filonava, L., Gualerzi, C.O., and Rodnina, M.V. (2012). Real-time assembly landscape of bacterial 30S translation initiation complex. Nat Struct Mol Biol *19*, 609-615. 10.1038/nsmb.2285.

Milon, P., and Rodnina, M.V. (2012). Kinetic control of translation initiation in bacteria. Crit Rev Biochem Mol Biol *47*, 334-348. 10.3109/10409238.2012.678284.

Mitra, P., Ghosh, G., Hafeezunnisa, M., and Sen, R. (2017). Rho Protein: Roles and Mechanisms. Annu Rev Microbiol *71*, 687-709. 10.1146/annurev-micro-030117-020432.

Miura, O., Ogake, T., and Ohyama, T. (2018). Requirement or exclusion of inverted repeat sequences with cruciform-forming potential in Escherichia coli revealed by genome-wide analyses. Curr Genet *64*, 945-958. 10.1007/s00294-018-0815-y.

Mohammad, F., Woolstenhulme, C.J., Green, R., and Buskirk, A.R. (2016). Clarifying the Translational Pausing Landscape in Bacteria by Ribosome Profiling. Cell Rep *14*, 686-694. 10.1016/j.celrep.2015.12.073.

Moreau, M., de Cock, E., Fortier, P.L., Garcia, C., Albaret, C., Blanquet, S., Lallemand, J.Y., and Dardel, F. (1997). Heteronuclear NMR studies of E. coli translation initiation factor IF3. Evidence that the inter-domain region is disordered in solution. J Mol Biol *266*, 15-22. 10.1006/jmbi.1996.0756.

Nakamura, K., and Inouye, M. (1979). DNA sequence of the gene for the outer membrane lipoprotein of E. coli: an extremely AT-rich promoter. Cell *18*, 1109-1117. 10.1016/0092-8674(79)90224-1.

Newbury, S.F., Smith, N.H., Robinson, E.C., Hiles, I.D., and Higgins, C.F. (1987). Stabilization of translationally active mRNA by prokaryotic REP sequences. Cell *48*, 297-310. 10.1016/0092-8674(87)90433-8.

Nissen, P., Hansen, J., Ban, N., Moore, P.B., and Steitz, T.A. (2000). The structural basis of ribosome activity in peptide bond synthesis. Science *289*, 920-930. 10.1126/science.289.5481.920.

Nurenberg, E., and Tampe, R. (2013). Tying up loose ends: ribosome recycling in eukaryotes and archaea. Trends Biochem Sci *38*, 64-74. 10.1016/j.tibs.2012.11.003.

Pai, R.D., Zhang, W., Schuwirth, B.S., Hirokawa, G., Kaji, H., Kaji, A., and Cate, J.H. (2008). Structural Insights into ribosome recycling factor interactions with the 70S ribosome. J Mol Biol *376*, 1334-1347. 10.1016/j.jmb.2007.12.048.

Pavlov, M.Y., Antoun, A., Lovmar, M., and Ehrenberg, M. (2008). Complementary roles of initiation factor 1 and ribosome recycling factor in 70S ribosome splitting. EMBO J *27*, 1706-1717. 10.1038/emboj.2008.99.

Peng, B.Z., Bock, L.V., Belardinelli, R., Peske, F., Grubmuller, H., and Rodnina, M.V. (2019). Active role of elongation factor G in maintaining the mRNA reading frame during translation. Sci Adv *5*, eaax8030. 10.1126/sciadv.aax8030.

Peske, F., Rodnina, M.V., and Wintermeyer, W. (2005). Sequence of steps in ribosome recycling as defined by kinetic analysis. Mol Cell *18*, 403-412. 10.1016/j.molcel.2005.04.009.

Peske, F., Savelsbergh, A., Katunin, V.I., Rodnina, M.V., and Wintermeyer, W. (2004). Conformational changes of the small ribosomal subunit during elongation factor G-dependent tRNA-mRNA translocation. J Mol Biol *343*, 1183-1194. 10.1016/j.jmb.2004.08.097.

Peters, J.M., Vangeloff, A.D., and Landick, R. (2011). Bacterial transcription terminators: the RNA 3'-end chronicles. J Mol Biol *412*, 793-813. 10.1016/j.jmb.2011.03.036.

Petrychenko, V., Peng, B.Z., de, A.P.S.A.C., Peske, F., Rodnina, M.V., and Fischer, N. (2021). Structural mechanism of GTPase-powered ribosome-tRNA movement. Nat Commun *12*, 5933. 10.1038/s41467-021-26133-x.

Pisarev, A.V., Skabkin, M.A., Pisareva, V.P., Skabkina, O.V., Rakotondrafara, A.M., Hentze, M.W., Hellen, C.U., and Pestova, T.V. (2010). The role of ABCE1 in eukaryotic posttermination ribosomal recycling. Mol Cell *37*, 196-210. 10.1016/j.molcel.2009.12.034.

Plaks, J.G., Falatach, R., Kastantin, M., Berberich, J.A., and Kaar, J.L. (2015). Multisite clickable modification of proteins using lipoic acid ligase. Bioconjug Chem *26*, 1104-1112. 10.1021/acs.bioconjchem.5b00161.

Platt, T. (1981). Termination of transcription and its regulation in the tryptophan operon of E. coli. Cell *24*, 10-23. 10.1016/0092-8674(81)90496-7.

Prabhakar, A., Capece, M.C., Petrov, A., Choi, J., and Puglisi, J.D. (2017). Post-termination Ribosome Intermediate Acts as the Gateway to Ribosome Recycling. Cell Rep *20*, 161-172. 10.1016/j.celrep.2017.06.028.

Preis, A., Heuer, A., Barrio-Garcia, C., Hauser, A., Eyler, D.E., Berninghausen, O., Green, R., Becker, T., and Beckmann, R. (2014). Cryoelectron microscopic structures of eukaryotic translation termination complexes containing eRF1-eRF3 or eRF1-ABCE1. Cell Rep *8*, 59-65. 10.1016/j.celrep.2014.04.058.

Puthenveetil, S., Liu, D.S., White, K.A., Thompson, S., and Ting, A.Y. (2009). Yeast Display Evolution of a Kinetically Efficient 13-Amino Acid Substrate for Lipoic Acid Ligase. Journal of the American Chemical Society *131*, 16430-16438. 10.1021/ja904596f.

Rabl, J., Leibundgut, M., Ataide, S.F., Haag, A., and Ban, N. (2011). Crystal structure of the eukaryotic 40S ribosomal subunit in complex with initiation factor 1. Science *331*, 730-736. 10.1126/science.1198308.

Ramakrishnan, V. (2014). The ribosome emerges from a black box. Cell *159*, 979-984. 10.1016/j.cell.2014.10.052.

Rodnina, M.V. (2013). The ribosome as a versatile catalyst: reactions at the peptidyl transferase center. Curr Opin Struct Biol *23*, 595-602. 10.1016/j.sbi.2013.04.012.

Rodnina, M.V. (2018). Translation in Prokaryotes. Cold Spring Harb Perspect Biol *10*. 10.1101/cshperspect.a032664.

Rodnina, M.V., Beringer, M., and Wintermeyer, W. (2007). How ribosomes make peptide bonds. Trends Biochem Sci *32*, 20-26. 10.1016/j.tibs.2006.11.007.

Rodnina, M.V., Fischer, N., Maracci, C., and Stark, H. (2017). Ribosome dynamics during decoding. Philos Trans R Soc Lond B Biol Sci *372*. 10.1098/rstb.2016.0182.

Rodnina, M.V., Peske, F., Peng, B.Z., Belardinelli, R., and Wintermeyer, W. (2019). Converting GTP hydrolysis into motion: versatile translational elongation factor G. Biol Chem *401*, 131-142. 10.1515/hsz-2019-0313.

Rodnina, M.V., Savelsbergh, A., Katunin, V.I., and Wintermeyer, W. (1997). Hydrolysis of GTP by elongation factor G drives tRNA movement on the ribosome. Nature *385*, 37-41. 10.1038/385037a0.

Rodnina, M.V., Savelsbergh, A., Matassova, N.B., Katunin, V.I., Semenkov, Y.P., and Wintermeyer, W. (1999). Thiostrepton inhibits the turnover but not the GTPase of elongation factor G on the ribosome. Proc Natl Acad Sci U S A *96*, 9586-9590. 10.1073/pnas.96.17.9586.

Rodnina, M.V., and Wintermeyer, W. (1995). GTP consumption of elongation factor Tu during translation of heteropolymeric mRNAs. Proc Natl Acad Sci U S A *92*, 1945-1949. 10.1073/pnas.92.6.1945.

Rodnina, M.V., and Wintermeyer, W. (2011). The ribosome as a molecular machine: the mechanism of tRNA-mRNA movement in translocation. Biochem Soc Trans *39*, 658-662. 10.1042/BST0390658.

Roy, R., Hohng, S., and Ha, T. (2008). A practical guide to single-molecule FRET. Nature Methods *5*, 507-516. 10.1038/nmeth.1208.

Rozov, A., Khusainov, I., El Omari, K., Duman, R., Mykhaylyk, V., Yusupov, M., Westhof, E., Wagner, A., and Yusupova, G. (2019). Importance of potassium ions for ribosome structure and function revealed by long-wavelength X-ray diffraction. Nat Commun *10*, 2519. 10.1038/s41467-019-10409-4.

Salgado, H., Moreno-Hagelsieb, G., Smith, T.F., and Collado-Vides, J. (2000). Operons in Escherichia coli: genomic analyses and predictions. Proc Natl Acad Sci U S A *97*, 6652-6657. 10.1073/pnas.110147297.

Savelsbergh, A., Katunin, V.I., Mohr, D., Peske, F., Rodnina, M.V., and Wintermeyer, W. (2003). An elongation factor G-induced ribosome rearrangement precedes tRNA-mRNA translocation. Mol Cell *11*, 1517-1523. 10.1016/s1097-2765(03)00230-2.

Savelsbergh, A., Matassova, N.B., Rodnina, M.V., and Wintermeyer, W. (2000). Role of domains 4 and 5 in elongation factor G functions on the ribosome. J Mol Biol *300*, 951-961. 10.1006/jmbi.2000.3886.

Savelsbergh, A., Rodnina, M.V., and Wintermeyer, W. (2009). Distinct functions of elongation factor G in ribosome recycling and translocation. RNA *15*, 772-780. 10.1261/rna.1592509.

Schagger, H. (2006). Tricine-SDS-PAGE. Nat Protoc *1*, 16-22. 10.1038/nprot.2006.4.

Schagger, H., and von Jagow, G. (1987). Tricine-sodium dodecyl sulfate-polyacrylamide gel electrophoresis for the separation of proteins in the range from 1 to 100 kDa. Anal Biochem *166*, 368-379. 10.1016/0003-2697(87)90587-2.

Schmitt, E., Coureux, P.D., Kazan, R., Bourgeois, G., Lazennec-Schurdevin, C., and Mechulam, Y. (2020). Recent Advances in Archaeal Translation Initiation. Front Microbiol *11*, 584152. 10.3389/fmicb.2020.584152.

Schneider, C.A., Rasband, W.S., and Eliceiri, K.W. (2012). NIH Image to ImageJ: 25 years of image analysis. Nat Methods *9*, 671-675. 10.1038/nmeth.2089.

Selmer, M., Al-Karadaghi, S., Hirokawa, G., Kaji, A., and Liljas, A. (1999). Crystal structure of Thermotoga maritima ribosome recycling factor: a tRNA mimic. Science *286*, 2349-2352. 10.1126/science.286.5448.2349.

Sette, M., van Tilborg, P., Spurio, R., Kaptein, R., Paci, M., Gualerzi, C.O., and Boelens, R. (1997). The structure of the translational initiation factor IF1 from E.coli contains an oligomer-binding motif. EMBO J *16*, 1436-1443. 10.1093/emboj/16.6.1436.

Sharma, H., Adio, S., Senyushkina, T., Belardinelli, R., Peske, F., and Rodnina, M.V. (2016). Kinetics of Spontaneous and EF-G-Accelerated Rotation of Ribosomal Subunits. Cell Rep *16*, 2187-2196. 10.1016/j.celrep.2016.07.051.

Shoji, S., Dambacher, C.M., Shajani, Z., Williamson, J.R., and Schultz, P.G. (2011). Systematic chromosomal deletion of bacterial ribosomal protein genes. J Mol Biol *413*, 751-761. 10.1016/j.jmb.2011.09.004.

Spahn, C.M., Beckmann, R., Eswar, N., Penczek, P.A., Sali, A., Blobel, G., and Frank, J. (2001). Structure of the 80S ribosome from Saccharomyces cerevisiae--tRNA-ribosome and subunit-subunit interactions. Cell *107*, 373-386. 10.1016/s0092-8674(01)00539-6.

Stryer, L. (1978). Fluorescence Energy Transfer as a Spectroscopic Ruler. Annual Review of Biochemistry *47*, 819-846. 10.1146/annurev.bi.47.070178.004131.

Takyar, S., Hickerson, R.P., and Noller, H.F. (2005). mRNA helicase activity of the ribosome. Cell *120*, 49-58. 10.1016/j.cell.2004.11.042.

Thornlow, D.N., Cox, E.C., Walker, J.A., Sorkin, M., Plesset, J.B., DeLisa, M.P., and Alabi, C.A. (2019). Dual Site-Specific Antibody Conjugates for Sequential and Orthogonal Cargo Release. Bioconjug Chem *30*, 1702-1710. 10.1021/acs.bioconjchem.9b00244.

Van Rossum, G., and Drake, F.L. (2009). Python 3 Reference Manual (CreateSpace).

Varadi, M., Anyango, S., Deshpande, M., Nair, S., Natassia, C., Yordanova, G., Yuan, D., Stroe, O., Wood, G., Laydon, A., et al. (2022). AlphaFold Protein Structure Database: massively expanding the structural coverage of protein-sequence space with high-accuracy models. Nucleic Acids Res *50*, D439-D444. 10.1093/nar/gkab1061.

Weisser, M., and Ban, N. (2019). Extensions, Extra Factors, and Extreme Complexity: Ribosomal Structures Provide Insights into Eukaryotic Translation. Cold Spring Harb Perspect Biol *11*. 10.1101/cshperspect.a032367.

Wells, S.E., Hillner, P.E., Vale, R.D., and Sachs, A.B. (1998). Circularization of mRNA by eukaryotic translation initiation factors. Mol Cell *2*, 135-140. 10.1016/s1097-2765(00)80122-7.

Wieden, H.J., Gromadski, K., Rodnin, D., and Rodnina, M.V. (2002). Mechanism of elongation factor (EF)-Ts-catalyzed nucleotide exchange in EF-Tu. Contribution of contacts at the guanine base. J Biol Chem *277*, 6032-6036. 10.1074/jbc.M110888200.

Wilson, D.N. (2014). Ribosome-targeting antibiotics and mechanisms of bacterial resistance. Nature Reviews Microbiology *12*, 35-48. 10.1038/nrmicro3155.

Wohlgemuth, I., Pohl, C., and Rodnina, M.V. (2010). Optimization of speed and accuracy of decoding in translation. EMBO J *29*, 3701-3709. 10.1038/emboj.2010.229.

Wu, A.M., and Platt, T. (1978). Transcription termination: nucleotide sequence at 3' end of tryptophan operon in Escherichia coli. Proc Natl Acad Sci U S A *75*, 5442-5446. 10.1073/pnas.75.11.5442.

Yamamoto, H., Wittek, D., Gupta, R., Qin, B., Ueda, T., Krause, R., Yamamoto, K., Albrecht, R., Pech, M., and Nierhaus, K.H. (2016). 70S-scanning initiation is a novel and frequent initiation mode of ribosomal translation in bacteria. Proc Natl Acad Sci U S A *113*, E1180-1189. 10.1073/pnas.1524554113.

Yan, B., Boitano, M., Clark, T.A., and Ettwiller, L. (2018). SMRT-Cappable-seq reveals complex operon variants in bacteria. Nat Commun *9*, 3676. 10.1038/s41467-018-05997-6.

Yokoyama, T., Shaikh, T.R., Iwakura, N., Kaji, H., Kaji, A., and Agrawal, R.K. (2012). Structural insights into initial and intermediate steps of the ribosome-recycling process. EMBO J *31*, 1836-1846. 10.1038/emboj.2012.22.

Yoo, J.H., and RajBhandary, U.L. (2008). Requirements for translation re-initiation in Escherichia coli: roles of initiator tRNA and initiation factors IF2 and IF3. Mol Microbiol *67*, 1012-1026. 10.1111/j.1365-2958.2008.06104.x.

Yusupov, M.M., Yusupova, G.Z., Baucom, A., Lieberman, K., Earnest, T.N., Cate, J.H., and Noller, H.F. (2001). Crystal structure of the ribosome at 5.5 A resolution. Science *292*, 883-896. 10.1126/science.1060089.

Zavialov, A.V., Hauryliuk, V.V., and Ehrenberg, M. (2005). Splitting of the posttermination ribosome into subunits by the concerted action of RRF and EF-G. Mol Cell *18*, 675-686. 10.1016/j.molcel.2005.05.016.

6 Supplement

Abbreviations

µM	micromolar
Å	Ångstroem
A site	aminoacyl site
a. u.	arbitrary units
aa	amino acids
aa-tRNA	aminoacyl-tRNA
Amp	amplitude
ATP	adenosine triphosphate
Cryo-EM	cryo-Electron microscopy
DNA	Desoxyribonucleic acid
DOL	degree of labeling
E site	exit site
E. coli	*Escherichia coli*
EF-G	elongation factor G
EF-Tu	elongation factor Tu
FRET	förster resonance energy transfer
g	gram
GDP	guanosine diphosphate
GTP	guanosine triphosphate
h	hour
IC	initiation complex
IF	initiation factor
k	rate constant
LAP	LplA acceptor peptide
LED	light emitting diode
LplA	lipoic acid ligase
Lpp	major outer membrane prolipoprotein
M	molar, mol/L
ME	methyl
min	minute
mL	milliliter
mM	millimolar
mRNA	messenger RNA
ms	millisecond
ng	nanogram
nm	nanometer
nM	nanomolar
nts	nucleotides
OD_{260}	absorbance at 260 nm

ORF	open reading frame
P site	peptidyl site
PAGE	poly-acrylamide gel electrophoresis
PCR	polymerase chain reaction
PDB	protein data bank
Pi	inorganic phosphate
pmol	picomole
PoTC	post-translation complex
PRC	pre-recycling complex
RBS	ribosome binding site
REP	repetitive extragenic palindromic
RF	release factor
RG	red glass
RNA	ribonucleic acid
RNASeq	RNA sequencing
rpm	rotation per minute
RRF	ribosome recycling factor
rRNA	ribosomal RNA
RT	room temperature
S	svedberg unit
s	second
SD	Shine-Dalgarno
smFRET	single molecule FRET
StD	standard deviation
T. thermophilus	*Thermus thermophilus*
TC	ternary complex
TIRF	total internal reflection fluorescence
tRNA	transfer RNA
TSS	transcription start site
TTS	transcription termination site
UTR	untranslated region
X_0	duration of delay phase

Table of Figures

List of Tables

Acknowledgements

I would like to thank Marina Rodnina for giving me the opportunity to work on this challenging topic for my PhD thesis and for all the support, encouragement and inspiration during the last years providing an exceptional environment for creativity and freedom for experimentation. I would also like to thank the members of my thesis advisory committee Kai Tittmann and Holger Stark for their helpful suggestions and motivating questions which helped to improve my studies. Furthermore, I thank Alex Faesen, Sonja Lorenz and Hauke Hillen for joining my examination board and the GGNB office for the helpful support.

Special thanks go out to Frank Peske for being a great daily supervisor, gifting me with rich scientific and non-scientific advice, patience and constructive criticism and rich conversations about science, politics and life. I want to further thank Tamara Senyushkina for the collaboration on smFRET TIRF microscopy, Ekaterina Samatova for her advice and help with in vitro translation.

Most of my experiments would not have been possible without extensive technical support and ribosomes from Sandra Kappler, tRNA from Olaf Geintzer, mRNAs from Vanessa Herold, translation factors from Michael Zimmermann and Christina Kothe and many other things prepared and maintained by Tessa Hübner, Manuela Beck-Corell, Theresia Steiger, Anna Pfeifer and Franziska Hummel. Many thanks go to Dimitra Papastavrou for keeping a great overview and help with all kinds of organizational issues and to Mario Klein for the IT support. Appreciation goes to Vladimir Belov, Jürgen Bienert, Jens Schimpfhauser and Jan Seikowski for the synthesis of the norbornene substrate.

I would like to thank my lab mates Natalie, Panos and Michael, former lab mates Betty, Natalia and Sarah for letting me use their precious stock solutions and having good conversations. Thanks to the rest of the lab who were always helpful and fun to chat with: Lena (a board game evening will happen again), Vitalii, Mani and Mario (beware when these three are in the kitchen, one might not be able to leave again), Ingo, Kärt, Shreya, Michele, Evan, Wolfgang, Nicola, Prajwal, Nilanjan, Sakshi, Vaishali, Céline, Justas and all those who just arrived or left the lab.

Further I want to thank all my friends and colleagues that helped me during my life before and during university. Without them I would not have been able to make it that far. And in that regard, I have to thank especially Natalie, Vitalii, Nessa, Lena, Lena and Lars for their kind words, suggestions and company during the final stages of this thesis.

I want to thank my family for supporting and encouraging me since I was born.

And last, I need to thank my wonderful wife Anni and my amazing son Oskar. Words cannot describe how grateful I am that you both exist.